Energy Science

MASTER THESIS

Combined Photovoltaic and Solar Thermal (PV-T) systems;
Design optimization and thermal annealing.

UTRECHT UNIVERSITY

Utrecht, The Netherlands

2013

Student:	Friso Huizinga
Supervisors:	Dr. W.G.J.H.M. van Sark (UU)
	Martin Ruiter (QING Sustainable)
	Jasper Lemmens (DNV KEMA)
Date:	5/2013 – 10/2013
Company:	QING Sustainable
University:	Utrecht University
Adress:	Westervoortsedijk 73
	6827 AV, Arnhem
	The Netherlands

ABSTRACT

Hybrid solar photovoltaic-thermal systems (PV-T) generate electricity and heat simultaneously. The Nanosol project aims to develop such a PV-T system by combining a thin-film flexible amorphous Silicon solar module with tube shaped lamination to extract the heat. However, it was unclear whether it was favorable to cool the solar cell with air or with water, what the optimal design would be, what annual yield could be expected in the Netherlands and how the solar cell would be affected by longer periods of elevated temperatures.

To investigate these issues, a theoretical model was presented to simulate different PV-T systems. The model was based on the one from Hegazy (2000) that was used to simulate air-cooled collectors. For the purpose of this study, this model was improved and extended to also simulate water-cooled collectors. Two designs were simulated with either air or water to cool the solar cell, resulting in a total of four models; 'P1 Air', 'P1 Water', 'P2 Air' and 'P2 Water'. Prototype 1 is cooled from both the front and the backside of the solar cell and prototype 2 is only cooled from the backside. These models were simulated under standard test conditions and under real Dutch climate conditions. Also an experiment was conducted to investigate the effect of thermal annealing. Three modules were degraded in a light soaker and subsequently heated in different ovens at 60°C, 90°C and 120°C for about 300 hours. The efficiencies were regularly measured during the degradation and heating process

Results from the simulations at mass flow rates of 0.015 $\frac{kg}{sm^2}$, showed annual electrical performances, including the required pumping power, of 7.88, 8.61, 7.46 and 8.64 percent for 'P1 Air', 'P1 Water', 'P2 Air' and 'P2 Water' respectively. A reference PV cell under the same conditions provided an annual electrical efficiency of 8.58 percent. The annual thermal efficiencies proved to be 23.77, 35.06, 14.52 and 29.70 percent for the four models. The annealing experiment showed a relative increase in efficiency of 0.031%, 0.130% and 0.339% per hour during the first 24 hours of thermal annealing at 60°C, 90°C and 120°C respectively. Thereafter, only a gradual improvement of the efficiency could be observed.

Model 'P1 Water' resulted to be the most favorable PV-T design. Water is beneficial for its superior properties compared to air, allowing for higher thermal and electrical yields. Additionally, water requires much less pumping power and is better compatible with other thermal applications. The effect of thermal annealing of this particular module in Dutch climate conditions is expected to be limited.

TABLE OF CONTENTS

LIST OF TABLES

LIST OF FIGURES

LIST OF CONSTANTS AND VARIABLES

Standard Test Conditions

Variable	Symbol	Value	Unit	Formula
Solar Radiation on Panel	I_r	1000.0	$\mathrm{Wm^{-2}}$	
Ambient Temperature	T_a	288.15	K	
Sky Temperature	T_s	270.00	K	$= 0.0552 \cdot T_a^{1.5}$
Wind speed	u_w	0.0	$\mathrm{ms^{-1}}$	

Constants

Constant	Symbol	Value	Unit	Formula
Boltzmann Constant	σ	$5.67 \cdot 10^{-8}$	$\mathrm{Wm^{-2}K^{-4}}$	
Gravitational Constant	g	9.81	$\mathrm{ms^{-2}}$	

Fixed parameters – PVT-module and dimensions

Variable	Symbol	Value	Unit	Formula
Tilt angle PVT-module	β	0.0	Degrees	
Efficiency Solar Cell	η_{sc}	0.10	–	
Temperature Coefficient	T_{coeff}	-0.2	$\%\mathrm{K^{-1}}$	
Inlet Temperature	T_i	288.15	K	
Length PVT-module	L	2.00	m	
Width channel	W	0.018	m	
Depth channel	D	0.008	m	
Wetted perimeter	p	0.052	m	$= (2 \cdot D) + (2 \cdot W)$
Hydraulic diameter	d	0.011	m	$= (4 \cdot D \cdot W)/p$
Tube Cross Section	O_{tube}	0.000108	$\mathrm{m^2}$	$= 0.75 \cdot (D \cdot W)$
Tube diameter (app.)	d_{tube}	0.0117	m	$= 2 \cdot SQRT(O_{tube}/\pi)$
Area panel for convection	X	1.009	m	$= (L + W)/2$
Thickness PV cell	t_{sc}	0.0005	m	
Thickness Foil	t_f	0.001	m	
Thickness Insulation	t_{in}	0.003	m	
Thermal conduction insulation	k_{in}	0.045	$\mathrm{Wm^{-1}K^{-1}}$	

Fixed parameters – Mass Flow Rates

Variable	Symbol	Value	Unit	Formula
Number of tubes in a row	n_{tubes}	49	#	$= \dfrac{(1 - 0.02)}{(W + t_f + t_f)}$
Mass Flow Rate (air/water)	G_{tot}	0.015	$\mathrm{kgs^{-1}m^{-2}}$	Varies from 0 to 0.05
Mass Flow Rate per tube	G_{tube}	0.00031	$\mathrm{kgs^{-1}}$	$= G_{tot}/n_{tubes}$
Mass Flow Rate per element	G_{el}	0.00061	$\mathrm{kgs^{-1}}$	$= G_{tube} \cdot L$
Mass Flow Rate Upper/Lower (P1)	$G_{el1,P2}$	0.00061	$\mathrm{kgs^{-1}}$	$= G_{el}$
Mass Flow Rate Upper/Lower (P1)	$G_{el1,P1}$	0.00031	$\mathrm{kgs^{-1}}$	$= G_{el}/2$

Fixed parameters – Equipment efficiencies

Variable	Symbol	Value	Unit	Formula
Efficiency Inverter	$\eta_{inverter}$	0.90	–	
Efficiency Fan (air)	η_{fan}	0.75	–	
Efficiency Pump (water)	η_{pump}	0.90	–	
Efficiency Electrical motor	$\eta_{e.motor}$	0.90	–	

Fixed parameters – Material and optical properties

Variable	Symbol	Value	Unit	Formula
Emissivity Foil	ϵ_f	0.90	–	
Emissivity Plate	ϵ_p	0.90	–	
Emissivity Base	ϵ_b	0.90	–	
Absorption Foil	α_f	0.035	–	
Absorption Plate	α_p	0.70	–	
Refractive index Air	n_{air}	1.00	–	
Refractive index Water (590nm)	n_{water}	1.33	–	

Refractive index Foil (590nm)	n_{foil}	1.45	–	
Refractive index Encaps. (590nm)	n_e	1.43	–	
Reflection interface Air-Foil	$R_{air,f}$	0.0337	–	$= \left[(n_{air} - n_{foil})/(n_{air} + n_{foil})\right]^2$
Reflection interface Water-Foil	$R_{wat,f}$	0.0018	–	$= \left[(n_{wat} - n_{foil})/(n_{wat} + n_{foil})\right]^2$
Reflection interface Air-Encaps.	$R_{air,e}$	0.0313	–	$= [(n_{air} - n_e)/(n_{air} + n_e)]^2$
Reflection interface Water-Encaps.	$R_{wat,e}$	0.0012	–	$= [(n_{wat} - n_e)/(n_{wat} + n_e)]^2$
Transmission Air-Foil	τ_{af}	0.9663	–	$= 1 - R_{air,f}$
Transmission Water-Foil	τ_{wf}	0.9982	–	$= 1 - R_{wat,f}$
Transmission Air-Foil-Air	τ_{afa}	0.9019	–	$= \tau_{total} = \frac{\tau_1(1-\alpha)\tau_2}{1 - R_1(1-\alpha)^2 R_2}$
Transmission Air-Foil-Water	τ_{afw}	0.9309	–	$= \tau_{total} = \frac{\tau_1(1-\alpha)\tau_2}{1 - R_1(1-\alpha)^2 R_2}$
Transmission Air-Encapsulent	τ_{ae}	0.9687	–	$= 1 - R_{air,e}$
Transmission Water-Encapsulent	τ_{we}	0.9988	–	$= 1 - R_{wat,e}$

Fixed parameters – Tube surfaces for heat transfer coefficients

Variable	Symbol	Value	Unit	Formula
Angle tube sides	A_t	75	Degrees	
Tube surface, Top	O_{top}	0.061	m^2	$= L\left[\left(2\frac{D}{sin(A_t)}\right) + \left(W - \left(2\frac{D}{tan(A_t)}\right)\right)\right]$
Tube surface, Inner Top	$O_{top,in}$	0.053	m^2	$= L\left[\left(2\frac{D}{sin(A_t)}\right) + \left(W - \left(2\frac{D}{tan(A_t)}\right)\right) - (4 \cdot t_f)\right]$
Tube surface, Plate	O_{plate}	0.040	m^2	$= L(W + t_f + t_f)$
Tube surface, Inner Base	$O_{base,in}$	0.053	m^2	$= L\left[\left(2\frac{D}{sin(A_t)}\right) + \left(W - \left(2\frac{D}{tan(A_t)}\right)\right) - (4 \cdot t_f)\right]$
Tube surface, Base	O_{base}	0.027	m^2	$= L\left[W - \left(2\frac{D}{tan(A_t)}\right)\right]$
Solar Cell Surface, Total	O_{sc}	0.980	m^2	$= \frac{O_{plate} \cdot n_{tubes}}{L}$

Air and Water properties (see Appendix A1 and A2 for their temperature dependencies)

Variable	Symbol	Value	Unit	Formula
Density	ρ	-	kgm^{-3}	
Kinetic Viscosity	ν	-	m^2s^{-1}	
Specific Heat Capacity	C	-	$Jkg^{-1}K^{-1}$	
Thermal Diffusivity	κ	-	m^2s^{-1}	
Thermal Conductivity	k	-	Wm^{-1}	

Heat Transfer Coefficient (HTC)

Variable	Symbol	Value	Unit	Formula
Heat transfer coefficient	h	-	$Wm^{-2}K^{-1}$	

Subscripts

Subscripts	Meaning	Subscripts	Meaning
a	Ambient	w	Wind
s	Sky	r	Radiation
i	Inlet	c	Convection
o	Outlet	cn	Conduction
f	Foil	sc	Solar Cell
p	Plate	in	Insulation
b	Base	tot	Total
m	Mean	1	Air/Water stream 1 (upper tube)
e	Encapsulent	2	Air/Water stream 2 (lower tube)

ACKNOWLEDGEMENTS

This research was primarily conducted at QING Sustainable in Arnhem. First of all, I am very grateful to my supervisors at QING Sustainable; Martin Ruiter and Arno Albers. Their supervision manifested in regular meetings which provided me with useful input throughout this project. Furthermore, they have lent me useful books, tools and knowledge to help me in my research. Also I would like to thank Martin, Arno and all other colleagues from QING Sustainable for the inspiring and joyful atmosphere that is present at the office.

The same gratitude applies to Jasper Lemmens who was my main contact person at DNV KEMA. He gave me the unique opportunity to be involved in the Nanosol Consortium and to perform this study. Jasper, together with Bas Vet and Friso Sikkema (also from DNV KEMA), were available for critical but constructive conversations to improve the quality of this study.

Also Edward Hamers and Klaus Jäger from Hyet Solar were essential for this research. The thermal annealing experiment was completely conducted at Hyet Solar in Arnhem. Klaus was helpful with the experimental setup; he offered me the modules for the experiment and an introduction for the instrumentation. Edward and Klaus also provided useful feedback on the PV-T model and the results of the annealing experiment.

In addition, I am indebted to my supervisor at Utrecht University, Dr. Wilfried van Sark. Wilfried was very effective in quickly assessing the functionality of my model and provided me with useful knowledge and literature to continue this study.

And finally, I would very much like to thank Martin and Arno again for offering me a full-time job at QING Sustainable as junior Consultant! I am very much looking forward to start at the 1st of November!

PREFACE

This research is part of a larger project which is usually referred to as the Nanosol project. Nanosol is founded via a consortium that consists of five main partners; DNV KEMA, Hyet Solar, NanoAnalytics, SMInnoTech and QING Sustainable.

The Nanosol project aims to develop an inexpensive, flexible and light weight PV-T system that could be applied at commercial offices. The advantage of a PV-T system is that it enables to cool the solar cell which improves its electrical efficiency. Furthermore, the energy yield per unit surface is increased as the solar energy is now converted in both electricity and heat. The heat can be used to further meet the energy demand of the office.

Via DNV KEMA I was notified of the Nanosol project. Subsequently, QING Sustainable offered me the opportunity to conduct this research at their office as a graduate student.

SECTION 1: INTRODUCTION

A growing demand for energy, the security of supply of fossil resources and the international agreements to mitigate climate change are key issues of modern society. These developments drastically increased the necessity of large scale implementation of renewable energy technologies over the past two decennia and will continue to do so in the near future (IPCC, 2007).

Electricity and heat are the most important energy requirements in the residential sector and the public and commercial services sector. The latter accounted for 32.5% (33.7 TWh) of the total final electricity consumption and 30.1% (25.9 PJ) of the total heat consumption of the Netherlands in 2009 (IEA, 2013). In the Netherlands, most of this energy is centrally produced from conventional energy carriers such as coal and natural gas. Alternatively, photovoltaic (PV) and solar thermal collector devices enable decentralized and renewable electricity and heat production. However, so far they only represented a share of 0.02% (361 TJ) of the final electricity consumption and a share of 0.05% (1041 TJ) of the final heat consumption in the Netherlands in 2011 (CBS, 2013).

FIGURE 1, COMBINED SOLAR PV AND THERMAL PANEL

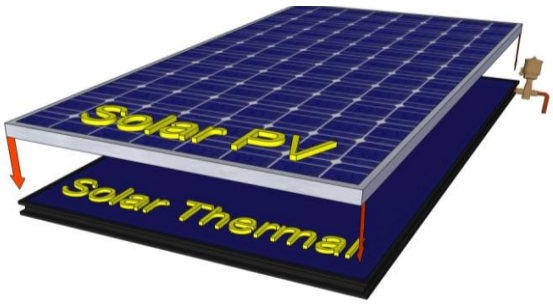

Combined photovoltaic and solar thermal systems (PV-T systems, see Figure 1) produce both electricity and heat simultaneously. In doing so, PV-T systems enable higher energy yields per square meter and thus more efficient use of the available roof space. Furthermore, the thermal collector now actively cools the photovoltaic solar cells, resulting in increased electrical performances. In addition, PV-T systems allow for a more uniform appearance on the roof and require less installation costs compared to two individual systems together. Although PV-T-systems have been researched extensively for the last three decades, still very few commercial systems are available on the market today (Zondag H. A., 2008).

To respond to this market opportunity, project Nanosol was initiated by five companies; DNV KEMA, QING Sustainable, Hyet Solar, MS Innotech and Nano Analytics. The Nanosol project aims to develop a new PV-T system, by using the flexible thin-film amorphous Silicon photovoltaic module from Hyet Solar as absorber, and should be ready for the market at the end of 2014. Amorphous Silicon (a-Si) has a lower temperature coefficient (-0.20%/K) compared to crystalline Silicon (-0.45%/K) which allows it to operate at higher temperatures without compromising much on efficiency (Schott-Solar, 2013a). However, there are still many uncertainties considering the design of the PVT-system. For example, what is the most optimal design, which heat extraction medium is preferred, other design features and what would the annual yield of such a system be in the Netherlands? Another interesting topic is the effect of seasonal thermal annealing. In a PV-T system, the temperature can by varied by adjusting the mass flow rate of the cooling fluid. Long term heating of an amorphous Silicon module is expected to increase its electrical performance. The latter has not yet been experimentally verified at module level and especially not at low operation temperatures (< 150°C).

To clarify the uncertainties of the Nanosol project, this research focuses on the following questions:

- What are optimal PV-T designs for the Nanosol Project and what is the annual yield?
- How does thermal annealing of thin-film a-Si modules depend on the temperature?

Obtaining this information is essential to develop an optimal PV-T system and to have an idea of the annual yields in the Netherlands. From a social point of view, the resulting PV-T system could provide low cost decentralized renewable electricity and heat. From a scientific point of view, especially the

thermal annealing experiment is of interest. Low temperature thermal annealing of amorphous Silicon modules is conducted for the first time.

This study combines information available from scientific literature, knowledge from experts, excel simulations and experimental data to obtain a thorough insight into the research questions. The report starts with a theoretical section to provide (1) an overview of the principles and development PVT-systems and (2) the required background for the effect of seasonal thermal annealing. Thereafter, in the methodology, the models, calculations and data for the numerical simulations are explained and the annealing experiment is described in detail. Subsequently, the results of the numerical simulations and the annealing experiment are summarized. In the analysis section, the outcomes of the excel simulations and the annealing experiment are compared and analyzed. The discussion, conclusion and recommendations can be found at the end of the report.

SECTION 2: THEORETICAL BACKGROUND

The theoretical section provides the required background information to have a good understanding of the concepts that are central for this research. This section is therefore divided in two chapters; the first chapter considers several aspects of hybrid photovoltaic-thermal module designs and the second chapter deals with the effect of thermal annealing.

2.1 PV-T COLLECTORS

To begin with, this chapter explains the principles of a solar photovoltaic-thermal (PV-T) system and provides a brief overview of the relevant literature that has been conducted over the past three decades. Subsequently, the designs that already have been researched are discussed and compared. Thereafter, some words are dedicated to the pros and cons of using water or air as working fluid to extract the heat. Furthermore, innovative designs are shown that could improve the heat extraction process and a few commercially available PV-T modules are reviewed. In addition, the potential of PV-T systems in the Netherlands is explained and some current applications. The chapter ends with the key factors that are important to increase the market potential of PV-T systems.

2.1.1 PV-T PRINCIPLES

Research and development into solar photovoltaic-thermal systems have been conducted since the 1970's. Especially after the oil embargo in 1973/4, there was an increased awareness about resource scarcity and the necessity to develop independent and local renewable energy resources. This was especially meaningful for the photovoltaic industry and hence also for the development of PV-T systems. The main characteristic of a PV-T system is that converts solar radiation into electricity and heat simultaneously. Electricity and heat are often required on the same location, which makes the photovoltaic and thermal system a particular interesting combination. In standard solar thermal systems, the heat is absorbed by a specially designed absorber plate. In PV-T systems, the photovoltaic solar cell is used is the heat absorber and thus has a dual function. (Zondag H. A., 2008)

Besides the main advantage of producing electricity and heat simultaneously where it is required, a PV-T system has additional advantages. The electrical performance of solar cells is reduced when they are operated at higher temperatures (see also section 2.2.2 on the temperature coefficient). Via the heat extraction process of a PV-T system, the photovoltaic cell is actively cooled and thus enables higher electrical performances. Furthermore, the total energy yield per unit surface is increased; two squared meter of PV-T yields more electricity and heat than one squared meter of photovoltaic and one squared meter of solar thermal panels together. Additionally, combined systems allow for a more uniform appearance on rooftops and less costs for the installation. (Chow, 2010)

FIGURE 2, PV-T WATER, MATERIAL STACK

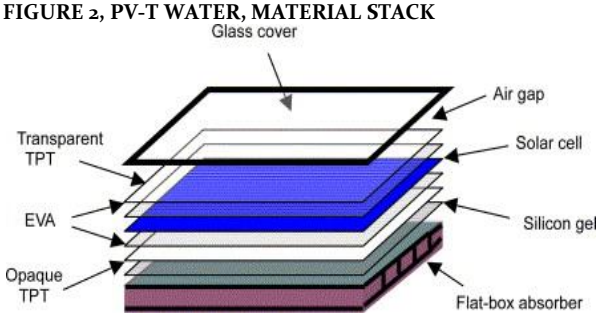

FIGURE 3, PV-T WATER SHEET AND TUBE DESIGN

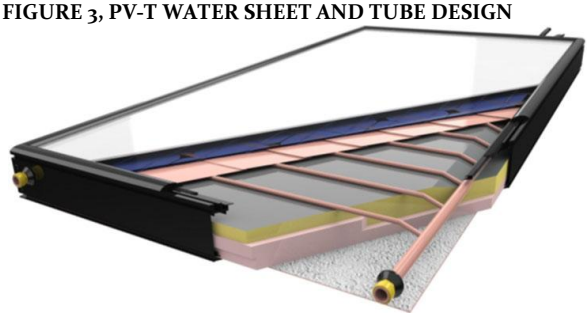

The easiest way to manufacture a PV-T collector is by gluing a photovoltaic solar cell on top of a solar thermal collector. This simple design can be improved by adding a transparent cover (e.g. glass with low

iron content) on top of the solar cell to limit heat losses on the front side of the collector. In addition, an appropriate adhesive is preferred to fix the solar cell onto the solar collector for two reasons; withstand thermal expansion differences of the materials (1), and to ensure effective heat transfer from the solar cell to the absorber (2). Figure 2 illustrates the material stack of a typical PV-T water collector, including TPT (Tedlar-Polyester-Tedlar) and EVA (Ethylene-Vinyl-Acetate) layers for encapsulation of the solar cell to protect it from moister, water and air and provides good electrical insulation (He, et al., 2006). Figure 3[1] also displays a PV-T water sheet and tube collector, where an absorptive sheet is placed at the backside of the solar cells which is connected to tubes to cool the sheet. Furthermore, the absorber is fully insulated and the whole collector is protected via an aluminum casing with a highly transparent front cover.

2.1.2 PV-T DESIGNS

In the past three decades, many different designs for PV-T systems were developed which can be classified in multiple ways. The most straight forward distinction is between the concentrating PV-T collectors and the flat plate PV-T collectors. In this research, only the flat plate collectors are considered. Flat plate PV-T collectors can be classified in PV-T water collectors, PV-T air collectors and PV-T collectors that use a combination of water and air to extract heat from a solar cell.

2.1.2.1 PV-T WATER COLLECTORS

In Figure 4, four typical designs for PV-T water collectors are illustrated; sheet & tube, channel, free flow and a two absorber design. The sheet & tube design is the most basic, where the sheet provides uniform heat transfer, while the absorber tubes subtract the heat from the back side. The absorber tubes can have various shapes, from round to square or rectangular tubes. The channel design consists of a wide channel at the front or backside of the PV-cell where the water flows through. Also an additional glass cover, separated by a thin layer of air, can be used to decrease thermal losses. In the free-flow design, a mixture of air, water and vapor flows through the channel to cool the solar cells. And fourthly, a two absorber design preferably uses a transparent solar cell and subtracts the heat from both the front and the backside of the solar cell (Charalambous, Maidment, Kalogirou, & Yiakoumetti, 2007).

FIGURE 4, FOUR TYPES OF PV-T WATER COLLECTORS; SHEET & TUBE, CHANNEL, FREE FLOW AND TWO ABSORBER

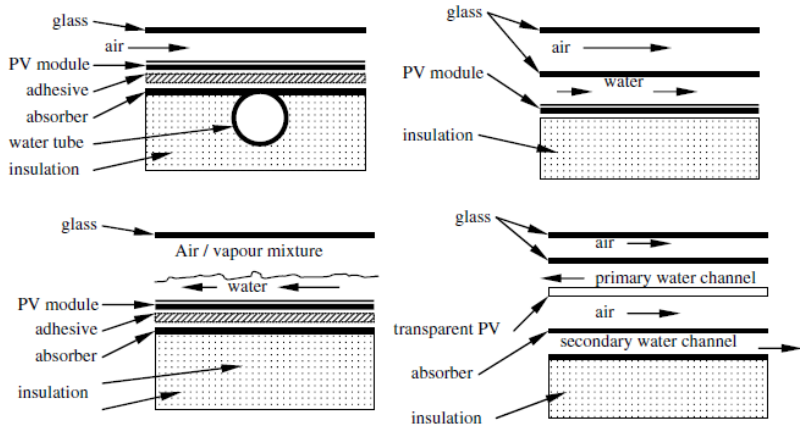

Zondag et al. (2003) simulated nine different PV-T water collectors and calculated their electrical and thermal efficiencies at zero reduced temperature and on an annual basis (see Table 1). Efficiencies are often displayed as a function of the difference between the inlet and the ambient temperature for a specific irradiance$\left(\frac{T_i - T_a}{G}\right)$. At zero reduced temperature ($T_{in} - T_a = 0$) implies that the solar cell is maximal cooled and thus illustrates to optimal efficiency. In Table 1 are the electrical and thermal

[1] *Picture retrieved from: http://www.newformenergy.com/technology/photovoltaic-thermal-pvt*

efficiencies summarized for the nine different collector designs. From the table it becomes clear that there exists a large difference between the efficiencies at zero reduced temperature and annual based efficiencies; approximately 45 and 25% lower for the thermal and electrical efficiencies respectively (Zondag, de Vries, van Helden, van Zolingen, & van Steenhoven, 2003).

TABLE 1, OVERVIEW OF THERMAL AND ELECTRICAL EFFICIENCIES FOR SEVERAL PV-T WATER COLLECTOR TYPES

PV-T water collector type (Zondag, de Vries, van Helden, van Zolingen, & van Steenhoven, 2003)	Thermal Efficiency Zero red.T	Thermal Efficiency Annual	Electrical Efficiency Zero red.T	Electrical Efficiency Annual
PV panel	-	-	0.097	0.072
Sheet and tube PV-T, no cover	0.52	0.24	0.097	0.076
Sheet and tube PV-T, 1 cover	0.58	0.35	0.089	0.066
Sheet and tube PV-T, 2 covers	0.58	0.38	0.081	0.058
PV-T collector with channel above PV	0.65	0.38	0.084	0.061
PV-T collector with channel below opaque PV	0.60	0.35	0.090	0.067
PV-T collector with channel below transp. PV	0.63	0.37	0.090	0.065
Free flow PV-T collector	0.64	0.34	0.086	0.063
Two-absorber PV-T collector (insulated)	0.66	0.39	0.085	0.061
Two-absorber PV-T collector (non insulated)	0.65	0.37	0.084	0.061
Thermal collector	0.83	0.51	-	-

2.1.2.2 PV-T AIR COLLECTORS

Most research articles are devoted to air-cooled PV-T collectors. Similar to PV-T water collectors, air collectors can have the absorber channel placed either in front of or behind the solar cell and can be equipped with or without additional glazing. Furthermore, the heat can also be extracted from both sides of the solar cell simultaneously, with single and double pass collectors. In single pass collectors, the air flows in one direction over both sides of the solar cell, while in double pass collectors the air flows in two opposite direction. For examples of PV-T air collector designs, please see Figure 5. Solar cells can also be integrated in the walls of a building, where different combinations of vent openings enable different ventilating flows for cooling or heating, see Figure 6. This flow can either be buoyant-induced (natural flow) or forced via a pumping system. However, the scope of this study is limited to roof systems (Chow, 2010).

The commercial acceptability of PV-T air collectors mainly depends on their cost-effectiveness and thermal performance. Many studies suggest that the most important parameter to increase the efficiency of PV-T air collectors is the heat transfer rate from the absorber to the airflows. Experimental designs that attempted to increase the heat transfer rate included configurations with additional fins, v-grooved tubes, corrugated absorbers, ceramic granulates and multiple-pass air flow. More details on design optimization and new innovations are explained in the subsequent chapters 2.2.3-2.2.5 (Kumar & Rosen, 2011).

FIGURE 5, TYPICAL PV-T AIR DESIGNS

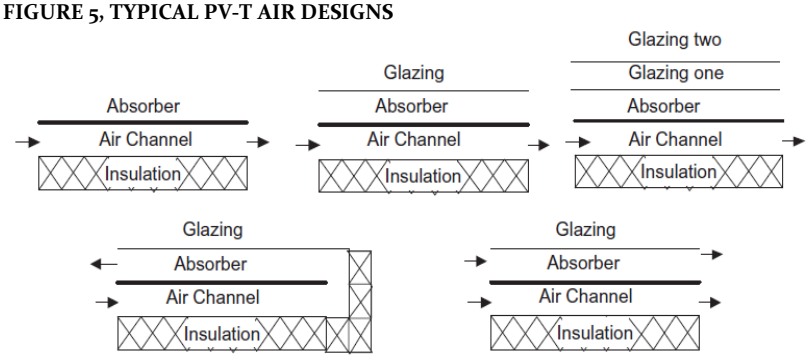

FIGURE 6, VENTILATED PV GLAZING

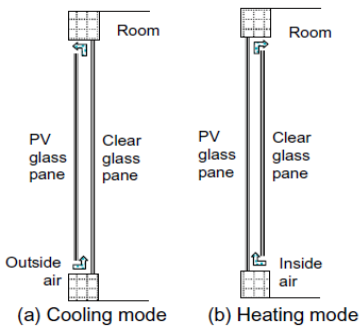

A comparative study of the performance of four PV-T air collectors was conducted by Hegazy (2000) via detailed simulations. The results of the four models can be found in Table 2. According to Hegazy, the single pass PV-T collector (model 3) showed the best performance and required relative little pumping power (Hegazy, 2000).

TABLE 2, THERMAL AND ELECTRICAL EFFICIENCIES OF TYPICAL PV-T AIR COLLECTORS

PV-T air collector types[2] (Hegazy, 2000)	Thermal efficiency	Electrical efficiency
PV-T collector with one channel above PV, (1 cover)	0.46	0.078
PV-T collector with one channel below PV, 1 cover	0.51	0.077
PV-T collector with two channels, single pass (1 cover)	0.56	0.081
PV-T collector with two channels, double pass (1 cover)	0.56	0.0805

2.1.2.3 PV-T BI-FLUID COLLECTORS

A few scientists have also experimented with PV-T bi-fluid collectors, where water and air is used simultaneously to cool the PV-cells. Figure 7 and Figure 8 show the prototype that was developed by Assoa, Menezo, Yezou, Fraisse and Lefebvre (2005). This prototype consists of a metal sheet with an air gap and a water tube at the backside of an insulated absorber. The PV-cells are located between the metal sheet absorbers. The air is either forced or circulated naturally through the gaps. Their simulations show that at a specific mass flow rate and for a certain collector length the thermal efficiency of this collector could reach approximately 80% (Assoa, Menezo, Yezou, Fraisse, & Lefebvre, 2005).

FIGURE 7, PV-T BI-FLUID COLLECTOR

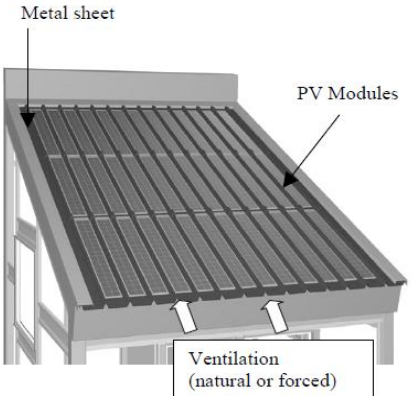

FIGURE 8, CROSS-SECTION OF THE PV-T BI-FLUID COLLECTOR

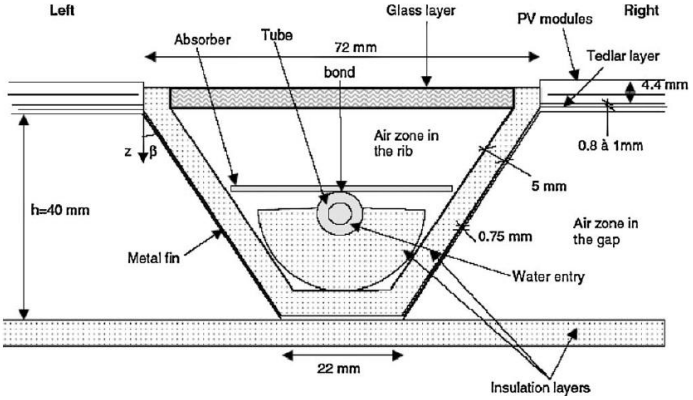

2.1.3 MODULE ASPECTS FOR MANUFACTURING

In 2008, Zondag published an extensive overview of all aspects relevant for flat-plate PV-Thermal collectors and systems. One chapter was completely devoted to manufacturing aspects for PV-T water and PV-T air collectors. This subchapter quickly treats three key aspects that should be taken into account during the design and production of PV-T collectors; thermal efficiency, electrical efficiency and reliability.

The thermal efficiency of the collector depends on various factors. First of all, reflection losses are very important which occur at the top cover, the PV-cell (also functions as absorber) and at the rear contact. PV-T collectors can be designed without a top cover, single glazed and double glazed; the more glazing the higher the thermal yield but the more reflection losses occur that limit the electrical performance. Also the reflection in the PV-cell itself is extremely important. Anti-reflection coatings are valuable to

[2] *Both thermal and electrical efficiencies are given for a mass flow rate of 0.02 and 0.04* $(\frac{kg}{s \cdot m^2})$ *for one and two channels respectively*

limit reflection losses especially for light with energy higher than the bandgap (ultraviolet and visible light), however these coatings are often transparent for light with energy below the bandgap (infrared), which is of particular interest for a PV-T collector. The use of texturing in the top layer and in the rear-contact of the solar cell greatly reduces the reflection of infrared light. The importance of selective coatings and textures is also visualized in Figure 9, which shows the absorption of specific wavelengths in different layers of a PV-T collector (Santbergen & Zolingen, 2006). After the reflection losses have been limited, it is essential to minimize the thermal resistance as much as possible. After the heat is absorbed in the solar cell or directly at the rear-contact, this heat should be conducted from the solar cell or rear-contact to the absorber and subsequently from the absorber to the water or air. Low heat transfer results in high temperature solar cells and thus lower electric and thermal efficiencies. Using thinner layers between the solar cell and the absorber increases the thermal conductivity, but it should not compromise on the electrical insulation. Finally, the whole collector should be well insulated to reduce thermal losses to the surroundings. This can be achieved via a top cover, good insulation of the absorber, air space between the solar cell and the front cover (Zondag H. A., 2008).

FIGURE 9, ABSORPTION IN DIFFERENT LAYERS OF A PV-T ABSORBER WITH TEXTURED C-SI SOLAR CELLS

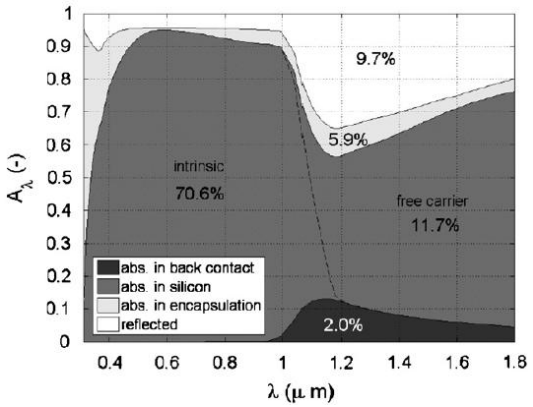

Besides the thermal efficiency, also the electrical efficiency plays an important role for the selection and use of materials. To begin with, which is discussed more in-depth in section 2.2.2, the temperature coefficient of solar cells varies widely; c-Si and a-Si cells have temperature coefficients of -0.45 and -0.20 %/K respectively, which stresses to advantage of a-Si in PV-T collectors. Since the solar cell also functions as the absorber, its absorptive capacity should be high. Another aspect is shading from the edges of the PV-T module onto the solar cell, which can significantly decrease the electrical efficiency and should thus be avoided. In addition, the front cover of PV-T collector is preferably as transparent as possible to maximize the incoming light at the solar cell.

Reliability is another major aspect for PV-T collectors. All materials should be able to withstand the stagnation temperatures of the collector. Stagnation temperature occurs when there is no heat demand and the heat is therefore not drawn from the system, resulting in high temperatures up to 130°C. The stagnation temperature for glazed PV-T collectors is of course much higher than for unglazed collectors. The effect of large temperature differences from the collector fluid and the collector after the pump was turned off appeared to be limited. Lastly, appropriate electrical insulation is required for long lifetime of the PV-T module.

2.1.4 WATER VERSUS AIR.

One of the most critical decisions during the design process of the PV-T collector for the Nanosol project is the use of water or air for the heat extraction process. In the upcoming sections, extensive modeling was performed on several water- and air-cooled prototypes, but this chapter quickly compares

the properties, advantages and disadvantages of water and air in PV-T collectors on a qualitative manner.

Table 3 demonstrates the different values of water and air that are essential in for heat transfer; heat capacity, conductivity and density. The heat capacity of water is approximately four times larger than air, and its thermal conductivity almost 20 times larger. For air, this means that it requires more volume to store the same amount of energy as water and it takes longer time before it reaches the same temperature. However, water weighs about 1000 times more than air and therefore the air can have much higher flow rates, enabling the air to compensate for its low heat capacity and conductivity. The next table (Table 4) provides qualitative considerations of the use of water and air in PV-T collectors. The lower heat capacity and conductivity of air compared to water demonstrates that heat transfer in air collectors is much more critical than in water collectors.

TABLE 3, PROPERTIES OF WATER AND AIR (SEE APPENDIX A FOR TEMPERATURE DEPENDENT PROPERTIES)

Properties at 25°C (Twidell & Weir, 2006)	Water	Air	Unit
Specific Heat Capacity	4.184	1.010	kJ/kgK
Thermal Conductivity	0.650	0.029	W/mK
Density	983.20	1.06	Kg/m^3

The flow rates of air collectors are therefore much larger than the flow rates in water collectors. PV-T water collectors have a flow rate of approximately 50 $\frac{L}{m^2h}$, or 0.014 $\frac{L}{m^2s}$. To obtain the same heat transfer, air collectors should use flow rates of 175 $\frac{m^3}{m^2h}$, or 48.6 $\frac{L}{m^2s}$, however for practical reasons flow rates of 40 $\frac{m^3}{m^2h}$ are used, or 11.1 $\frac{L}{m^2s}$ (Zondag H. A., 2008).

TABLE 4, ADVANTAGES AND DISADVANTAGES OF THE USE OF WATER AND AIR IN PV-T COLLECTORS

	Water	Air
Advantages	• High energy capacity • Good conductivity • Easy/economic to pump • Thermal efficiency of ± 60% • Cheap and safe	• Light weight • Easy to manufacture • Less damage in case of leakage • Thermal efficiency of ± 50% • Cheap and safe
Disadvantages	• Phase changes (is fixed with glycol) • Heavy weight	• Low energy capacity • Low conductivity • Less applications (mainly for drying) • Additional heat exchanger required

2.1.5 NEW INNOVATIONS AVAILABLE

Since 1990, many scientists have experimented with innovative concepts to increase the performance of PV-T systems, mainly in terms of thermal output. This chapter includes a selection of designs that have been developed during the past few decades.

For example, Tripanagnostopoulos, Nousia, Souliotis and Yianoulis (2002) equipped a PV-T system with an additional diffuse collector to improve its performance (see Figure 10). The reflectors were placed in between two rows of PV-T modules to reflect extra sunlight onto the PV-T modules and resulted in a concentration factor of $1 \leq C \leq 1.5$. At a concentration factor of 1.35, the reflector increased the electrical output by 16% and also the thermal output was greatly increased.

FIGURE 10, A PV-T ARRAY WITH ADDITIONAL DIFFUSE REFLECTORS TO BOOST THE PERFORMANCE

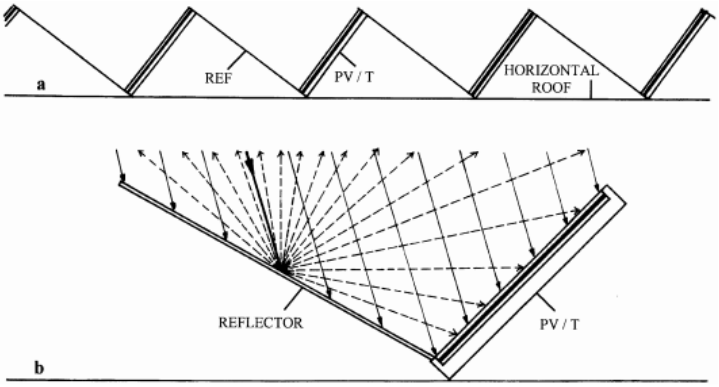

Ibrahim et al. (2009), simulated seven different absorber collector designs, among others configurations with square or rectangular and round hollow tubes. The best results were obtained for the spiral flow design (see Figure 11), with a thermal efficiency of over 50% and a cell efficiency of almost 12% (Ibrahim, et al., 2009). Furthermore, Sandnes and Rekstad (2002) performed both theoretical and experimental analyses on an innovative PV-T collector design. The absorber collector, located behind a single crystalline photovoltaic solar cell, was made from square polymer tubes with black surfaces, see Figure 12). The internal and wall-to-wall channels are filled with ceramic granulates. As the water fills up the vacant space in between the granulates, the granulates are brought in contact with the top absorber sheet, enabling efficient heat transfer and a thermal efficiency of approximately 60% (Sandnes & Rekstad, 2002).

FIGURE 11, SPIRAL FLOW DESIGN ABSORBER

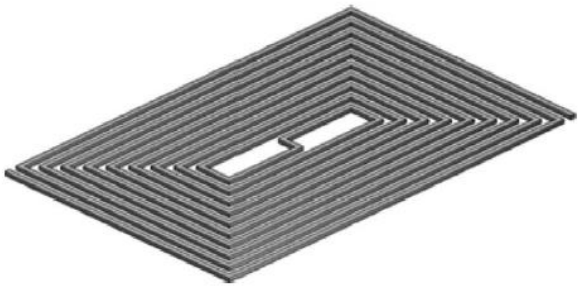

FIGURE 12, PV-T SYSTEM WITH CERAMIC GRANULATES

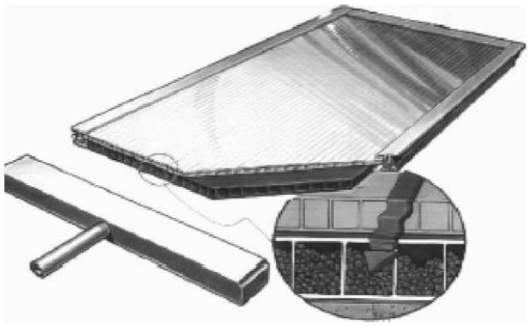

Another way to improve the heat transfer process is to increase the effective surface that can be brought in contact with the working fluid. For this reason, Alfegi, Sopian, Othman and Yatim developed several PV-T air collectors with additional fins at the backside of the absorber collector, of which one is illustrated in Figure 13. The fins enabled an increase in total efficiency from 49.1 to 62.8 percent (Alfegi, Sopian, Othman, & Yatim, 2008). In Figure 14, a PV-T air collector is displayed with V-groves to increase the absorber surface and thus the heat transfer process (Othman, Sopian, Yatim, & Daud, 2006).

FIGURE 13, PV-T AIR COLLECTOR WITH FINS

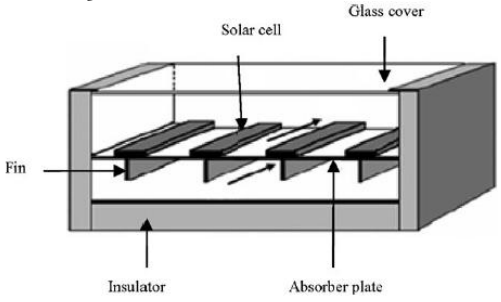

FIGURE 14, PV-T AIR COLLECTOR WITH V-GROVES

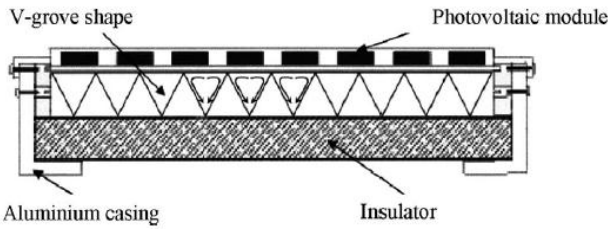

2.1.6 COMMERCIAL AVAILABLE PV-T SYSTEMS

Via a quick internet search, it became clear that the market for PV-T systems is still in its development phase. Only little PV-T modules are currently commercially available, of which most systems are water-cooled and a few air cooled. This is quite remarkable since most research was conducted on air-cooled prototypes. The amount of available PV-T systems is expected to increase in the near future as the prices for photovoltaic modules will drop further. A summary of the commercial products available is provided in Table 5 below.

TABLE 5, OVERVIEW OF COMMERCIALLY AVAILABLE PV-T SYSTEMS AND THEIR SPECIFICATIONS

Manu-facturer	Modules	PV-cell	Air/ Water cooled	Length/ Width [m]	Typ. Flow [L/m²/h]	Elect. P. [Wp/m²]	Thermal Power [Wp/m²]	Price [€/mod.]
AnafSolar	H-NRG[3]	pc-Si	Water	1.65 / 1.00	43.6	140	500	n.a.
Everlight	EL-54/6P[4]	pc-Si	Water	1.48 / 0.99	40.5	190	500	n.a.
Fototherm	FT250AL[5]	mc-Si	Water	1.66 / 0.99	72.3	150	550	526
Millennium Electric	MSS MIL 250W[6]	mc-Si	Water & Air	1.65 / 0.99	n.a.	153	700	n.a.
Solar Wall	Solar Duct[7]	n.a.	Air	18.00 / 1.00	73000	100	400	n.a.
Solimpeks	Power Therm[8]	mc-Si	Water	1.64 / 0.87	45.5	190	440	800
SunWin	AF24US4[9]	pc-Si	Water	2.06 / 1.15	n.a.	n.a.	607	n.a.
Tes Solar	TESZEUS[10]	mc-Si	Water	1.65 / 0.99	n.a.	168	640	n.a.

From Table 5, several important observations can be made. The typical flow rate of water cooled PV-T collectors is in the range of 40 to 50 liters per m² per hour. Furthermore, most PV-T systems use a poly- or mono-crystalline solar cell as absorber plate with a module efficiency (electric) ranging from 10 to 19%. The thermal efficiencies vary between 40 and 70%. Prices were only found for the PV-T panel from Fototherm and Solimpeks, of which Solimpeks provided the most complete data. Still, the specifications of both Solimpeks and Fototherm modules provide us with a good estimate of the values we could aim for in project Nanosol. Taking into account a module price of € 800 and a size of 1.427 m² ($= 1.64m \cdot 0.87m$), the module costs € 569.70 per m². Under standard test conditions (1000 W/m² and 25°C) this module has an electrical and thermal power output of 190Wp/m² and 440Wp/m² respectively, which results in a total power output of 630 Wp/m². The latter results in a price of 0.90 €/Wp ($= \frac{596.70\ €}{630\ Wp}$) for the Solimpeks module. For the Fototherm module this results in a price of 0.45 €/Wp.

2.1.7 TEST STANDARDS

In the PV-T market, standard methods to test the performance and reliability of PV-T modules do not exist. Development of international standards forms an important step in order to promote PV-T systems in the commercial market. PV-T tests can be performed outdoor and indoor. Outdoor testing provides more realistic performances but requires longer measurement times. Indoor testing on the other hand allows for quick and repeatable results, but standards are still lacking (Chow, 2010).

Also for the analysis of the effects of different materials, constructions and geometrics in PV-T systems, accurate and appropriate testing is required. Dupeyrat, Helmers, Fortuin and Kramer from the Fraunhofer Institute for Solar Energy Systems in Freiburg, Germany, conducted a detailed study to test

[3] Retrieved from: http://www.anafsolar.eu/eng/download/anafsolar_HNRGY.pdf
[4] Retrieved from: http://www.everlight-solar.com/home/downloads/datasheets/pv/EL-54-6P.pdf
[5] Retrieved from: http://www.fototherm.com/images/certificazioni/seriecs/scheda_tecnicafototherm-cs.pdf
[6] Retrieved from: http://www.millenniumsolar.com/files/Products/Mil-PVT-250w-M-02-Data-sheet.pdf
[7] Retrieved from: http://solarwall.com/media/download_gallery/SolarWallPVT_Sellsheet.pdf
[8] Retrieved from: http://www.solimpeks.com/wp-content/uploads/2012/12/Volther-Datasheet.pdf
[9] Retrieved from: http://www.sunwin-energy.com/uploads/media/datasheet_AF24US4_EN_2013-02.pdf
[10] Retrieved from: http://www.tessolarwater.com/docs/TEZEUS_brochure.pdf

the performance of flat-plate and concentrating PV-T collectors; of which the first is relevant for this study. By combining the standards for solar thermal collectors (EN 12975-2) and for photovoltaic modules (IEC 61215) they developed a test procedure to accurately measure the thermal and electrical performances of PV-T systems (Dupeyrat, Helmers, Fortuin, & Kramer, 2011).

They measured the performance of two PV-T systems in two steps, first in 'thermal only' mode and second in 'hybrid' mode. This allows for a good comparison with conventional 'thermal only' collectors and with other PV-T collectors. There is no need for 'electrical only' measurements because this performance is comparable to operation in 'hybrid' mode at stagnation temperature. The electrical performance depends on ambient conditions, integration in the PV-T system and on the operation modes, therefore 'electrical only' mode could provide misleading results. In addition, PV-T systems will practically never operate in 'electrical only' mode. The two mode testing method proved to provide accurate and realistic results (Dupeyrat, Helmers, Fortuin, & Kramer, 2011).

2.1.8 Energy demand of commercial offices

The commercial PV-T systems that are summarized in the previous chapter were mainly intended for the residential sector. The Nanosol aims to develop a PV-T system that could enable the energy demand of a commercial office. Table 6 illustrates the energy demand of a typical office in the Netherlands, divided over its functions (Senternovum, 2008). The annual gas and electricity demand accounted for 146.1 and 197.8 kWh/m² respectively, of which the gas usage is for 95 percent explained by the demand for space heating. The electricity is primarily used for lightning, ICT equipment and cooling. PV-T systems have a great potential in partly or completely fulfilling these needs.

TABLE 6, ENERGY DEMAND OF A TYPICAL COMMERCIAL OFFICE, DIVIDED OVER ITS FUNCTIONS

	Office [MJ/m²]	**Gas [MJ/m²]**	**Share [%]**	**Electricity [MJ/m²]**	**Share [%]**
Space Heating	500	500	95.1		
Cooling	70			70	9.8
Hot tapwater	6	6	1.1		0.0
Humidification	2			2	0.3
Other	25	5	1.0	20	2.8
Catering	50	15	2.9	35	4.9
ICT-central	150			150	21.1
ICT-decentral	90			90	12.6
Pumps	15			15	2.1
Product preparation	0				0.0
Product cooling	0				0.0
Transport	15			15	2.1
Ventilation	40			40	5.6
Lighting inside	260			260	36.5
Lighting outside	10			10	1.4
Lighting Emergency	5			5	0.7
Total	**1238**	**526**	**MJ/m²**	**712**	**MJ/m²**
		146.1	**kWh/m²**	**197.8**	**kWh/m²**
		15.0	**m3 gas/m²**		

However, the values above only represent the total annual demands. PV-T systems are completely dependent on the solar irradiance for producing electricity and heat. Figure 15 Illustrates the solar irradiance (in Wh/m²) on an hourly basis in Deelen (nearest weather station to Arnhem) in 2012 (KNMI, 2013). It can be observed that by far the most solar energy is available during and around the summer months. For this reason, the electrical and thermal yield of PV-T systems is highest during summer and lowest during the winter.

On the contrary, Figure 16[11] and Figure 17[12] show the heat, cold and electricity demands of a typical commercial office on an hourly basis (VREG, 2012). What immediately becomes clear from these figures is that the demand for heat and electricity is highest during the winter and lowest during the summer, the exact opposite pattern of the solar irradiance. Only the pattern of the cooling demand, quite logical, matches the irradiance pattern. Note that in all graphs the energy yield and demands are given per square meter of office area. From the figures above two aspects become clear that are important for the development of the PV-T system; the electrical and thermal yield should be as high as possible (1) and seasonal storage is required to satisfy the annual energy needs (2).

FIGURE 15, SOLAR IRRADIANCE, DEELEN 2012

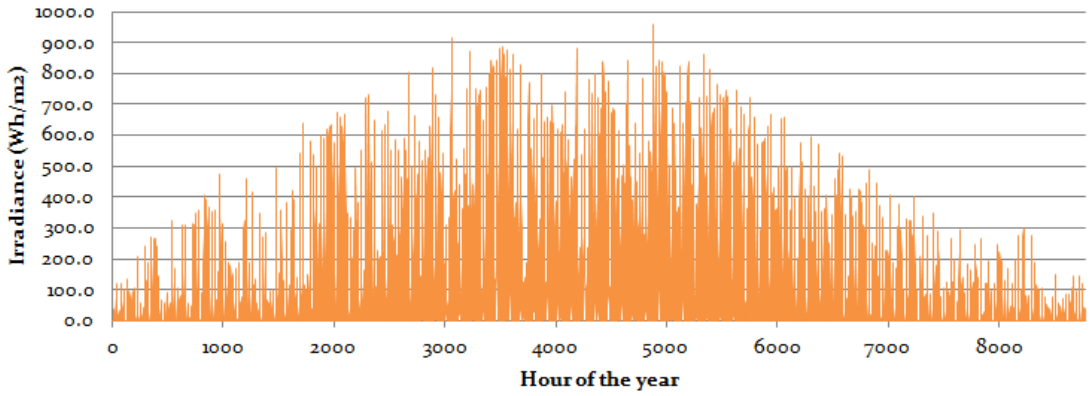

FIGURE 16, HEAT AND COLD DEMAND OF A TYPICAL COMMERCIAL OFFICE IN THE NETHERLANDS

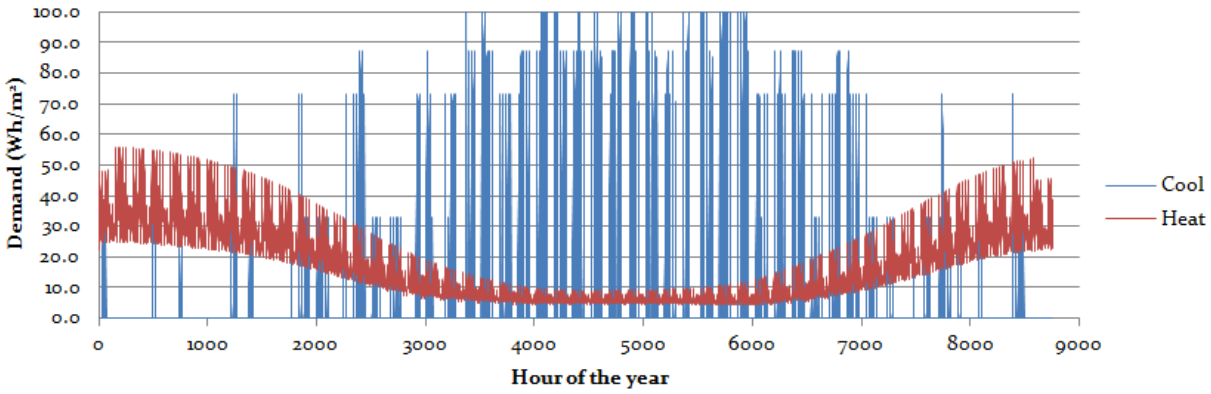

FIGURE 17, ELECTRICTY DEMAND OF A TYPICAL COMMERCIAL OFFICE (<56KVA)

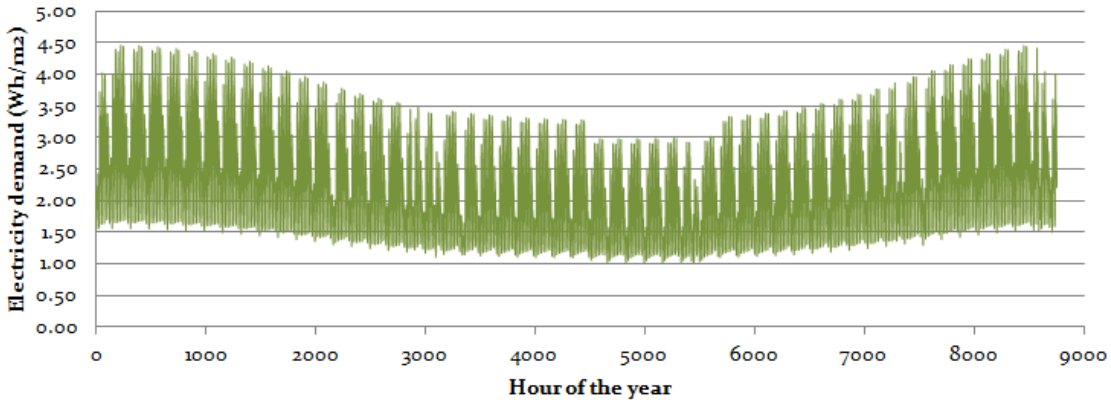

[11] *The heat demand is based on typical user profiles from VREG for commercial users (>0.15GW), the cold demand is constructed from data retrieved from DNV KEMA. The heat demand is corrected via the values from Table 6.*
[12] *The electricity demand is based on typical user profiles from VREG for commercial users (<56kVA)*

The figures above not only show the seasonal variations, but also the daily and weekly variations in the energy demands can be observed. In the weekends most companies are closed and therefore their energy demand is low. If the x-axis would only show 24 hours, a clear daily pattern would become visible between 8.00 and 18.00, when most activities take place.

2.1.9 PV-T APPLICATIONS

In general, solar thermal systems are in principal used for preheating of tap-water in the residential sector or for swimming pools (Chow, 2010). However, in commercial offices, tap-water represents only a fraction of the total energy requirement of an office. As was explained in section 2.1.8, by far the largest energy demand in commercial offices is for space heating and cooling and for electricity to run their equipment. In order to meet these energy demands of offices in the Netherlands, smart combinations of systems are required. Three combinations of systems that are thought of in the Nanosol project are very briefly described below.

2.1.9.1 HEAT PUMP

Heat pumps usually run on electricity and are used to upgrade a certain heat flow by subtracting additional heat from its surroundings. For this reason, its efficiency exceeds 100 percent and therefore its performance is usually given as a Coefficient of Performance (COP). A heat pump with a COP factor of 3 implies that the heat pump delivers 3 units of heat (e.g. 3 $kW_{thermal}$) for each unit of electrical input (1 $kW_{electrical}$). In doing so, the heat pump also subtracts two units of heat (2 $kW_{thermal}$) from its surroundings. For this reason, heat pumps always consist of a split system of which one part is placed inside the building and the other outside of the building. Via this principle, a heat pump could be used in combination with a PV-T system; the heat of the PV-T systems could be upgraded to a higher value ($3kW_{thermal}$) and simultaneously cooling the building (2 $kW_{thermal}$). The upgraded heat can either be utilized or could be disposed of (Bakker, Zondag, Elswijk, Strootman, & Jong, 2005) (Fang, Hu, & Liu, 2010).

2.1.9.2 HEAT PUMP WITH ATES

An expensive but very effective system is the combination of a heat pump with Aquifer Thermal Energy Storage (ATES). In this system, the heat pump exchanges heat from the inside of a building with two large storages (a cold and a hot storage) below the ground. During summer, heat from inside the building is pumped and stored into the ground (charging the warm aquifer) while the cold aquifer is uncharged and thus cooling the building. In the winter, the stored heat is used for heating of the building and simultaneously the cold source is recharged again. A drawback of this system however, is the fact that in general more heat is subtracted from the ground than is replaced again, resulting in an unbalanced system. A PV-T system could perfectly be combined with this system to replenish the hot source of aquifer thermal energy storage.

2.1.9.2 SOLAR COOLING

A third option is utilizing the heat of the PV-T in combination with an absorption chiller to cool the building. Commercially available absorption chillers use input water of approximately 85 degrees Celsius to vaporize Ammonia and normally have COP factors between 0.7 and 1.2. In this way, the Ammonia cools down another stream of water potentially even below its freezing point so it can be used to cool the building. However, the PV-T system will not be able to provide water of 85°C. In order to overcome the temperature gap between the PV-T outlet and the absorption chiller inlet, an additional heat pump as described above could be an option to upgrade the heat. Besides the upgraded heat to drive the absorption chiller, the heat pump also delivers a cold flow that can be used to cool the building. Recently, Solabcool introduced a new absorption chiller. Instead of Ammonia, this new absorption chiller uses Silica gel as its working fluid, allowing for lower input temperatures. The system is preferably operated at temperatures of 70°C, but it should already be able to function at temperatures of

55-60°C. PV-T in combination with an absorption chiller could be an interesting option when direct utilization is cheaper than seasonal storage.

2.1.10 FUTURE ROAD MAP

In a paper that was presented at the 20th European Photovoltaic Solar Energy Conference in Spain in 2005, ECN proposed a roadmap for the development and market introduction of PV-T technology. ECN demonstrated that until 2005, the work on PV-T was mainly focused on technical issues; efficiency optimization and system design. For this reason ECN suggested to focus on other non-technical issues as well; marketing, building integration, financing, testing guidelines and training and education. For an overview of the issues and requested actions, please see Table 7 below (ECN, 2005).

TABLE 7, PV-T ROADMAP - ISSUES AND ACTIONS (ECN, 2005)

PV-T Roadmap	Priority actions
Technical	• Stagnation temperature resistant materials for encapsulation • Minimization of reflection losses over entire solar spectrum • Optimize heat transfer from solar cell to collector fluid
Marketing	• Detailed market studies; PV-T market • Drivers and barriers for PV-T applications
Building integration	• Plug-and-play methods to integrate PV-T in buildings • Plug-and-play methods for combinations of PV-T and PV • Map demand for aesthetics of PV-T for architects and end users • Integration of parties; R&D, engineering, manufacturers, installers. • Plug-and-play components to integrate PV-T into space and tap water heating • Develop high temperature resistant electrical connections • Develop optimized for PV-T in combinations with heat pumps and for concentrator PV-T and solar cooling • Standardization issues; manufacturers, research and testing institutes • Develop standardized testing of performance and reliability • Gain experience via field tests
Financing	• Development of low-cost finance schemes
Subsidy	• Decide for which subsidies is PV-T eligible; e.g. combined with PV
Training & Education	• Demonstration projects to show performance and potential of PV-T • Develop tools for engineers and installers for reliable PV-T systems • Training of installers in PV-T installation

2.2 THERMAL ANNEALING

Temperature affects the performance of solar cells in two opposite ways. On the one hand, during the solar cell operation, increased temperature directly hampers its electrical performance. On the other hand however, after longer periods of elevated temperatures, the electrical performance is improved due to thermal annealing. This chapter is mainly focused on the latter effect, why it occurs and how this effect influences the solar cell performance. The effect of thermal annealing could be interesting for combined PV-T systems, as it might occur during stagnation temperatures. Or it might not occur anymore because the solar cell is actively cooled. A better understanding of this effect is therefore important.

2.2.1 AMORPHOUS SILICON

Silicon is a group 14 element with four of its electrons located in the valence shell (shell structure; 2, 8, 4), which means that it can bond with four other elements i.e. silicon or hydrogen atoms. Silicon crystal

lattices, depending on the preparation conditions, are structured in different manners, ranging from perfectly ordered crystalline silicon (c-Si), to micro crystalline (µc-Si) to completely disordered amorphous silicon (a-Si), see Figure 18[13] below. In the case of amorphous silicon, the disordered structure disables some silicon atoms to make four bonds and leaves one valence electron left vacant. The idle valence electron is called a dangling bond and is regarded as a defect, which hampers the electrical conductivity of the material. By introducing hydrogen into the preparation process, called passivation, hydrogen atoms can fill up the dangling bonds and significantly reduce the amount of defects (Peercy, 1981).

FIGURE 18, DIFFERENT SILICON STRUCTURES; CRYSTALLINE, MICRO-CRYSTALLINE AND AMORPHOUS

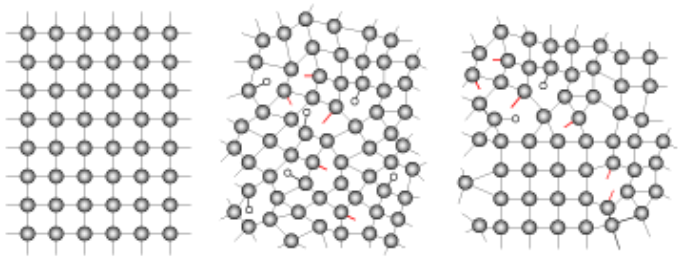

2.2.2 TEMPERATURE COEFFICIENT

A common value that is often provided on technical data sheets of solar cells is the temperature coefficient. This value displays in what extent the electrical performance is influenced as a function of solar cell temperature. Polycrystalline and amorphous Silicon have temperatures coefficients of -0.45 and -0.20 $\%K^{-1}$ respectively (Schott-Solar, 2013a) (Schott-Solar, 2013b). This implies that the electrical performance of amorphous Silicon solar cells is much less affected by an increase in temperature compared to poly crystalline solar cells, see also Figure 19. These values apply for solar cells in operation. In summer, solar cell temperatures can reach up to 50-60 degrees Celsius.

FIGURE 19, MODULES EFFICIENCY VERSUS TEMPERATURE

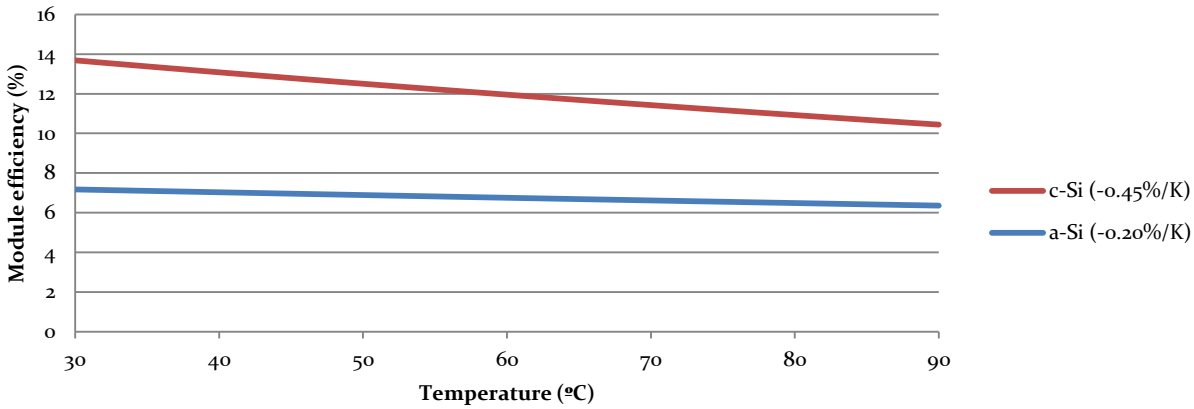

2.2.3 STAEBLER WRONSKI EFFECT

Another effect that occurs during solar cell operation is the Staebler Wronski effect. D. Staebler and C Wronski found that the structure of amorphous Silicon deteriorates after exposure to long periods of intense light. This degradation results in an increase in the amount of dangling bonds in the structure which in turn leads to more recombination in the solar cell. Dangling bonds or gap states are 'unoccupied' valence electrons. When photons provoke electron-hole pairs to be separated within the

[13] Picture retrieved from: *http://www.energyresearch.nl/energieopties/zonnecellen/achtergrond/typen/dunne-lagen/*

Silicon layer, the liberated electron has a change of being bonded to such an unoccupied valence electron, which is known as recombination. Electrons that are recombined within the solar cell are not able to contribute towards an external load. Thus, degradation of the solar cell, also referred to as the Staebler Wronski effect, leads to shorter electron lifetimes and thus diminishing electrical performance (Dersch, Stuke, & Beichler, 1981).

However, in their study, Staebler and Wronski (1977) also discovered this process to be reversible when heat was applied to the amorphous Silicon. Heating the Silicon structure enables it to stabilize again which reduces the amount of dangling bonds in the material; this process is called thermal annealing. Moreover, Staebler and Wronski found that heating up the amorphous Silicon up to 150 degrees Celsius was sufficient to regain its initial electrical conductivity (Staebler & Wronski, 1977).

2.2.4 SEASONAL THERMAL ANNEALING

Thermal annealing effects are also observed in several studies to the variations in outdoor performances of amorphous Silicon modules. For example, King, Kratochvil and Boyson (2000) obtained data from outdoor testing of multiple commercial modules in Albuquerque, New Mexico. Figure 20 present the results of two modules over three years, which clearly show a shark teeth trend of the normalized power output over time. During the summer months the performance of the modules was improved automatically. They suggest this effect to be a result of two effects; namely the seasonal variations in the solar spectrum and from the thermal annealing effect (King, Kratochvil, & Boyson, 2000).

However, a study from Merten and Andreu (1998) suggest that the improved performance of a-Si solar modules was mainly caused by effects in the spectral response and that the effect of thermal annealing is negligible (Merten & Andreu, 1998).

FIGURE 20, SEASONAL THERMAL ANNEALING OF TWO TANDEM-JUNCTION A-SI MODULES

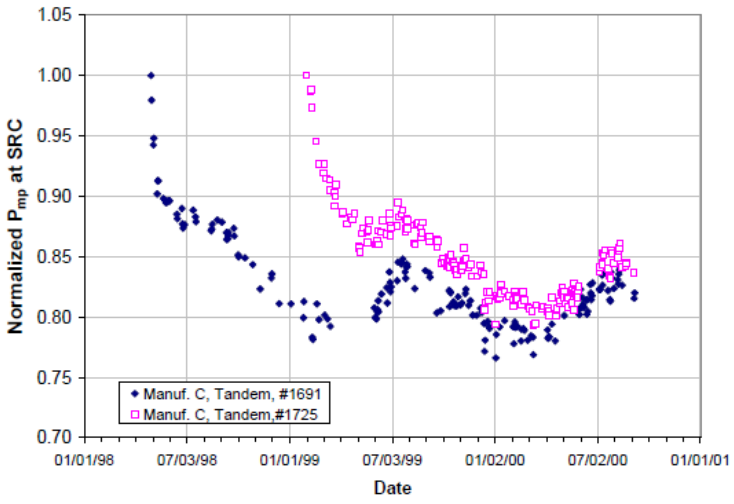

More recent studies provide clarity on the contributions of the two effects that cause the improved performance of the amorphous Silicon solar cells. For example, Virtuani & Fanni (2012) examined the different contributions that lead the variations in the power production and they also distinguished between spectral variations and Staebler-Wronski Effects. According to their findings these effects accounted for 10.5% and 8% respectively, which are in good agreement with the findings of King, Kratochvil and Boyson (Virtuani & Fanni, 2012). In addition, Ishii, Otani, Takshima and Ikeda (2013) presented comparable results. For hydrogenated amorphous Silicon modules (a-Si:H) they observed a decrease of 20% in the performance as a result from increased degradation. After exposed to high temperature conditions the modules showed an improvement in the performance again of approximately 4-6%. From the latter they also assume that the effects of seasonal thermal annealing and

light soaking contribute 4-6% towards the performance improvements. Similar to Virtuany & Fanni, they also detected a performance enhancement of 10% due to the variations in the solar spectrum (Ishii, Otani, Takashima, & Ikeda, 2013). From these two studies, the effect of seasonal thermal annealing is expected to contribute between 4% and 8% to the improved performance of amorphous Silicon solar cells.

Another interesting article from Pathak, Girotra, Harrison and Pearce (2012) examined the effect of different temperatures (25°C, 50°C and 90°C) on the performance of a-Si:H solar cells with different layer thicknesses to find optimal operating temperatures in photovoltaic-thermal (PV-T) systems. As shown above, amorphous Silicon solar cells are little influenced by increased operating temperatures, and they have an additional gain from the effect of thermal annealing. The main finding of their investigation was that relative thick Silicon layers (± 840 nm) displayed the highest increase in power output when operated at 90°C (Pathak, Girotra, Harrison, & Pearce, 2012).

SECTION 3: METHODOLOGY

The methodology section is divided in two chapters. The first chapter introduces the two prototypes that are compared in this study and the numerical simulations are explained in detail. The two prototypes were simulated with both air and water as their working fluids, resulting in four models in total. Also a reference scenario is modeled which only considers the PV module from Hyet Solar. In addition, these models are simulated under standard test conditions (STC) and under real climate conditions (RCC). In the second chapter, the thermal annealing experiment and its required equipment is described.

3.1 MODELING PV-T DESIGNS

This section starts with the introduction of the two prototypes that were simulated which enable to cool the thin-film solar cell with air or water. Also the reference case is quickly described. After that, the principles behind the numerical simulations are explained in detail by formulating and solving the heat balances. The next chapter describes the heat transfer coefficients that are required to calculate the solved heat balances; convection, radiation and conduction. Also the formulas are given that are used to calculate the key performance indicators such as the final electrical and thermal efficiencies, which allow for a good comparison of the different models. The section ends with the two conditions under which these models are simulated; standard test conditions (STC) and real climate conditions (RCC).

3.1.1 TWO PV-T DESIGNS AND THE REFERENCE

Hyet Solar produces thin-film amorphous Silicon solar cells (total thickness of the laminate < 0.5 mm!) with electrical efficiencies of approximately 10 percent (Figure 21). These cheap, light weight (~600 grams/m^2) and flexible solar cell are very well suited to cover large flat roofs of commercial offices. The amorphous Silicon has the advantage to operate at higher temperatures without compromising much on its electrical efficiency. But of course, cooling the modules also increases the electrical performance.

FIGURE 21, HYET SOLAR MODULES

FIGURE 22, NANOTEXTURES

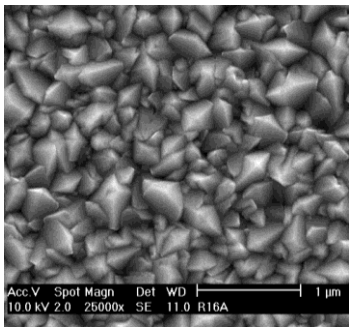

FIGURE 23, INTERNAL REFLECTION

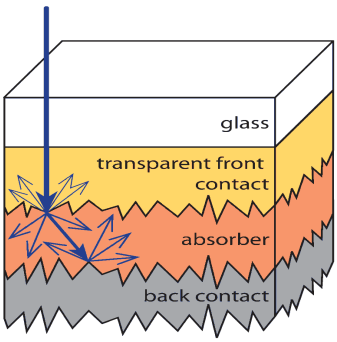

The Hyet Solar modules have been optimized with nanotextures, see Figure 22. The pyramid shaped textures have an anti-reflective effect because they increase the internal reflection of incoming light (Figure 23). In addition, the modules have improved heat transfer features to effectively conduct the heat towards the backside of the module.

For the reasons mentioned above, the Hyet Solar module is an excellent solar cell and absorber for the development of a PV-T system for commercial offices with large flat roofs. Based on the literature and expert knowledge, the partners of the Nanosol project agreed to simulate two models; Prototype 1 where the solar module is cooled from both the front- and the backside simultaneously, and Prototype 2 where

the solar module is only cooled from the backside. Figure 24 and Figure 25 illustrate 3 dimensional images of prototype 1 (P1) and prototype 2 (P2).

FIGURE 24, PROTOTYPE 1 (P1); THE SOLAR CELL IS COOLED FROM BOTH THE FRONT- AND BACKSIDE

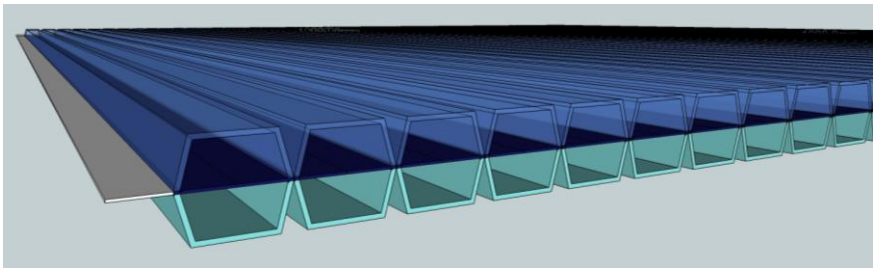

FIGURE 25, PROTOTYPE 2 (P2); THE SOLAR CELL IS COOLED FROM THE BACKSIDE ONLY

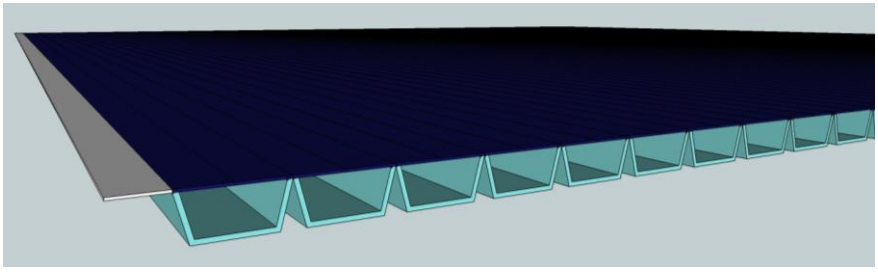

The simulation of these two prototypes would clarify two essential factors for the Nanosol project. On the one hand it shows which design is preferred and what the expected annual yields are, and on the other hand it helps with the decision to use air or water as the working fluid. It is expected that the electrical performance of prototype 1 will be lower than prototype 2 due to optical losses, but the thermal efficiency should be higher. The trapezoidal shape of the tubes could be laminated on top of the Hyet Solar module and enables air or water to flow over the surfaces of the module. To limit the optical losses on the front side, the tubes should be optically transparent. On the back side on the other hand, the tubes do not need to be transparent, allowing for thicker, non transparent and better insulated tubes. The shapes of the tubes can of course be altered to for example circular tubes, but for practical reasons the rectangular shaped tubes are chosen.

FIGURE 26, CROSS-SECTIONS OF THE TWO PROTOTYPES WITH AIR AND WATER, INCLUDING DIMENSIONS

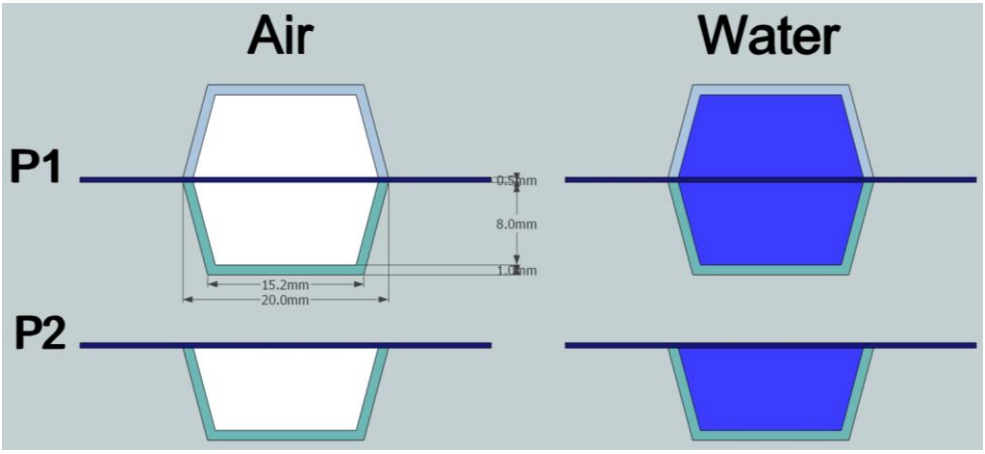

Figure 26 displays the cross-sections of Prototype 1 and Prototype 2 with both air and water as working fluids. Also the dimensions are provided; the solar cell thickness (0.5 mm), tube foil thickness (1.0 mm), tube width (20.0 mm) and tube depth (9.0 mm). With these dimensions, and taking into account one

centimeter at each side of the solar module for the connectors, a total of 49 tubes could fit next to each other per meter width of solar module.

3.1.2 HEAT BALANCES

The model described below is primarily based on the model that was proposed by Hegazy (2000) for the simulation of four air-cooled collectors (Hegazy, 2000). In this study, that model is extended to also simulate the water-cooled designs. At some points the model was somewhat simplified, at other points it has been improved. This section describes how the temperatures are calculated based on the heat balances approach and the next section explains in detail how the heat transfer coefficients are defined. Excel was used to perform the numerical simulations.

Looking closely to the cross-sections of the prototypes, it can be observed that prototype 1 consists of five layers (foil, air/water gap, solar cell, air/water gap, foil) and prototype 2 of three layers (solar cell, air/water gap, foil). Figure 27 visualizes the five layers of prototype 1 and the associated heat flows based on the three heat transfer mechanisms; radiation, convection and conduction. The temperature of each individual layer can be approached by solving the heat balance ($Energy\ in\ =\ Energy\ out$). However, the temperatures of the layers are dependent on the heat transfer coefficients, which in turn are dependent on the temperature. To cope with this problem, an iteration process is required to accurately estimate the final temperature of each layer, depending on the other temperatures and heat transfer coefficients. To start the iteration process, first an estimate is made of the temperatures of each layer. These temperatures are used to calculate the heat transfer coefficients, which in turn enable to estimate more accurate temperatures. Between 50 and 100 iterations are sufficient to estimate the final temperatures[14]. After the iteration process is completed, the results represent the temperatures of the system in a steady state. The latter is accurate enough since hourly data will be used to calculate the annual yields of the system in the Dutch climate. Via the heat balance approach, the air or water flow in one particular tube can be precisely calculated. To obtain the yields per square meter, the values are multiplied by the number of tubes and divided by length of the tube.

FIGURE 27, HEAT BALANCES OF PROTOTYPE 1

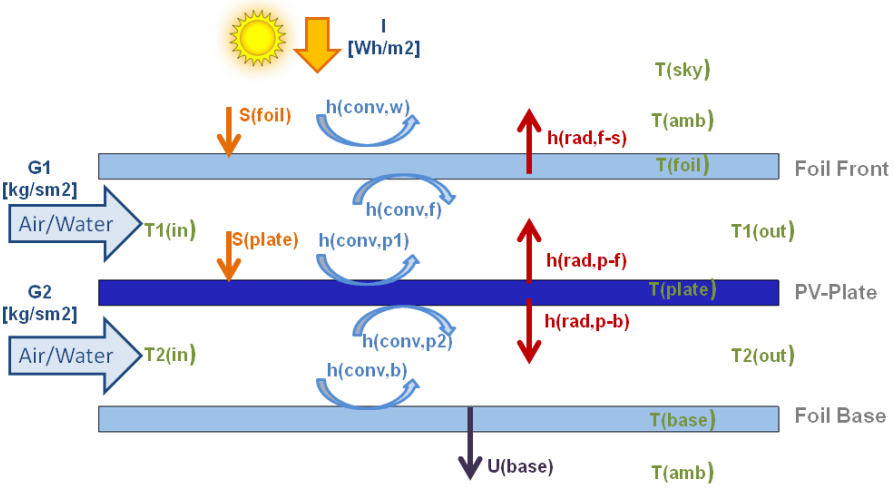

Table 8 shows the heat balances for each layer. The left hand sides of the equations contain the input energy flows, while the right hand side represents the output energy flows. Table 9 displays the same equations but then solved to the temperatures of interest. Note that each layer depends on the heat transfer coefficients and on the temperatures of the neighboring layers. Also the solar irradiance and the

[14] *This process can be automated in excel via 'Excel options' (see start menu), 'Formulas' and 'Enable iterative calculations'*

two air or water flows play an important role. Finally, the output temperatures of the fluid can be calculated via the flow temperatures and the inlet temperatures, see Table 10. An overview of the definitions of the constants, variables and subscripts can be found at the beginning of this thesis, under *'List of constants and variables'*.

TABLE 8, HEAT BALANCES FOR PROTOTYPE 1

Layer	Heat Balance (Energy in = Energy out)	Equation
Foil	$S_f + h_{c,f}(T_{m1} - T_f) + h_{r,pf}(T_p - T_f) = h_{c,w}(T_f - T_a) + h_{r,fs}(T_f - T_a)$	1
Flow 1	$h_{c,p1}(T_p - T_{m1}) = h_{c,f}(T_{m1} - T_f) + 2G_{el1,P1}C(T_{m1} - T_{i1})$	2
Plate	$S_p = h_{c,p1}(T_p - T_{m1}) + h_{r,pf}(T_p - T_f) + h_{c,p2}(T_p - T_{m2}) + h_{r,pb}(T_p - T_b)$	3
Flow 2	$h_{c,p2}(T_p - T_{m2}) = h_{c,b}(T_{m2} - T_b) + 2G_{el2,P1}C(T_{m2} - T_{i2})$	4
Base	$h_{c,b}(T_{m2} - T_b) + h_{r,pb}(T_p - T_b) = h_{cn,b}(T_b - T_a)$	5

TABLE 9, HEAT BALANCES OF PROTOTYPE 1 SOLVED TO OBTAIN TEMPERATURES

Temp.	Heat Balances solved to obtain the required temperatures $[K]$	Equation
Foil	$T_f = \frac{(S_f + h_{c,f}T_{m1} + h_{r,pf}T_p + h_{c,w}T_a + h_{r,fs}T_a)}{(h_{c,w} + h_{c,f} + h_{r,pf} + h_{r,fs})}$	6
Flow 1	$T_{m1} = \frac{(h_{c,p1}T_p + h_{c,f}T_f + 2G_{el1,P1}CT_{i1})}{(h_{c,p1} + h_{c,f} + 2G_{el1,P1}C)}$	7
Plate	$T_p = \frac{(S_p + h_{c,p1}T_{m1} + h_{r,pf}T_f + h_{c,p2}T_{m2} + h_{r,pb}T_b)}{(h_{c,p1} + h_{r,pf} + h_{c,p2} + h_{r,pb})}$	8
Flow 2	$T_{m2} = \frac{(h_{c,p2}T_p + h_{c,b}T_b + 2G_{el2,P1}CT_{i2})}{(h_{c,p2} + h_{c,b} + 2G_{el2,P1}C)}$	9
Base	$T_b = \frac{(h_{c,b}T_{m2} + h_{r,pb}T_p + h_{cn,b}T_a)}{(h_{c,b} + h_{r,pb} + h_{cn,b})}$	10

TABLE 10, CALCULATION OF THE OUTPUT TEMPERATURES

Temp.	Output Temperatures, essential to determine thermal yield $[K]$	Equation
Out 1	$T_{o1} = (2 \cdot T_{m1}) - T_{i,1}$	11
Out 2	$T_{o2} = (2 \cdot T_{m,2}) - T_{i,2}$	12

Figure 28 visualizes the energy flows in the situation of Prototype 2 where only the backside of the solar module is cooled with air or water. The solar module itself is now in direct contact with the ambient conditions. In Table 11 the heat balance of the plate temperature is given which replaces equation 8. Equation 6 and 7 are not relevant in this situation and equations 9 and 10 remain almost unchanged; in equation 9, the mass flow rate of prototype 2 should be used ($= G_{el1,P2}$). Figure 29 and Table 12 provide the same information for the reference case of the solar module only. However, in this case equation 8 is replaced by equation 16, and the other equations become irrelevant.

The heat balances and the iteration process forms the heart of the numerical simulations, the equations in the next section are mainly to calculate the solved heat balances.

FIGURE 28, HEAT BALANCES FOR PROTOTYPE 2

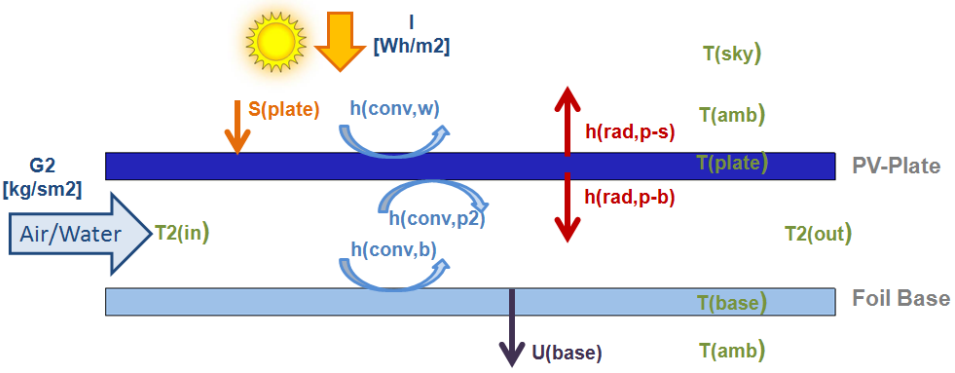

TABLE 11, HEAT BALANCES FOR PLATE TEMPERATURE PROTOTYPE 2

Layer	Heat Balance (Energy in = Energy out), and solved to plate temperature	Equation
Plate	$S_p = h_{c,w}(T_p - T_a) + h_{r,ps}(T_p - T_a) + h_{c,p2}(T_p - T_{m2}) + h_{r,pb}(T_p - T_b)$	13
Plate	$T_p = \frac{(S_p + h_{c,w}T_a + h_{r,ps}T_a + h_{c,p2}T_{m2} + h_{r,pb}T_b)}{(h_{c,w} + h_{r,ps} + h_{c,p2} + h_{r,pb})}$	14

FIGURE 29, HEAT BALANCE FOR REFERENCE SCENARIO; PV ONLY

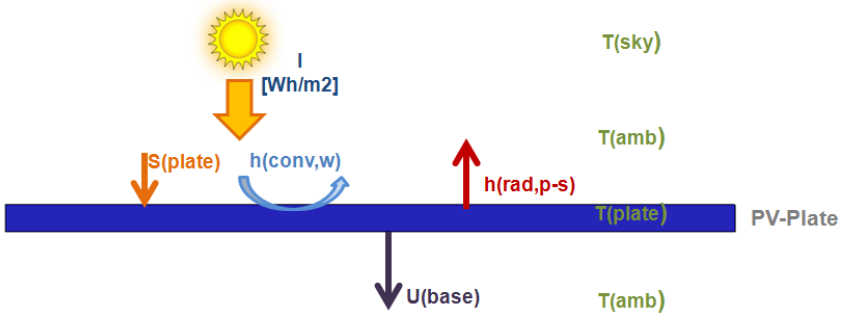

TABLE 12, HEAT BALANCES FOR PLATE TEMPERATURE FOR REFERENCE CASE (PV ONLY)

Layer	Heat Balance (Energy in = Energy out), and solved to plate temperature	Equation
Plate	$S_p = h_{c,w}(T_p - T_a) + h_{r,ps}(T_p - T_a) + h_{cn,b}(T_p - T_a)$	15
Plate	$T_p = \frac{\left(S_p + T_a(h_{c,w} + h_{r,ps} + h_{cn,b})\right)}{(h_{c,w} + h_{r,ps} + h_{cn,b})}$	16

3.1.3 HEAT TRANSFER COEFFICIENTS

In the previous section, the heat balances were explained and solved. The solved equations mainly depend on the amount of incoming solar irradiance, the mass flow rates and the heat transfer coefficients (HTC's) from the three heat transfer mechanisms; convection, radiation and conduction. This sections describes in detail how these variables are defined; the absorbed solar radiation, natural and forced convection, radiation and conduction. In the first column of each table is always mentioned for which prototype the formulas apply and what the units are.

3.1.3.1 ABSORBED SOLAR RADIATION

To calculate how much energy is coming in, it is important to take into account the amount of solar irradiance that is reflected, transmitted and absorbed in the upper layers. The reflection, and thus transmission, depends strongly on the different refractive indices; the higher the difference, the more reflection. These values and relations are also stated in the *'List of constants and variables'*. Another essential factor is the efficiency of the solar cell; the amount of irradiance that is converted into electricity cannot be converted into heat anymore. The resulting equations 17-21 are summarized in Table 13 below.

TABLE 13, ABSORBED SOLAR RADIATION

System	Solar radiation for different elements and materials	Equation
P1 Air: Foil $\left[\frac{W}{tube}\right]$	$S_f = I_r \cdot O_{plate} \cdot \tau_{af} \cdot \alpha_f$	17
P1 Air: Plate $\left[\frac{W}{tube}\right]$	$S_p = I_r \cdot O_{plate} \cdot \tau_{afa} \cdot \tau_{ae} \cdot \alpha_p \cdot (1 - \eta_{sc})$	18
P1 Water: Foil $\left[\frac{W}{tube}\right]$	$S_f = I_r \cdot O_{plate} \cdot \tau_{af} \cdot \alpha_f$	19
P1 Water: Plate $\left[\frac{W}{tube}\right]$	$S_p = I_r \cdot O_{plate} \cdot \tau_{afw} \cdot \tau_{we} \cdot \alpha_p \cdot (1 - \eta_{sc})$	20
P2 A/ P2W/ Ref: Plate $\left[\frac{W}{tube}\right]$	$S_p = I_r \cdot O_{plate} \cdot \tau_{ae} \cdot \alpha_p \cdot (1 - \eta_{sc})$	21

3.1.3.2 NATURAL AND FORCED CONVECTION

Convection occurs naturally but can also be forced as a result of high velocity air or water flows. Table 14 shows al the heat transfer relations (equation 22-46) for convection of wind, air and water flows. Reynolds numbers determine if flows are laminar or turbulent, which in turn determines which Nusselt relations are required. For temperature dependent properties of air and water, please see Appendix A.

TABLE 14, HEAT TRANSFER COEFFICIENTS FOR CONVECTION; WIND, AIR AND WATER FLOWS

HTC Convection	Heat transfer coefficients	Equation
Wind		
P1: Wind total, Foil top $\left[\frac{W}{tube \cdot K}\right]$	$h_w = O_{top} \cdot \sqrt{{h_{w,free}}^2 + {h_{w,forced}}^2}$	22
P2: Wind total, Plate top $\left[\frac{W}{tube \cdot K}\right]$	$h_w = O_{plate} \cdot \sqrt{{h_{w,free}}^2 + {h_{w,forced}}^2}$	23
P1: Wind free, top $\left[\frac{W}{tube \cdot K}\right]$	$h_{w,free} = \frac{k \cdot \mathrm{N}_{free}}{X}$	24
P1: Wind forced, top $\left[\frac{W}{tube \cdot K}\right]$	$h_{w,forced} = \frac{k \cdot \mathrm{N}_{forced}}{X}$	25
Nusselt Nr: wind, free [−]	$\mathrm{N}_{free} = 0.54 \cdot \mathrm{Ą}^{0.25} = 0.54 \cdot \left(\frac{g\beta X^3 \Delta T}{\kappa\nu}\right)^{0.25}$	26
Nusselt Nr: wind, forced [−]	$\mathrm{N}_{forced} = 0.664 \cdot \mathrm{R}^{0.5} \cdot \mathrm{P}^{0.33} = 0.664 \cdot \left(\frac{u_w X}{\nu}\right)^{0.5} \cdot \left(\frac{\nu}{\kappa}\right)^{0.33}$	27
Air Flows		
P1: Air Flow, Foil $\left[\frac{W}{tube \cdot K}\right]$	$h_{c,f} = \left(\frac{k_{m1} \cdot \mathrm{N}_{air,1}}{d}\right) \cdot O_{top,in}$	28
P1: Air Flow, Plate 1 $\left[\frac{W}{tube \cdot K}\right]$	$h_{c,p1} = \left(\frac{k_{m1} \cdot \mathrm{N}_{air,1}}{d}\right) \cdot O_{plate}$	29
P1/P2: Air Flow, Plate 2 $\left[\frac{W}{tube \cdot K}\right]$	$h_{c,p2} = \left(\frac{k_{m2} \cdot \mathrm{N}_{air,2}}{d}\right) \cdot O_{plate}$	30
P1/P2: Air Flow, Base $\left[\frac{W}{tube \cdot K}\right]$	$h_{c,b} = \left(\frac{k_{m2} \cdot \mathrm{N}_{air,2}}{d}\right) \cdot O_{base,in}$	31
Nusselt Nr: Air 1 [−]	$\mathrm{N}_{air,1} = 0.0158 \cdot \mathrm{R}_{air,m1}^{0.8} + \left(0.00181 \cdot \mathrm{R}_{air,m1} + 2.92\right)^{\frac{-0.03795 \cdot L}{d}}$	32

Nusselt Nr: Air 2 [−]	$\mathrm{N}_{air.2} = 0.0158 \cdot \mathrm{R}_{air,m2}^{0.8} + \left(0.00181 \cdot \mathrm{R}_{air,m2} + 2.92\right)^{\frac{-0.03795 \cdot L}{d}}$	33
P1: Reynolds Nr: Air 1 [−]	$\mathrm{R}_{air,m1} = \frac{4 \cdot G_{el,1}}{\nu_{m1} \cdot p}$	34
P1/P2: Reynolds Nr: Air 2 [−]	$\mathrm{R}_{air,m2} = \frac{4 \cdot G_{el2,P1}}{\nu_{m2} \cdot p}$ and $\mathrm{R}_{air,m2} = \frac{4 \cdot G_{el2,P2}}{\nu_{m2} \cdot p}$	35
Water Flows		
P1: Water Flow, Foil $\left[\frac{W}{tube \cdot K}\right]$	$h_{c,f} = \left(\frac{k_{m1} \cdot \mathrm{N}_{wat,1}}{d}\right) \cdot O_{top,in}$	36
P1: Water Flow, Plate 1 $\left[\frac{W}{tube \cdot K}\right]$	$h_{c,p1} = \left(\frac{k_{m1} \cdot \mathrm{N}_{wat,1}}{d}\right) \cdot O_{plate}$	37
P1/P2: Water Flow, Plate 2 $\left[\frac{W}{tube \cdot K}\right]$	$h_{c,p2} = \left(\frac{k_{m2} \cdot \mathrm{N}_{wat,2}}{d}\right) \cdot O_{plate}$	38
P1/P2: Water Flow, Base $\left[\frac{W}{tube \cdot K}\right]$	$h_{c,b} = \left(\frac{k_{m2} \cdot \mathrm{N}_{wat,2}}{d}\right) \cdot O_{base,in}$	39
Nusselt Nr: Water 1 [−]	$\mathrm{N}_{wat,1} = 1.86 \cdot (\mathrm{P}_{m1})^{\frac{1}{3}} \cdot (\mathrm{R}_{wat,m1})^{\frac{1}{3}} \cdot \left(\frac{d_{tube}}{L}\right)^{\frac{1}{3}} \cdot \left(\frac{\nu_{m1}}{\nu_f}\right)^{0.14}$	40
Nusselt Nr: Water 2 [−]	$\mathrm{N}_{wat,2} = 1.86 \cdot (\mathrm{P}_{m2})^{\frac{1}{3}} \cdot (\mathrm{R}_{wat,m2})^{\frac{1}{3}} \cdot \left(\frac{d_{tube}}{L}\right)^{\frac{1}{3}} \cdot \left(\frac{\nu_{m2}}{\nu_b}\right)^{0.14}$	41
Reynolds Nr: Water 1 [−]	$\mathrm{R}_{wat,m1} = \frac{u_{wat} \cdot d_{tube}}{\nu_{m1}}$	42
Reynolds Nr: Water 2 [−]	$\mathrm{R}_{wat,m2} = \frac{u_{wat} \cdot d_{tube}}{\nu_{m2}}$	43
Prandtl Nr: Water 1 [−]	$\mathrm{P}_{m1} = \frac{\nu_{m1}}{\kappa_{m1}}$	44
Prandtl Nr: Water 2 [−]	$\mathrm{P}_{m2} = \frac{\nu_{m2}}{\kappa_{m2}}$	45
P1/P2: Water Velocity $\left[\frac{m}{s}\right]$	$u_{wat} = \frac{G_{el1,P1}}{\rho_{wat,1} \cdot O_{tube}} = \frac{G_{el2,P1}}{\rho_{wat,2} \cdot O_{tube}}$ and $\frac{G_{el2,P2}}{\rho_{wat,2} \cdot O_{tube}}$	46

3.1.3.3 RADIATION

As the individual layers heat up as a result of the incoming solar irradiance, the layer radiate heat (infrared radiation) towards the sky or other towards grey bodies. Equations 47-50 enable to quantify this radiation towards the sky and towards the other layers. Please note that in equations 47 and 48 it is recommended to have a minimum temperature difference in the denominator. Otherwise the outcome would approach an infinite value as the temperature differences between two layers approaches zero.

TABLE 15, HEAT TRANSFER COEFFICIENTS FOR RADIATION

HTC Radiation	Heat transfer coefficients	Equation
P1: Radiation, Foil to Sky $\left[\frac{W}{tube \cdot K}\right]$	$h_{r,fs} = \left[\sigma \cdot \epsilon_f \cdot \left(\frac{{T_f}^4 - {T_s}^4}{T_f - T_a}\right)\right] \cdot O_{top}$	47
P2: Radiation, Plate to Sky $\left[\frac{W}{tube \cdot K}\right]$	$h_{r,ps} = \left[\sigma \cdot \epsilon_p \cdot \left(\frac{{T_p}^4 - {T_s}^4}{T_p - T_a}\right)\right] \cdot O_{top}$	48
P1: Radiation, Plate to Foil $\left[\frac{W}{tube \cdot K}\right]$	$h_{r,pf} = \left[\frac{\sigma \cdot \left(T_f + T_p\right) \cdot \left(T_f^2 + T_p^2\right)}{\frac{1}{\epsilon_f} + \frac{1}{\epsilon_p} - 1}\right] \cdot O_{plate}$	49
P1/P2: Radiation, Plate to Base $\left[\frac{W}{tube \cdot K}\right]$	$h_{r,pb} = \left[\frac{\sigma \cdot \left(T_p + T_b\right) \cdot \left(T_p^2 + T_b^2\right)}{\frac{1}{\epsilon_p} + \frac{1}{\epsilon_b} - 1}\right] \cdot O_{plate}$	50

3.1.3.4 CONDUCTION

The last heat transfer mechanism is conduction and occurs between the backside of the PV-T system and the roof on which it is mounted, see equation 51 in Table 16. Please note that the thicker the insulation at the backside, the less heat is transferred per degree Kelvin.

TABLE 16, HEAT TRANSFER COEFFICENT FOR CONDUCTION

HTC Conduction (flat plate)	Heat transfer coefficients	Equation
P1/P2: Conduction, Base $\left[\frac{W}{tube \cdot K}\right]$	$h_{cn,b} = \frac{k_{in}}{t_{in}} \cdot O_{base}$	51

3.1.4 FAN AND PUMPING POWER

Via the equations formulated in sections 3.1.2 and 3.1.3 it is possible to accurately calculate the electrical and thermal yield of each prototype. However, in order to actively cool the solar module forced air or water flows through the tubes are required. More efficient cooling results in higher electric yields but also requires additional fan or pumping power. Table 17 (equations 52-59) and Table 18 (equations 60-69) provide the relations for the required fan and pumping power respectively. In Equations 56 and 65, 0.5, 1 and 10 represent the loss coefficients at the entrance, exit and various fittings.

TABLE 17, REQUIRED FAN POWER FOR THE AIR FLOWS

Fan (air)	Fan in Operation (*see Hegazy, 2000*)	Equation
P1/P2: Air, Fan Power $\left[\frac{W}{m^2}\right]$	$P_{fan} = \frac{P_{flow,air,meter2}}{\eta_{fan} \cdot \eta_{e,motor}}$	52
P1: Air, Fan Required Flow $\left[\frac{W}{m^2}\right]$	$P_{flow,air,meter2} = \frac{P_{flow,tube} \cdot 2 \cdot n_{tubes}}{L}$	53a
P2: Air, Fan Required Flow $\left[\frac{W}{m^2}\right]$	$P_{flow,air,meter2} = \frac{P_{flow,tube} \cdot n_{tubes}}{L}$	53b
P1/P2: Air, Fan Required Flow $\left[\frac{W}{tube}\right]$	$P_{flow,air,tube} = (W \cdot L) \cdot \frac{G_{tot} \cdot p_{drop}}{\rho_{air}}$	54
P1/P2: Pressure drop total $\left[\frac{kg}{ms^2} = \boldsymbol{Pa}\right]$	$p_{drop} = (p_{drop,air,friction} + p_{drop,air,other})$	55
P1/P2: Pressure drop other $\left[\frac{kg}{ms^2} = \boldsymbol{Pa}\right]$	$p_{drop,air,other} = \frac{(0.5 + 1 + 10) \cdot \rho_{air} \cdot u_{air}^2}{2}$	56
P1/P2: Pressure drop friction $\left[\frac{kg}{ms^2} = \boldsymbol{Pa}\right]$	$p_{drop,air,friction} = \rho_{air} \cdot \left(0.079 \cdot \mathrm{R}_{air,m1}^{-0.25}\right) \cdot u_{air}^2 \cdot \frac{L}{D}$	57
P1/P2: Reynolds Nr. [−]	$\mathrm{R}_{air,m1} = \mathrm{R}_{air,m2} = \frac{4 \cdot G_{el}}{\nu_m \cdot p}$	58
P1/P2: Air, velocity $\left[\frac{m}{s}\right]$	$u_{air} = \frac{G_{el1,P1}}{\rho_{air,1} \cdot O_{tube}} = \frac{G_{el2,P1}}{\rho_{air,2} \cdot O_{tube}}$ *and* $\frac{G_{el2,P2}}{\rho_{air,2} \cdot O_{tube}}$	59

TABLE 18, REQUIRED PUMPING POWER FOR THE WATER FLOWS

Pump (water)	Pump in Operation	Equation
P1/P2: Water, Pump Power $\left[\frac{W}{m^2}\right]$	$P_{pump} = \frac{P_{flow,wat,meter2}}{\eta_{pump} \cdot \eta_{e,motor}}$	60
P1: Water, Pump Flow $\left[\frac{W}{m^2}\right]$	$P_{flow,wat,meter2} = \frac{P_{flow,wat,tube} \cdot 2 \cdot n_{tubes}}{L}$	61a
P2: Water, Pump Flow $\left[\frac{W}{m^2}\right]$	$P_{flow,wat,meter2} = \frac{P_{flow,wat,tube} \cdot n_{tubes}}{L}$	61b
P1/P2: Water, Pump Flow $\left[\frac{W}{tube}\right]$	$P_{flow,wat,tube} = \frac{G_{tot} \cdot p_{drop}}{\rho_{wat}}$	62
P1/P2: Total pressure drop $\left[\frac{kg}{m \cdot s^2} = \boldsymbol{Pa}\right]$	$p_{drop} = (p_{drop,wat,pipes} + p_{drop,wat,shapes} + p_{drop,wat,heights})$	63

P1/P2: Pressure drop pipes $[\frac{kg}{m \cdot s^2} = \boldsymbol{Pa}]$	$p_{drop,wat,pipes} = f_{friction} \cdot \frac{L}{D} \cdot \frac{\rho_{wat}}{2} \cdot u_{wat}^2$	64
P1/P2: Pressure drop shapes $[\frac{kg}{m \cdot s^2} = \boldsymbol{Pa}]$	$p_{drop,wat,shapes} = \frac{(0.5 + 1 + 10) \cdot \rho_{wat} \cdot u_{wat}^2}{2}$	65
P1/P2: Pressure drop height $[\frac{kg}{m \cdot s^2} = \boldsymbol{Pa}]$	$p_{drop,wat,height} = \frac{\rho_{wat} \cdot g \cdot [L \cdot sin(\beta)]}{\left(\frac{2 \cdot n_{tubes}}{L}\right)}$	66
P1/P2: Friction Coefficient $[-]$	$f_{friction} = \frac{64}{\mathrm{R}_{wat,m1}}$	67
P1/P2: Reynolds Nr. $[-]$	$\mathrm{R}_{wat,m1} = \mathrm{R}_{wat,m2} = \frac{u_{wat} \cdot d_{tube}}{\nu_m}$	68
P1/P2: Water, velocity $\left[\frac{m}{s}\right]$	$u_{wat} = \frac{G_{el1,P1}}{\rho_{wat,m} \cdot O_{tube}} = \frac{G_{el2,P1}}{\rho_{wat,m} \cdot O_{tube}}$ and $\frac{G_{el2,P2}}{\rho_{wat,m} \cdot O_{tube}}$	69

3.1.5 Key Performance Indicators

For a fair comparison between the prototypes, key performance indicators are essential. Table 19 contains the equations to determine the electrical yield, thermal yield and the mean temperatures of the prototypes. The final efficiencies of the systems are given in Table 20.

TABLE 19, KEY PERFORMANCE INDICATORS; ELECTRICAL AND THERMAL YIELDS

Key Performance Indicators	PVT in Operation	Equation
P1: Electric Yield PV, Air $\left[\frac{W}{m^2}\right]$	$P_{sc,P1,air} = I_r \cdot O_{sc} \cdot \tau_{afa} \cdot \tau_{ae} \cdot \left[\eta_{sc} \cdot \left(\frac{100 + T_{coef}}{100}\right)^{T_p - 298.15}\right]$	70
P1: Electric Yield PV, Water $\left[\frac{W}{m^2}\right]$	$P_{sc,P1,wat} = I_r \cdot O_{sc} \cdot \tau_{afw} \cdot \tau_{we} \cdot \left[\eta_{sc} \cdot \left(\frac{100 + T_{coef}}{100}\right)^{T_p - 298.15}\right]$	71
P2: Electric Yield PV, Air/Water $\left[\frac{W}{m^2}\right]$	$P_{sc,P2} = I_r \cdot O_{sc} \cdot \left[\eta_{sc} \cdot \left(\frac{100 + T_{coef}}{100}\right)^{T_p - 298.15}\right]$	72
P1/P2: Net Electric Yield, air $\left[\frac{W}{m^2}\right]$	$P_{sc,net,fan} = (\eta_{inverter} \cdot P_{sc}) - P_{fan}$	73
P1/P2: Net Electric Yield, water $\left[\frac{W}{m^2}\right]$	$P_{sc,net,pump} = (\eta_{inverter} \cdot P_{sc}) - P_{pump}$	74
P1: Thermal Yield $\left[\frac{W}{m^2}\right]$	$P_{therm,P1} = \{[G_{el1,P1} C \cdot (T_{o1} - T_{i1})] + [G_{el2,P1} C \cdot (T_{o2} - T_{i2})]\} \cdot \frac{n_{tubes}}{L}$	75
P2: Thermal Yield $\left[\frac{W}{m^2}\right]$	$P_{therm,P2} = [G_{el2,P2} \cdot C \cdot (T_{o2} - T_{i2})] \cdot \frac{n_{tubes}}{L}$	76
P1: Mean Temperature In $[\boldsymbol{K}]$	$T_{in,P1} = \frac{T_{i1} + T_{i2}}{2}$	77
P2: Mean Temperature In $[\boldsymbol{K}]$	$T_{in,P2} = T_{i2}$	78
P1: Mean Temperature Out $[\boldsymbol{K}]$	$T_{out,P1} = \frac{T_{o1} + T_{o2}}{2}$	79
P2: Mean Temperature Out $[\boldsymbol{K}]$	$T_{out,P2} = T_{o2}$	80

TABLE 20, KEY PERFORMANCE INDICATORS; EFFICIENCIES

Efficiency	Efficiency	Equation
Electrical Efficiency PV [%]	$\eta_{PV} = \frac{P_{sc}}{I_r} \cdot 100\%$	81
Electrical Efficiency Net [%]	$\eta_{net} = \frac{P_{sc,net}}{I_r} \cdot 100\%$	82
Thermal Efficiency PVT [%]	$\eta_{therm} = \frac{P_{therm}}{I_r} \cdot 100\%$	83
Overall Efficiency [%]	$\eta_{overall} = \frac{P_{sc,net} + P_{therm}}{I_r} \cdot 100\%$	84

3.1.6 Standard Test Conditions

The best way to compare the performance of the different systems is by simulating them under standard test conditions (STC). The standard test conditions are defined as followed; 1000 W/m^2 of irradiance, 15 °C (288.15 K) as ambient temperature and 0.0 m/s wind speed. A small difference with standard test conditions of normal solar photovoltaic modules is the ambient temperature, which is usually around 25 °C. In this study was deliberately chosen for an ambient temperature of 15 °C to test the PV-T modules to avoid an overestimation of the thermal yield, because the inlet temperatures of the air and water flows are also 15 °C. If the ambient temperature is higher than the inlet temperatures, a temperature rise inside the tubes is also affected by the ambient temperature, while we are only interested in the thermal yield as a result of the solar irradiance.

In addition, under standard test conditions, the effect of the mass flow rate and other design features can be accurately examined. For example the tube sizes, foil thickness or wind speeds can easily been altered. Another advantage of the simulations under standard test conditions is that a real prototype could also be tested under these conditions to see how well the simulations match experimental results.

3.1.7 Real Climate Conditions

After the prototypes are extensively simulated under test conditions, real data retrieved from KNMI can be used as input as well. Via data of the solar irradiance, ambient temperature and wind speeds, the steady states of the prototypes can be accurately estimated for each hour throughout the year. Because most partners of the Nanosol project are located in Arnhem, data was retrieved from Deelen (nearest weather station to Arnhem) for 2012. It should be noted that this method provides a rough estimate of the potential of each prototype, in this approach is no storage taken into account or other systems to utilize or convert the heat.

The air or water inlet temperature is always set at 10 °C, unless the ambient temperature is larger than 10 °C, in that case the inlet temperature equals the ambient temperature. The thermal system (PT part) is only turned on if the thermal efficiency is larger than zero and the solar cell (PV part) is only in operation when the electrical efficiency exceeds zero. Figure 30, Figure 31 and Figure 32 demonstrate the solar irradiance, wind speed and ambient temperatures in Deelen, 2012 (KNMI, 2013).

FIGURE 30, SOLAR IRRADIANCE ON A FLAT SURFACE, DEELEN 2012 (KNMI)

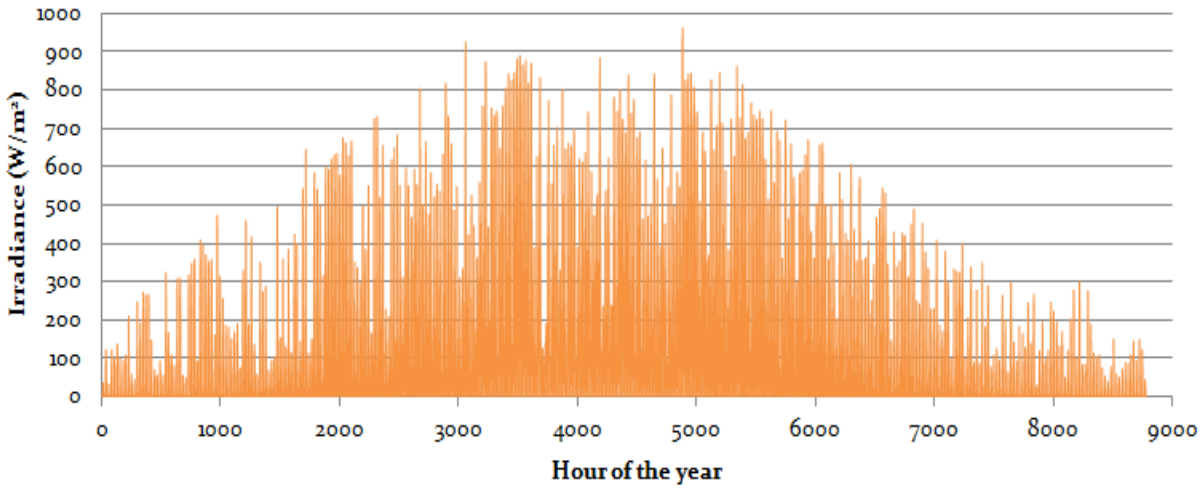

FIGURE 31, WIND SPEED AVERAGE, DEELEN 2012 (KNMI)

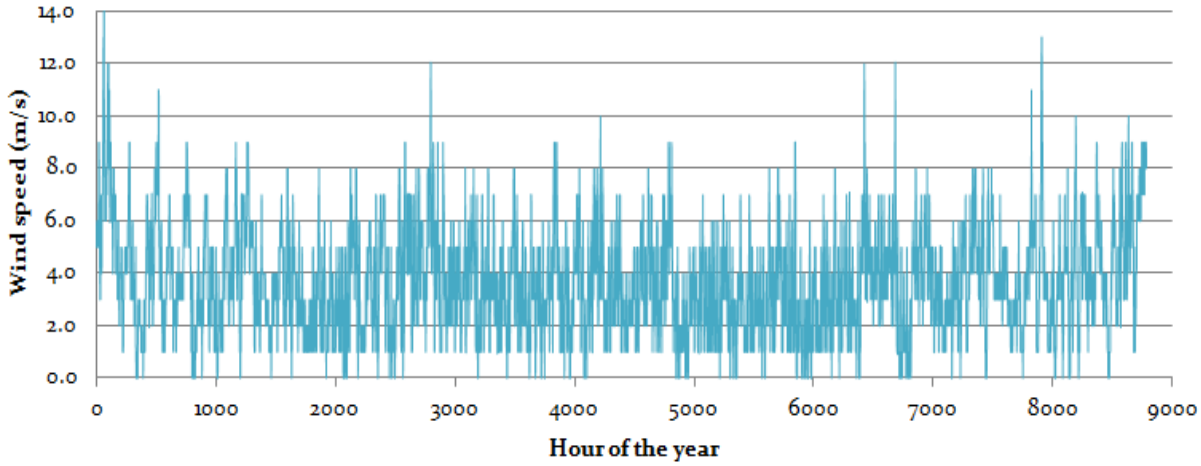

FIGURE 32, AMBIENT TEMPERATURE, DEELEN 2012 (KNMI)

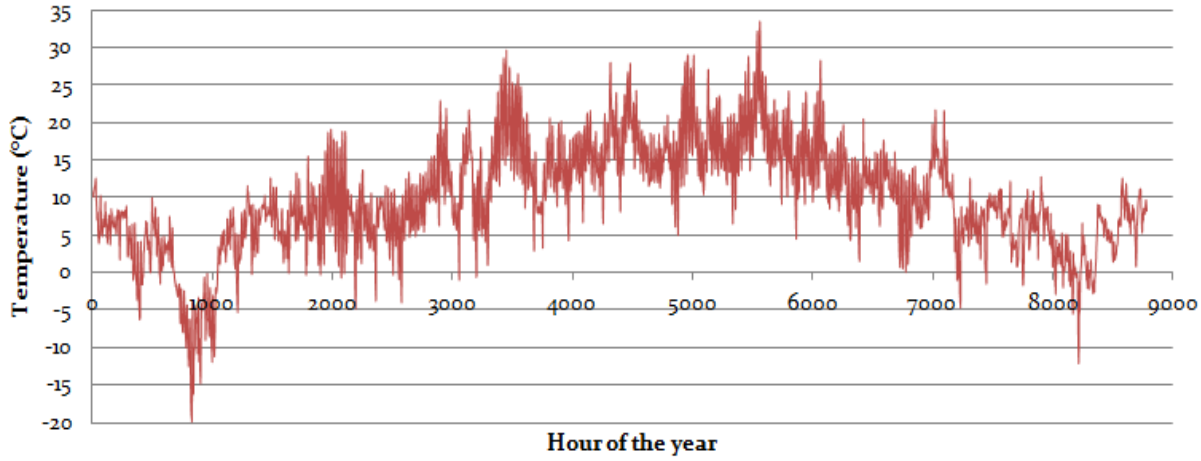

3.2 THERMAL ANNEALING EXPERIMENT

The previous section explained how the simulations for the prototypes and the reference are conducted. These simulations took into account the temperature coefficient, however that was not the case with the effect of thermal annealing. Section 2.2.4 already showed that natural seasonal annealing can have a significant effect on the electrical performance, however, the speed and temperature dependency of this effect has not been experimentally verified yet on the module scale.

In order to study the process of thermal annealing of thin-film amorphous Silicon modules, an experiment was conducted in two steps at Hyet Solar. For this experiment it was essential to start with three similar and 'fresh' modules. The first step was to degrade these modules in a light soaker for approximately 300 hours to ensure that the modules have reached their stabilized efficiency. In step two, these three modules were placed in ovens at different temperatures, again for approximately 300 hours. During both steps their efficiencies were regularly measured in the Pulsar, a flashing device to measure the I-V characteristics of the Hyet Solar modules. The purpose of this experiment is to examine the speed and the temperature dependence of the annealing process. If this effect occurs at reasonable temperatures and within a feasible time-span, this information is valuable to actively stimulate the annealing process within PV-T-systems. Furthermore, if this process could be accurately predicted, it could be taken into account in the simulations as well to obtain more precise results.

3.2.1 MODULES

At Hyet Solar, single junction thin-film amorphous Silicon modules were available together with instrumentation to measure module efficiencies (the pulsar), accelerate degradation (in the light soaker) and to heat up the modules (oven). This section briefly describes the modules that were used.

Hyet Solar provided three single junction amorphous Silicon modules for this experiment which are manufactured on a Roll-to-Roll basis. The modules were produced in June 2010 and since then they have been stored in stacks in the dark. All three modules come from the same roll and were selected on their performances.

FIGURE 33, HYET SOLAR MODULE

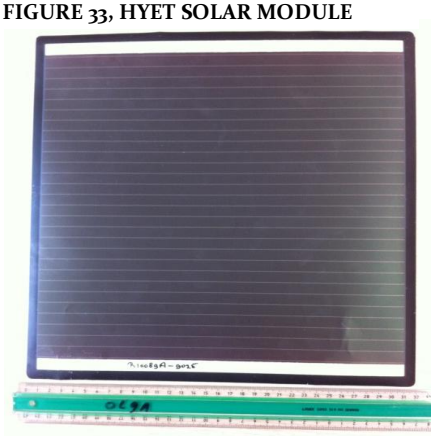

A typical Hyet Solar module has a length and width of 0.30m x 0.30m respectively and consists of 28 cells of 1cm width which are connected in series and on the sides two white strokes that form the connectors (see Figure 33). The whole module is protected by a flexible encapsulation and is less than 0.5 mm thick[15]. Table 21 summarizes the characteristics of the three selected modules.

TABLE 21, CHARACTERISTICS OF THE MODULES AVAILABLE FOR THE EXPERIMENT

Module	Roll Number	PoF	State	Date/Time Production	Number of Cells	Efficiency (%)	Oven temp. experiment (K)
A	R10034A	17480	R2REncap	08/06/2010 17:32	28	7.15	333.15
B	R10034A	17430	R2REncap	08/06/2010 17:35	28	7.21	363.15
C	R10034A	16730	R2REncap	08/06/2010 17:51	28	7.06	393.15

3.2.2 INSTRUMENTATION

This section describes the instrumentation that was used in the experiment; the light soaker, the pulsar and the oven. For more pictures and information on the operation of the instrumentation, please also see the lab journal in Appendix B.

3.2.2.1 LIGHT SOAKER

The light soaker simulates one sun at 1.5 AM (air mass), which results in a radiation of 1000 Wm^{-2}, see Figure 34. After 1000 hours of light irradiation a solar cell can be considered stable at its final efficiency. However, taking into account the exponential decrease of the efficiency, most degradation takes place within the first 300 hours of light soaking, in the last 700 hours the degradation is very minimal. For the experiment therefore, 300 hours of light soaking will be sufficient to have the modules at their stabilized efficiency. In order to determine if the solar cell is stabilized, the following assumption (see next page) needs to be met for two measurements with a minimal time difference of 24 hours (Arndt & Puto, 2003).

FIGURE 34, THE LIGHT SOAKER

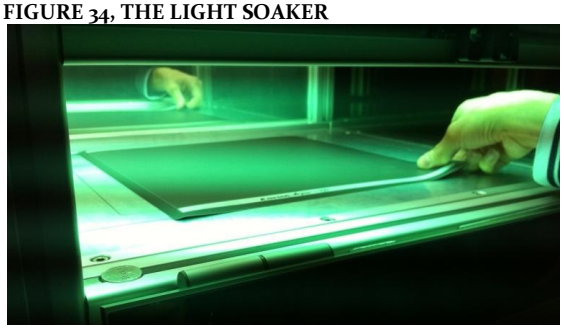

[15] *Detailed datasheets can be obtained from: http://www.hyetsolar.nl/our-product/performance/data-sheets*

$$Solar\ cell\ is\ stabilized\ if: \frac{(P_{max}-P_{min})}{P_{average}} < 2\% = \frac{(\eta_{max}-\eta_{min})}{\eta_{average}} < 2\%$$ 85

3.2.2.2 OVEN

As explained in the theoretical section, complete thermal annealing is expected to occur at temperatures of 150°C and above. During the summer, modules can reach temperatures up to 60 or 80 degrees Celsius. The modules of Hyet Solar are tested to withstand temperatures of maximum 120 °C. Because of these temperature limits, for this experiment was chosen to heat the modules up to 60, 90 and 120 degrees Celsius. A straightforward oven was used to heat up the modules to the required temperatures, see Figure 35. To make sure the modules were heated up and cooled down gradually, the modules were sandwiched between two metal plates. At least one hour before efficiency measurements were performed, the metal plates were taken out of the oven to let the module cool down to room temperature. In total, the modules were kept in de oven for approximately 300 hours.

FIGURE 35, MODULE PLACED BETWEEN TWO PLATES IN THE OVEN AT THREE TEMPERATURES: 60, 90 AND 120 °C

3.2.2.3 PULSAR

During the light soaking process and heating process, the efficiencies of the modules was regularly measured with the Pulsar, see Figure 36. The Pulsar is a flashing device that measures the I-V characteristics of the modules and provides data for at least thirteen parameters.

FIGURE 36, THE PULSAR

Within the first two days of the light soaking process and the annealing process the efficiency is expected to decrease rapidly. Because of this reason, in these time spans the efficiency was measured very often. After these two days less efficiency measurements were required as the efficiency is not changed that quickly anymore. Both after the light soaking or the oven process, the modules were cooled down to room temperature before efficiency measurements were performed. The Pulsar consists of a vacuum table where the modules are sucked upon to make sure the module is placed perfectly flat on the table. Two cupper arms can be placed on the connectors of the module to measure its performance, while a strong flash light simulates the solar irradiance. The whole setup is connected to a computer where the measured data is saved.

3.2.3 EXPERIMENTAL DESIGN

In the Netherlands temperatures of solar collectors varies approximately between -10°C (winter) and +90°C (summer). Complete annealing of amorphous silicon is most likely to appear at 150°C (Staebler & Wronski, 1977). However, during summertime, annealing also occurs at temperatures below 150°C, but in this case the modules are kept warm for longer periods of time (Virtuani & Fanni, 2012). Based on these typical values, the following temperatures and times for this experiment have been chosen.

During the experiment, the three modules (A, B and C) will be heated up to three different temperatures (60°C, 90°C and 120°C) for 336 hours (14 days). In order to compare the performance of the modules during the annealing experiments, their efficiencies will be measured multiple times; immediately after production, during the 300 hours of light soaking process and during the heating process.

Preferable new modules will be used for the experiment. All modules will undergo the same process. First, the efficiency of the new module is measured. Secondly, the module is placed in the light soaker for 300 hours to accelerate degradation of the module and its efficiency is measured several times. Thirdly, the module is placed between two metal plates in the oven at a specific temperature for approximately 336 hours. During the heating process, the module is taken out of the oven multiple times for approximately one hour. In that hour, the module is cooled down, its efficiency is measured and afterwards the module is placed back in the oven again. The new efficiencies will be compared to its original efficiency in order to examine the effect of thermal annealing.

After the experiment has been conducted, an estimate can be made of the required times and temperatures for thermal annealing process. Due to practical reasons the experiment only includes a selection of temperatures and heating times, more measurements would of course increase the accuracy of the final results. In Appendix B, the lab journal of the annealing experiment is attached.

SECTION 4: RESULTS

This section provides an overview of the results from the PV-T simulations and the thermal annealing experiment. Section 4.1 starts with comparing the key performance indicators of the two prototypes with air and water under standard test conditions (STC) and under real climate conditions (RCC). Section 4.2 discusses the results of the thermal annealing experiment, starting with the light soaking process, and thereafter the thermal annealing process.

4.1 PV-T MODELING PROTOTYPES

Via the approach described in section 3.1 the four models (see Figure 37) are accurately simulated. First, these models are simulated under standard test conditions to elucidate the tradeoff between air and water as working fluids. Secondly, also under standard test conditions, some design features are altered to investigate how they affect the electrical and thermal performances. The section ends with the four models simulated under real Dutch climate conditions to have a better understanding of the annual yields in the Netherlands.

FIGURE 37, CROSS-SECTIONS OF THE FOUR MODELS

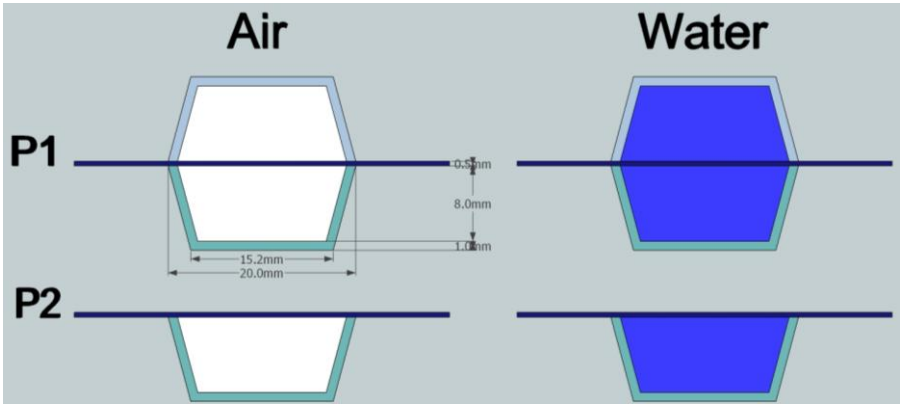

4.2.1 PV-T PROTOTYPES STC; AIR VERSUS WATER

Standard test conditions (irradiance of 1000 W/m², ambient temperature of 15°C and no wind) are required to examine the tradeoff between air and water in the PV-T models. The following key performance indicators (obtained via the relations defined in section 3.1.5) are plotted as a function of the mass flow rate make a fair comparison between the models; the electrical efficiency of the solar cell, the electrical efficiency minus pump requirements, the thermal efficiency and the output temperatures. From the section 2.1.4 it became clear that typical mass flow rates for air and water PV-T systems are 11.1 and 0.014 $\frac{L}{sm^2}$ respectively, which in both cases is approximately 0.015 $\frac{kg}{sm^2}$.

The following remarks hold for Figure 38 to Figure 42. In al graphs, the red lines always depict the air-cooled models and the blue lines always depict the water-cooled models. The darker lines always represent the double cooled models (prototype 1) and the lighter lines always represent the single cooled models (prototype 2). A black dashed line illustrates the electrical performance of the reference model; the Hyet Solar module under the same conditions.

Error! Reference source not found. displays the electrical efficiencies as a function of the mass flow rate $\left(\frac{kg}{sm^2}\right)$ of each model, with and without pumping losses and also include the efficiency of a single PV-module. Please note that the scale on the y-axis is shown from 6.5 to 10.0 percent. The solid lines only represent the electrical efficiencies, while the dashed lines also include the electrical losses at the pump. From the graph, several observations become clear.

FIGURE 38, ELECTRICAL EFFICIENCIES WITH AND WITHOUT PUMP LOSSES OF THE FOUR MODELS

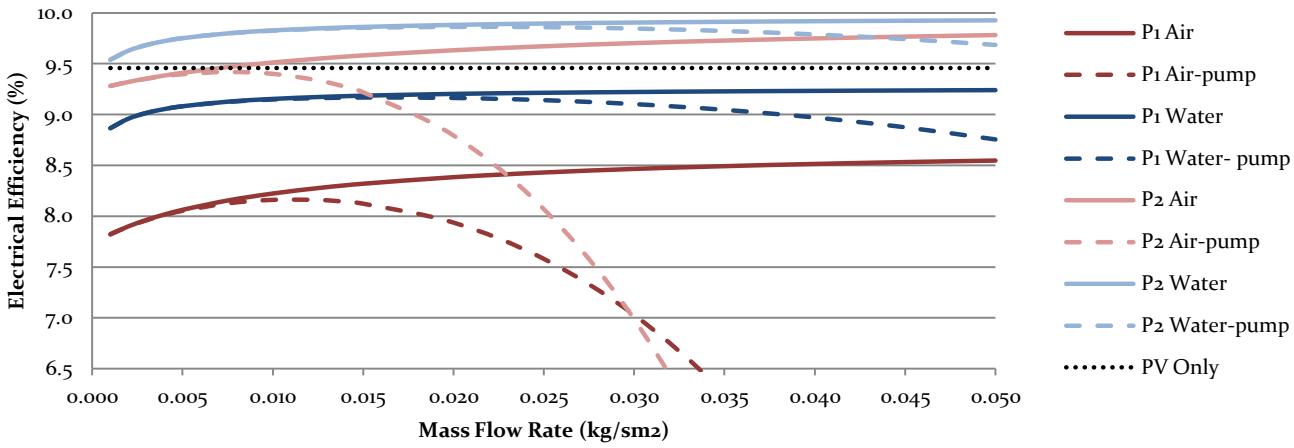

First of all, as the mass flow rate is increased, the electrical performance is increased as well. This can be explained by the fact that higher flow rates enable more efficient cooling, and solar cells have improved electrical performances when operated at lower temperatures. However, also observed is the apparent tradeoff between the increased electrical yield and the electric power required to pump the fluids (see dashed lines) as a function of the mass flow rate, where the effect for air is more dominant compared to water. The latter is due to the increased pressure losses in air, which does not occur in water as the fluid is incompressible. By comparing graph 'P2 Air-pump' with 'P1 Air-pump', it can be seen that similar flow rates result in different flow velocities in the two prototypes and thus different pressure losses and required pumping powers. Another observation that can be made is that the electrical performance of prototype 2 for both air and water is higher than the electrical performance of prototype 1. This can be explained by the optical losses from the tubes on the front side of the solar module in prototype 2 which hampers the electrical efficiency. Yet, this effect is smaller for prototype 1 on water because of the limited optical losses as a result of the smaller differences in the refractive indices at the different interfaces. The final observation that can be made from this graph is that the electrical performance of the water systems is higher than those of the air-cooled models. The heat capacity of water is four times higher than the heat capacity of air, and therefore, the same amount of energy input results in a much smaller temperature increase for the case of water than for air. And again, the lower the temperature of the solar cell, the higher its electrical performance.

The thermal efficiencies of the modules are demonstrated in Figure 39. Again, the main effect that is visible in the graph is that the thermal efficiency is increased with the mass flow rate. In general, the water-cooled prototypes show 10-17 percent higher efficiencies than the air-cooled prototypes; around 43 percent for the water collectors and about 26-30 percent for the air collectors at a mass flow rate of 0.015 $\frac{kg}{sm^2}$. The reciprocal differences between the results for individual prototypes are relatively small. Because the single cooled collectors have a much higher flow rate per tube, the efficiencies almost match those of the double cooled collectors. The air-cooled prototype 2, approaches the efficiency of prototype 1 for mass flow rate larger than 0.035 $\frac{kg}{sm^2}$. In water cooled collectors on the contrary, this is the case for mass flow rate below 0.025 $\frac{kg}{sm^2}$. This is most likely a result of the differences between the heat transfer properties of water and air.

FIGURE 39, THE THERMAL EFFICIENCIES OF THE MODELS AS A FUNCTION OF THE MASS FLOW RATE

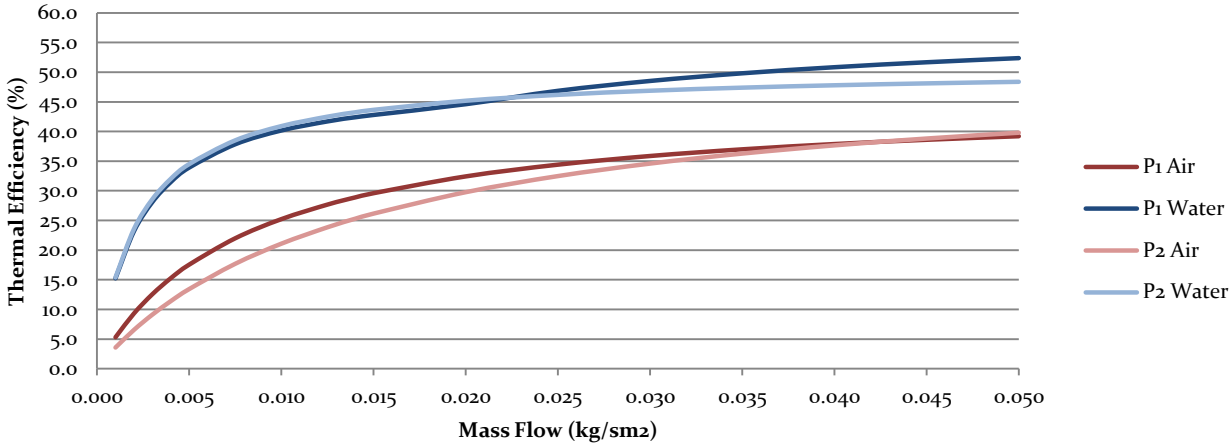

The output (solid lines) and plate (dashed lines) temperatures of the models are negatively related to the mass flow rate, which is visible in Figure 40. The temperatures of water-cooled collectors are approximately 5 to 15 degrees Kelvin lower than the output temperatures of the air-cooled collectors, leading to improved electrical performances. Again, this is a result of the different properties of the fluid, the heat capacity in specific; it takes about four times more energy to increase one kilogram of water with one degree Kelvin, than it takes for one kilogram of air. The difference between the temperature output of 'P1 Water' and 'P2 Water' is negligible, which implies that they both subtract exactly the same amount of energy. At low mass flow rates, 'P2 Air' provides much lower temperature output than 'P1 Air'. Apparently, the single air-cooled collector captures much less energy at low mass flow rates, probably because it has higher losses at the front side compared to the double air-cooled collector. In water-cooled collectors, the plate temperatures are lower than the output temperatures, while the opposite is true for air-cooled collectors.

FIGURE 40, OUTPUT AND PLATE TEMPERATURES OF THE MODELS AS A FUNCTION OF THE MASS FLOW RATE

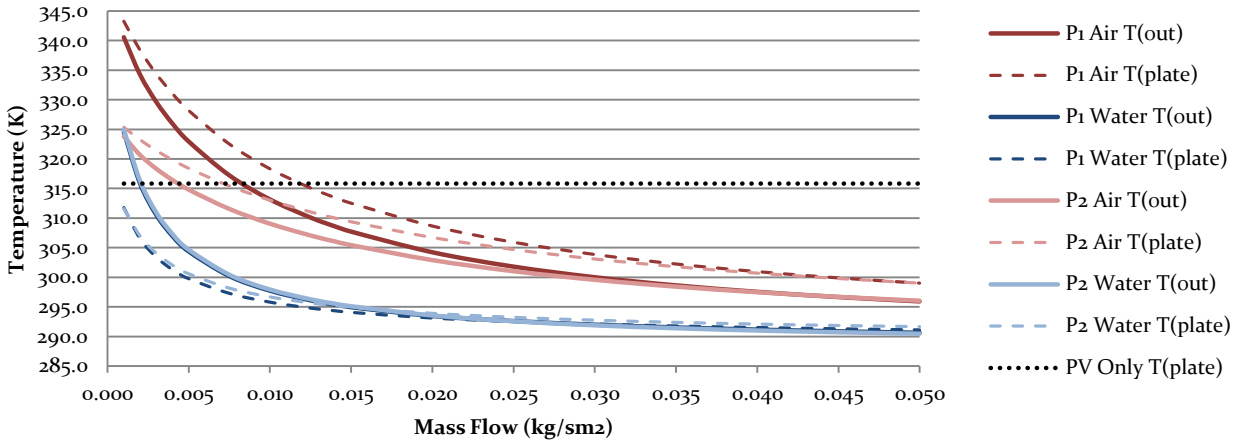

The results so far were obtained under standard test conditions and thus excluded the effect of the wind. To examine the magnitude of this effect, Figure 41 shows the thermal efficiencies at a mass flow rate of 0.015 $\frac{kg}{sm^2}$ of the modules as a function of the wind speed. In prototype 1, the front tubes provide shelter from the wind and prototype is therefore much less affected by the wind compared to prototype 2. The thermal efficiency of 'P2 Water' is more stable than the thermal efficiency of 'P2 Air'. In this case the convection losses in 'P2 Water' are less than in 'P2 Air' because water has superior conductive properties and allows the system to operate at lower temperatures.

FIGURE 41, THERMAL EFFICIENCIES AS A FUNCTION OF THE WIND SPEED

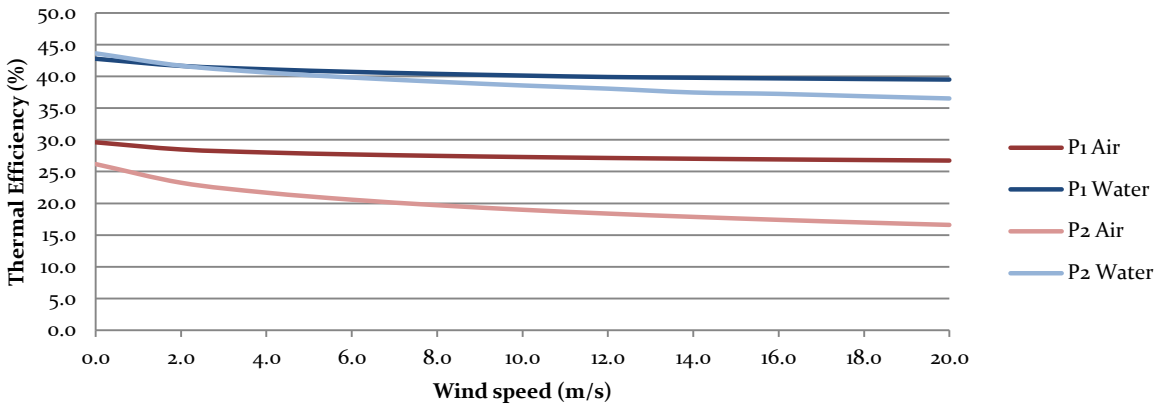

Another interesting factor is shown in Figure 42, namely the temperature rise of the working fluid as a function of the tube distance. This figure shows after what distance the final temperatures are achieved. This figure was constructed by modeling thirty tube lengths of 0.10 meter and using the output temperature of the previous element, as input temperature for the next element. The rate of temperature increase is also dependent on the mass flow rate and therefore the temperature rise in each model is given for three different mass flow rates; 0.005, 0.015 and 0.025 $\frac{kg}{sm^2}$. The main trend is that the higher the mass flow rate, the latter the final temperature is reached. For 0.005, 0.015 and 0.025 $\frac{kg}{sm^2}$, the final temperatures are reached after 0.20, 0.70 and 1.50 meter respectively. Furthermore, it seems that in general, air reaches its final temperature slightly earlier than water does.

FIGURE 42, FLUID TEMPERATURE RISE VERSUS TUBE DISTANCE

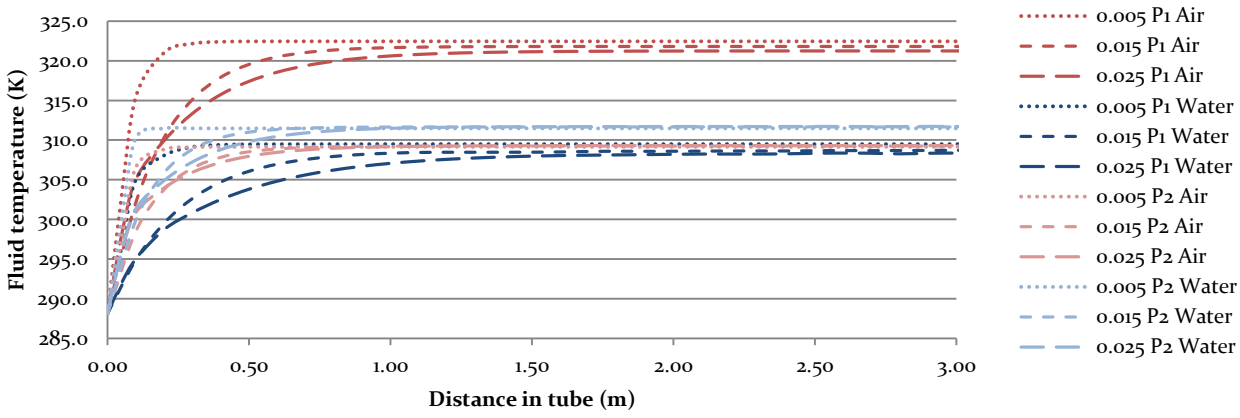

4.2.2 PV-T PROTOTYPES STC; DESIGN OPTIMIZATION

The previous section compared the key performance indicators of the four models. This section investigates the effect on the thermal efficiency of five different design parameters under the same standard test conditions; channel depth, channel width, tube length, angle of tube shape and the foil thickness. The normal dimensions of the five parameters (the 100% value) are given at a mass flow rate of 0.015 $\frac{kg}{sm^2}$. In the following graphs, these values are varied (where possible) between 20% and 200% compared to its original 100% value, depending on the variable (see Table 22 for an approximation of the varied values). Furthermore, when the channel width was altered, the model automatically changed the number of tubes that would fit per square meter of module. Note that not all parameters could be varied

from 20 to 200 percent because this was not always physically possible. For example, decreasing the angle of the tube too much would lead to crossing tube sides in a triangular shape instead of trapezoidal.

TABLE 22, VARIED VALUES OF FIVE DESIGN PARAMETERS

Design parameter	Unit	20% value	100% value	200% value
Channel depth	m	0.0016	0.008	0.016
Channel width	m	0.0036	0.018	0.036
Tube length	m	0.40	2.00	4.00
Angle tube shape	Degrees	15	75	150
Foil thickness	m	0.0002	0.001	0.002

Figure 43 to Figure 46 below illustrate the effects of the five design parameters on the thermal efficiencies of the four models. The y-axis of the graphs consider a range of 10 percent. The cross-section of multiple variables depict the thermal efficiency with the original values of the design parameters under standard test conditions.

FIGURE 43, P1 AIR THERMAL EFF.

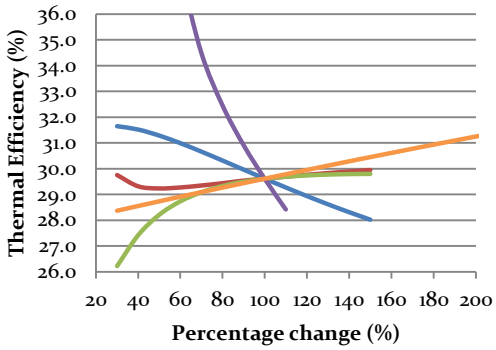

FIGURE 44, P1 WATER THERMAL EFF.

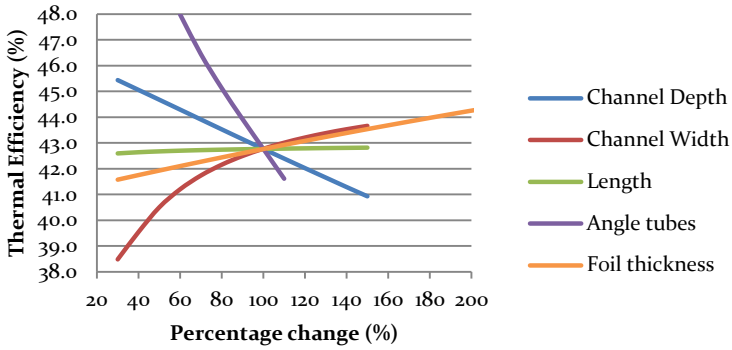

FIGURE 45, P2 AIR THERMAL EFF.

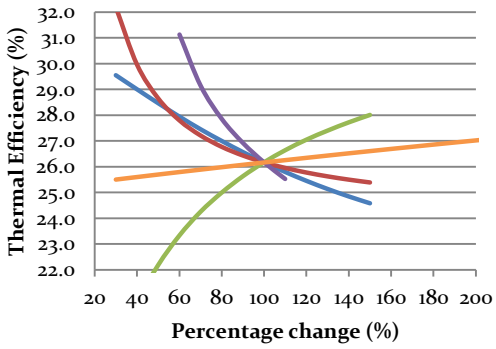

FIGURE 46, P2 WATER THERMAL EFF.

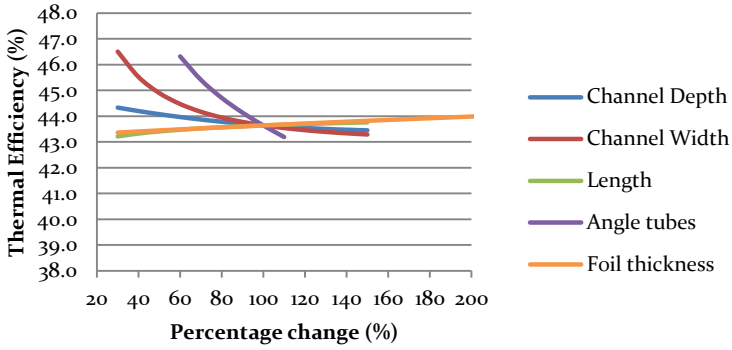

According to the results, it applies to all models that the thermal efficiency is increased by several percents if the channel depth is decreased. This increases the effective heat transfer surface of the tube with respect to the air or water flow, and a smaller channel dept increases the flow velocity through the tubes. For prototype 2, the thermal efficiency is also increased by using thinner tubes, most likely for the same reason. Strangely however, is that the opposite is true for the water-cooled prototype 1. For the air-cooled prototype 1, the effect of the channel width is indifferent. The thermal efficiency is also increased as the length of the tube is decreased. This effect was already visible in Figure 42, which showed that the final temperature was often reached within the first meter of tube distance; thereafter the thermal gains were limited. In addition, decreasing the angle of the tubes has a positive effect on the thermal efficiency of all models, probably because it increases the effective heat transfer surface too. Finally, the effect of the foil thickness was the same for all models; the thermal efficiency is improved by a few percents as the foil thickness was increased from 2 to 3 millimeter.

4.2.3 PV-T PROTOTYPES RCC; ANNUAL PERFORMANCES

In this chapter the exact same models are used as in chapter 4.2.1, however, now the data from Real Climate Conditions is used as input for the solar irradiance, ambient temperature and wind speed. The climate data, retrieved from KNMI, contains hourly data from Deelen (nearest weather station to Arnhem, the Netherlands) for 2012. In all upcoming simulations the mass flow rate was set at 0.015 $\frac{kg}{sm^2}$, because this rate provides a good thermal performance and is also in agreement with the general flow rates found in the literature and in commercial available PV-T systems.

To calculate the yields throughout the year, several assumptions were made. The most important is that the yields only represent the potential yields at each hour of the year of an individual PV-T system; storage is not included. Furthermore, the PV-cell is only turned on when the solar irradiance is larger than zero. The PT-system is only turned on when both the solar irradiance and its thermal efficiency are larger than zero. The final restriction that was made for the simulation of the PV-T models under real climate conditions is that the inlet temperature is usually set at 288.15 degrees Kelvin (or 15°C), unless the ambient temperature exceeds this temperature. In that case the inlet temperature is set equal to the ambient temperature.

In Figure 47, the annual electric yield of 'P1 Water' is shown in a 3D plot. On the x-axis, the 365 days of the years are shown, and on the y-axis the 24 hours of each days. On the z-axis stands the electric yield, ranging from 0 to 80 Wh/m². The flat surfaces on the front and backside of the plot imply a yield of zero Wh/m², which is logical during early morning and the nights when the sun is down. Furthermore, the seasonal variations are clearly visible, starting with low yields in the winter (left and right) and with clear peaks during the spring, summer and autumn (middle of the graph). Electricity production is directly related to solar radiation and can therefore be generated during the whole year.

FIGURE 47, ANNUAL ELECTRIC YIELD OF PROTOTYPE 1 WATER

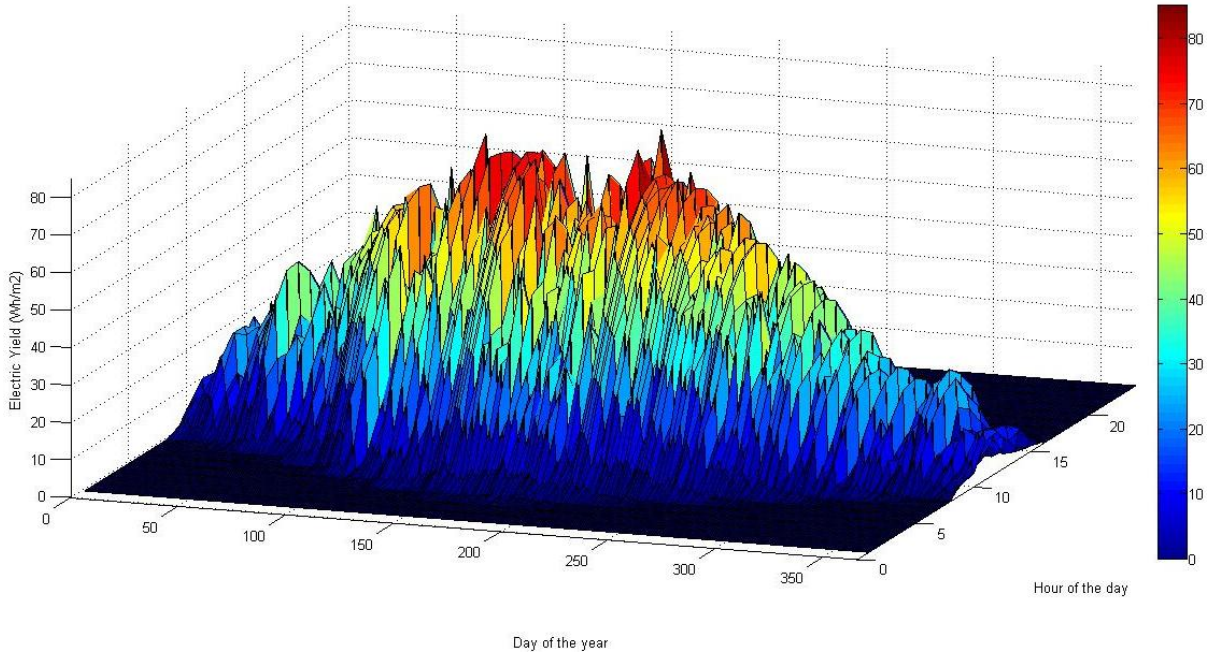

The annual thermal yield of 'P1 Water' is illustrated in the 3D plot in Figure 48. Note that the z-axis now ranges from 0 to 400 Wh/m². In contrast to the electrical yield, heat cannot be generated throughout the year. Certain threshold values for weather conditions need to be met to produce heat; a sufficient ambient temperature and a relative high solar irradiance. For this reason, thermal energy can mainly be harvest from spring to autumn, and less in wintertime.

FIGURE 48, ANNUAL THERMAL YIELD OF PROTOTYPE 1 WATER

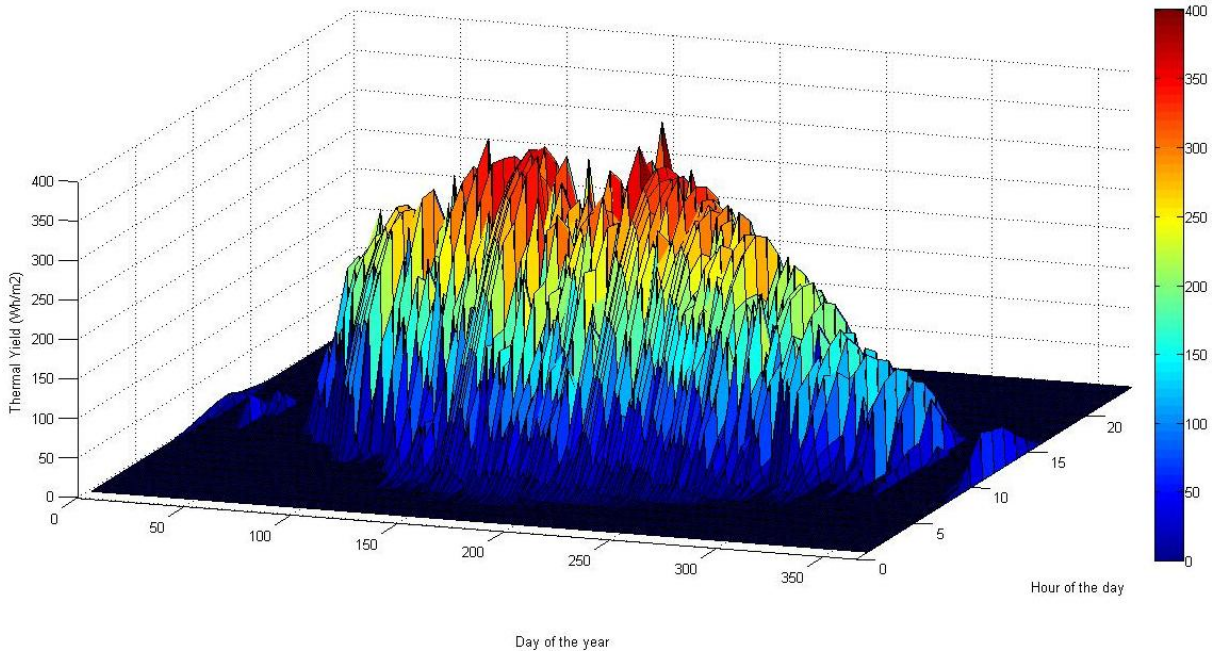

In Figure 49 to Figure 52 below, the same information is provided as in Figure 48, only now the plots are viewed from above. This means that the x-axis (left to right) depicts the days of the year and the y-axis (bottom to top) illustrates the 24 hours in each day. This allows for a good comparison of the annual thermal yields of the four prototypes. The water-cooled models clearly have better thermal yields than the air-cooled models. And regarding the designs, prototype 1 is preferred above prototype 2 from an efficiency perspective. All models operate best during summer, in the middle of the day. The maximum yield during these moments is around 400 Wh/m² of thermal energy.

FIGURE 49, P1 AIR ANNUAL THERMAL YIELD

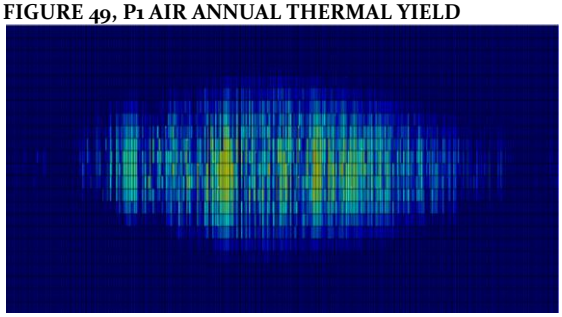

FIGURE 50, P1 WATER ANNUAL THERMAL YIELD

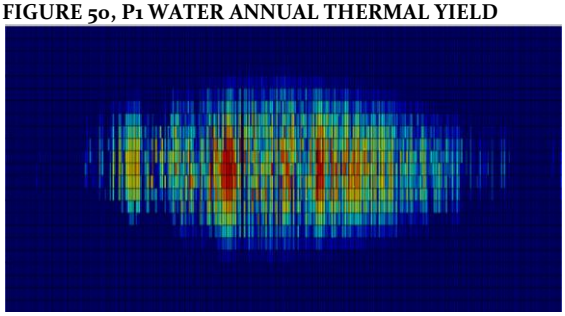

[Wh/m²]

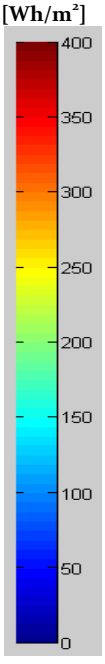

FIGURE 51, P2 AIR ANNUAL THERMAL YIELD

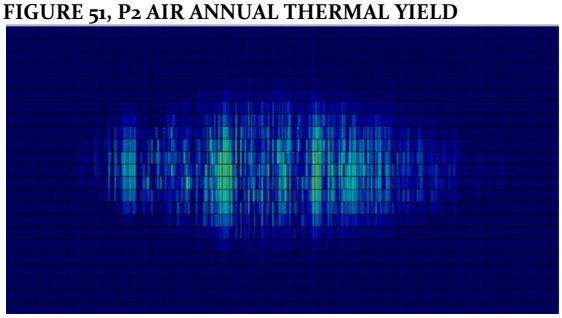

FIGURE 52, P2 WATER ANNUAL THERMAL YIELD

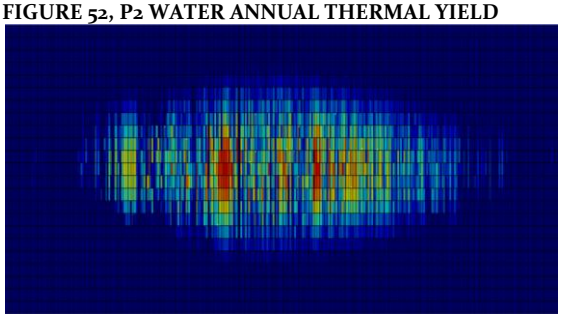

The electrical and thermal yields are also tabulated in Table 23 and Table 24 respectively. The values are provided per month and also totals per year are shown in the bottom rows. Furthermore, the solar irradiance and the average ambient temperatures are given in column two and three. Table 23 contains the electrical performances of the four models, with and without the losses at the pump. Also the

electrical performance of the reference PV-model is demonstrated in the last column. Table 24 includes the thermal performance and the output temperatures of the four models on a monthly basis.

TABLE 23, ANNUAL ELECTRICAL PERFORMANCE OF THE FOUR MODELS

			P1 Air		P1 Water		P2 Air		P2 Water		PV Only
	Solar Irr. [kWh /m²]	Amb. Temp [K]	PV Yield [kWh /m²]	PV - Pump [kWh /m²]	PV Yield [kWh /m²]	PV - Pump [kWh /m²]	PV Yield [kWh /m²]	PV - Pump [kWh /m²]	PV Yield [kWh /m²]	PV - Pump [kWh /m²]	PV Yield [kWh /m²]
Jan	20.01	277.11	1.76	1.68	1.77	1.76	1.77	1.70	1.77	1.77	1.78
Feb	37.92	273.11	3.34	3.23	3.35	3.35	3.37	3.28	3.35	3.35	3.39
Mar	80.84	281.01	6.96	6.47	7.06	7.02	7.02	6.26	7.06	7.04	6.99
Apr	98.54	281.12	8.51	7.90	8.63	8.58	8.58	7.60	8.63	8.61	8.56
May	150.34	287.50	12.72	11.83	12.96	12.88	12.83	11.22	12.96	12.92	12.77
Jun	127.47	287.66	10.87	9.92	11.03	10.94	10.95	9.25	11.04	10.99	10.91
Jul	150.43	290.10	12.71	11.73	12.93	12.83	12.81	10.97	12.93	12.88	12.76
Aug	143.79	291.46	12.11	11.21	12.32	12.23	12.21	10.53	12.32	12.28	12.15
Sept	89.46	286.65	7.64	6.91	7.74	7.67	7.70	6.35	7.75	7.71	7.68
Oct	50.89	283.04	4.41	3.88	4.45	4.40	4.44	3.51	4.45	4.43	4.43
Nov	22.47	279.46	1.97	1.77	1.98	1.97	1.98	1.73	1.98	1.98	1.98
Dec	15.02	277.24	1.33	1.26	1.33	1.32	1.33	1.26	1.33	1.33	1.34
Ann.	**987.18**	**283.00**	**84.34**	**77.80**	**85.55**	**84.95**	**84.99**	**73.66**	**85.58**	**85.28**	**84.73**

TABLE 24, ANNUAL THERMAL PERFORMANCE OF THE FOUR MODELS

			P1 Air		P1 Water		P2 Air		P2 Water	
	Solar Irr. [kWh /m²]	Amb. Temp [K]	Therm. Yield [kWh /m²]	Output Temp [K]	Therm. Yield [kWh /m²]	Output Temp [K]	Therm. Yield [kWh /m²]	Output Temp [K]	Therm. Yield [kWh /m²]	Output Temp [K]
Jan	20.01	277.11	0.52	284.32	0.20	284.13	0.09	284.07	0.22	283.95
Feb	37.92	273.11	1.37	284.84	1.03	283.94	0.36	284.38	0.84	283.91
Mar	80.84	281.01	18.34	290.28	25.80	287.97	11.03	289.54	21.76	287.64
Apr	98.54	281.12	22.29	289.26	30.00	286.56	12.38	287.92	25.32	286.32
May	150.34	287.50	39.55	295.68	59.21	292.30	26.03	294.11	51.76	292.05
Jun	127.47	287.66	33.86	293.75	51.09	291.07	20.66	292.28	42.70	290.81
Jul	150.43	290.10	40.73	296.81	62.07	293.43	26.60	294.96	53.43	293.16
Aug	143.79	291.46	38.74	298.87	59.42	295.37	25.43	296.96	51.13	295.08
Sept	89.46	286.65	24.06	293.28	36.50	290.63	14.01	291.62	29.80	290.37
Oct	50.89	283.04	12.08	289.24	17.29	287.64	5.79	288.06	13.62	287.36
Nov	22.47	279.46	2.68	285.15	3.03	284.15	0.84	284.32	2.28	284.03
Dec	15.02	277.24	0.39	284.73	0.46	284.53	0.12	284.68	0.35	284.46
Ann.	**987.18**	**283.00**	**234.61**	**293.46**	**346.11**	**291.01**	**143.33**	**292.34**	**293.22**	**290.75**

Model 'P2 Water' has the best electrical performance; no optical loss at the front side, the water enables effective cooling via the backside and requires the least pumping power. However, the direct electric yields of the four models and the reference do not differ much. Only when the pumping power is

considered as well, the air-cooled collectors show a decrease in electrical yield of 8-13%, while the water-cooled collectors only loose 1%. Again, electricity can be generated throughout the year, while thermal heat is mostly available from spring to autumn. The thermal performance varies among the different models. Model 'P1 Water' has the highest thermal yield, followed by 'P2 Water' and 'P1 Air'. On the other hand, the output temperatures are best in the air-cooled models. During summer months almost a 30-50% of the heat is extracted, while during the winter months this is only about 1-2%.

4.2 THERMAL ANNEALING EXPERIMENT

The thermal annealing experiment that was performed at Hyet Solar was conducted in two steps; first the modules were degraded in the light soaker until they reached their stabilized efficiency, secondly the modules were placed in the oven at different temperatures to initiate the annealing process.

4.2.1 EFFICIENCY STABILIZATION

During the light soaking process the efficiencies of the different modules were regularly measured in the Pulsar (the flashing device to measure the performance of the modules). Figure 53, shows the results of the degradation process, please note that the scale on the y-axis starts at 6.0 percent. Module A was measured first to obtain some more knowledge about the light soaking process, from which we noticed that more measurements were preferred especially within the first 24 hours. For this reason, much more measurements were done during the first day for modules B and C. The results show that by and large the most degradation takes place within the first two days, thereafter the efficiency decreases only slightly. After approximately 300 hours, the efficiency of Modules A, B and C all decreased by 1.00, 088, and 0.84 absolute percents respectively, see also equation 85 in section 3.2.2.1. For the purpose of this research, 300 hours of degradation was sufficient to start the heating process.

FIGURE 53, RESULTS OF THE LIGHT SOAKING PROCESS

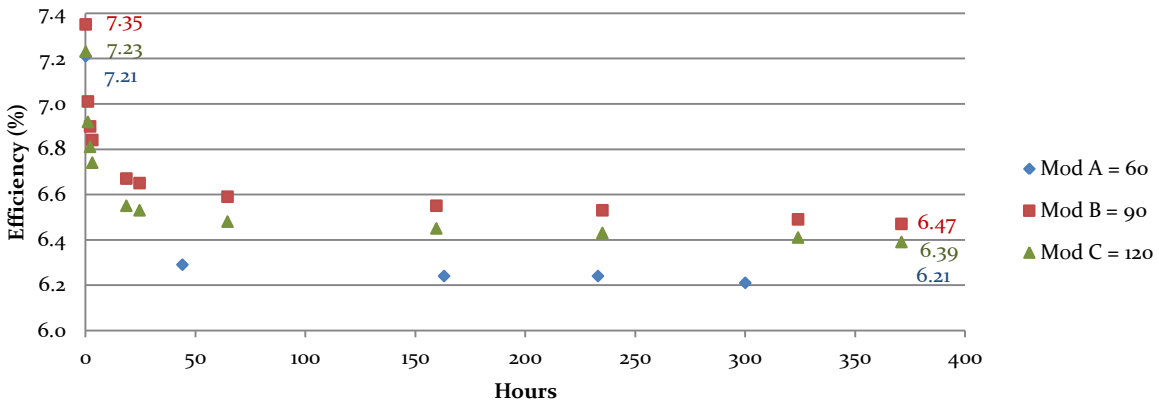

4.2.2 THERMAL ANNEALING

The result of the heating process is depicted in Figure 54. After the models were degraded in the light soaker, modules A, B and C were placed in the oven at temperatures of 60 °C, 90 °C and 120°C respectively. Before each efficiency measurement the modules were cooled down for at least one hour to make sure they were at room temperature. Again, please note that the scale on the y-axis is similar to the one of Figure 53. Modules A and B both show a gradual increase in efficiency after they have been heated up for a certain period of time. Furthermore, the results show that again the largest efficiency improvements take place within the first 24 hours, and the effect is clearly accelerate at higher temperatures. This is especially clear when only the first 24 hours of the three modules are considered,

the efficiency improvements within the first 24 hours for modules A, B and C are respectively +0.04, +0.16 and +0.38 percent. After the first day of heating, the modules show a gradual increase in the efficiencies. Because the experiment was finished after approximately 300 hours of heating, it is unclear if the efficiency would eventually reach is initial performance. In about 280 hours, the total efficiency improvements of modules A, B are +0.18 and +0.31 percent. Another effect that is clearly visible is that after 30 hours the efficiency of module C is declined again. The modules were supposed to be able to withstand temperatures of 120 °C, however maybe not for such long periods of time.

FIGURE 54, ANNEALING PROCESS IN THE OVEN UNDER TEMPERATURES OF 60, 90 AND 120 DEGREES CELSIUS

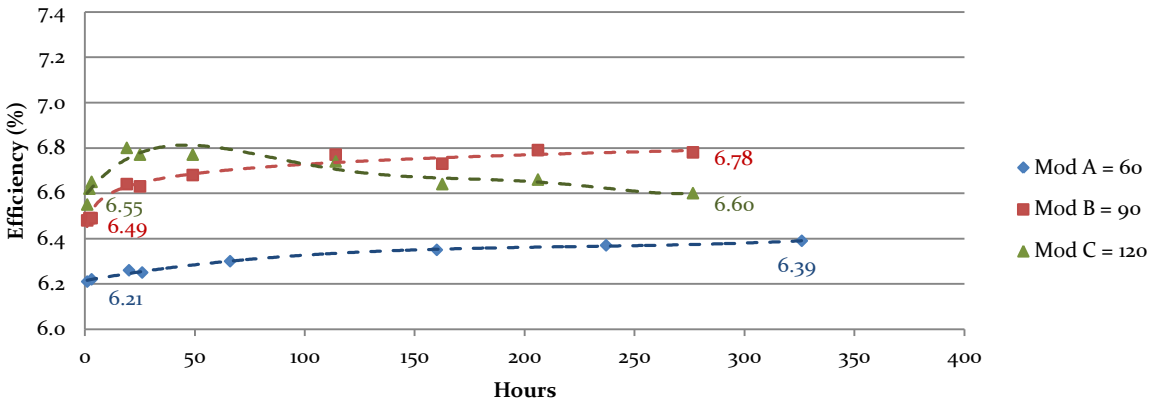

In order to explain the declining efficiency of module C after 30 hours, the other measured parameters of the Pulsar were compared to one another for their behavior under different temperatures and times. One parameter that clearly showed deviations for module C and which could explain the decrease in efficiency is the open circuit resistance, or the R_{oc}, see Figure 55. In the graph module A and B follow the same trend; their open circuit resistance does not vary much and even slightly decreases. Module C on the other hand clearly shows an upward trend, in particular the data measured after 30 hours show much higher Ohms per centimeter squared. According to Edward Hamers and Klaus Jäger (Hyet Solar) could the increase in the open circuit resistance imply a defect in the interconnections between the solar cells of the module. High temperatures are very likely to destroy the interconnections which lead to a higher current loss within the cells and thus lower efficiencies.

FIGURE 55 , DIFFERENCES IN OPEN CIRCUIT RESISTANCE FOR THE DIFFERENT TEMPERATURES

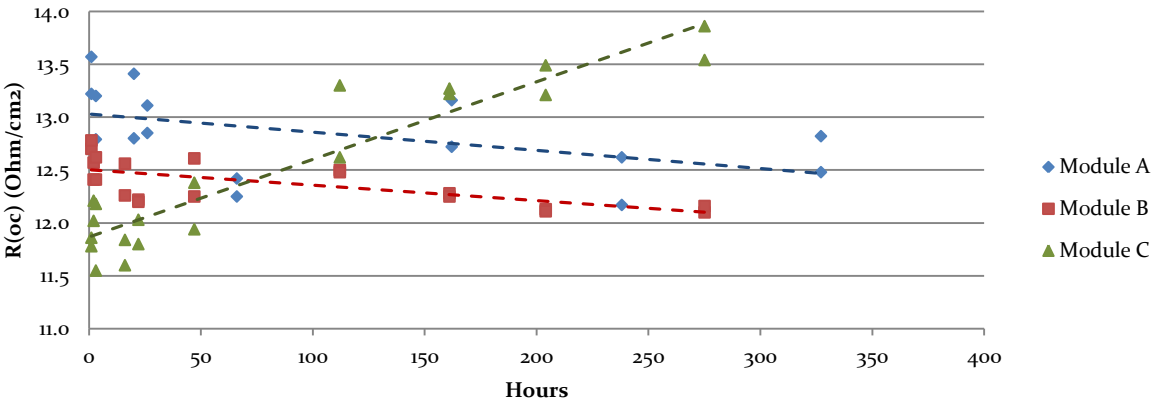

SECTION 5: ANALYSIS

The purpose of this section is to combine the obtained results and analyze which model is preferred and how it can be optimized. In order to do so, first the most important findings of the modeling results are summarized and subsequently this information is used to find the optimal model. Also the experimental results are analyzed and how they could be combined with the modeling part and in the final product that should be ready for the market by the end of 2014.

5.1 SUMMARY RESULTS

5.1.1 PV-T MODELING

The final results of the key performance indicators under standard test conditions and at mass flow rates of 0.015 $\frac{kg}{sm^2}$ are summarized in Table 25. Prototype 2 provides the best electrical performance, water-cooled collectors show the best optimal performance and air-cooled collectors provide the highest temperature output. But from a qualitative perspective, air is advantageous for its light weight, while water has more possible applications.

TABLE 25, THE KEY PERFORMANCE INDICATORS OF THE FOUR MODELS AT A MASS FLOW RATE OF 0.015 KG/SM²

Model	Electrical Eff. [%]	Elec. Eff. inc. pump [%]	Thermal Eff. [%]	Output Temp. [K]
Prototype 1 Air	8.32	8.12	29.61	307.7
Prototype 1 Water	9.19	9.17	42.77	295.0
Prototype 2 Air	9.58	9.22	26.17	305.4
Prototype 2 Water	9.86	9.85	43.64	295.1

In Table 26, a summary is shown of the most important findings from the simulations of the models under Dutch climate conditions. Again a mass flow rate of 0.015 $\frac{kg}{sm^2}$ was used. In total, 987.18 kWh of solar energy is radiated per square meter of area in Deelen, the Netherlands in 2012. The average temperature was 283.0K (or 9.9°C) in the Netherlands.

TABLE 26, ANNUAL PERFORMANCES OF THE FOUR MODELS AND THE REFERENCE

	Thermal Yield [kWh/m²]	Thermal Efficiency [%]	Output Temp. [K]	Elec. Yield [kWh/m²]	Electrical Efficiency [%]	Elec. incl. Pump [kWh/m²]	Elec. incl. Pump [%]
P1 Air	234.61	23.77	293.46	84.34	8.54	77.80	7.88
P1 Water	346.11	35.06	291.01	85.55	8.67	84.95	8.61
P2 Air	143.33	14.52	292.34	84.99	8.61	73.66	7.46
P2 Water	293.22	29.70	290.75	85.58	8.67	85.28	8.64
PV Only	0	0	0	84.73	8.58	0	0

Compared to the standard PV-cell, almost all models have increased electrical output as a result of the active cooling (0.26-0.85 kWh or 0.03-0.09% efficiency more), except for model 'P1 Air'. Also note that the addition of the transparent tubes on the front side of the solar cell only slightly affects the electrical performance and is partly compensated via the increased electric yield as a result of the active cooling. However, when also taking into account the pumping power of the air and water flows, the air-cooled models show a decrease of about 6.54 kWh ('P1 Air') and 11.33 kWh ('P2 Air'), while the water-cooled models used only 0.6 kWh ('P1 Water') and 0.3 kWh ('P2 Water') for the pumps during the year. The thermal output varies greatly amongst the four models. Water-cooled collectors (annual efficiency 29.7-35.0%) clearly show an advantage over air-cooled collectors (annual efficiency 14.5-23.7%). Also

prototype 1 seems extract more heat than prototype 2. Although the amount of embedded energy is lower, the temperature of the air-cooled systems is generally higher.

Considering the design parameters, it became clear that it was beneficial to decrease the channel depth of the tubes to increase the heat transfer surface. The effect of the channel width was less clear; for prototype 2 it seemed better to decrease the channel width, while in prototype 1 it was slightly better to actually increase the width. The length of the system appears to have a slight positive effect on the thermal efficiency. The tube angles should be made smaller; again smaller tubes increase the heat transfer surface. Maybe even spherical shapes would be very advantageous. Finally, also from a thermal efficiency perspective, the foil thickness should be increased to improve the insulating properties.

5.1.2 THERMAL ANNEALING

The thermal annealing experiment was conducted over a time span of approximately 300 hours and showed a gradual increase in efficiency as a result of the heating process. Also it became clear that most of the electrical gains could be observed during the first 24 hours, and occurred more rapidly at higher temperatures. A few key values of the annealing process are displayed in Table 27, where module A and B show improved efficiencies, while module C didn't function very well after 24 hours of heating at 120°C. Also from a practical point of view, heating outdoor modules at these temperatures for longer than 12 hours is very difficult. For these two reasons, in the analysis the focus is mainly aimed at the efficiency improvements within the first 24 hours. Within those 24 hours, modules A, B and C showed an increase in absolute electrical efficiencies of 0.04 (+0.65%), 0.16 (+2.47%) and 0.38 (+5.95%) percentages respectively.

TABLE 27, ELECTRICAL EFFICIENCIES OF THE MODULES DURING THE ANNEALING PROCESS

Hours	Module A (60°C) [%]	Module B (90°C) [%]	Module C (120°C) [%]
0	6.21	6.47	6.39
24	6.25	6.63	6.77
50	6.28	6.68	6.77
300	6.38	6.78	6.59

In Figure 56, the thermal annealing process depicted as relative efficiency improvement during the first 24 hours. At 120°C however, the annealing trend is not clear; very rapid improvement in the first 4 hours, but regarding the whole 24 hours the improvement occurred less quickly. This could imply that the module was already defect after four hours of heating at 120°C. All graphs have a linear trend line with its origin through 0.0, and also include the linear relations. In 24 hours, the relative efficiency increases for 60, 90 and 120°C are approximately 0.8, 3.2 and 8.0% respectively. According to the linear relations included in Figure 56, the relative increase in efficiency is improved with 0.031%/hour at 333K, 0.130%/hour at 363K and 0.339%/hour (or 1.565%/hour) at 393K.

FIGURE 56, RELATIVE EFFICIENCY IMPROVEMENTS AT THE FIRST 24 HOURS OF THERMAL ANNEALING EXPERIMENT

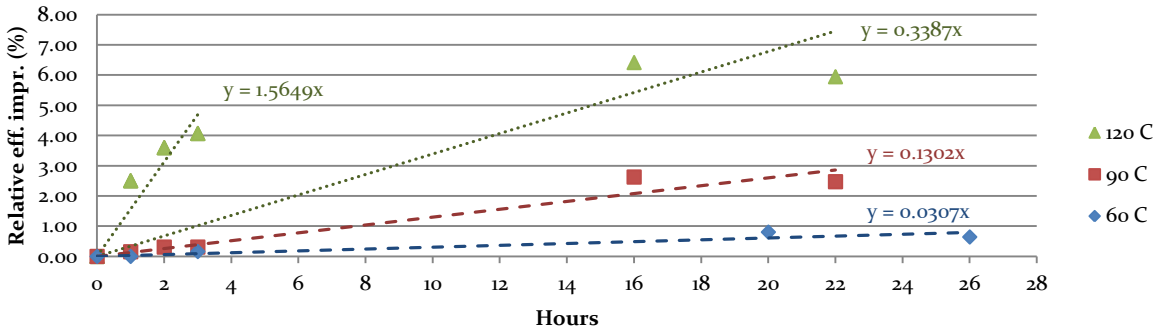

In Figure 40 of section 4.2.1, the plate and output temperatures were demonstrated as a function of the mass flow rate. When heat demand is completely satisfied, the system will stop the cooling process and as a consequence the temperature of the system rises, also known as the stagnation temperature. According to the results under standard test conditions (1000 Wh/m² solar irradiance, 15°C ambient temperature), the stagnation temperature of 'P1 Water' and 'P2 Water' is 51°C. For 'P2 Air', the stagnation temperature is 50°C and for 'P1 Air' this temperature can rise up to 67°C. Also remarkable was that the temperature of the solar cells compared to the output temperatures was three degrees higher in the air-cooled systems, while in the water-cooled systems the solar cells were almost 13 degrees lower than the output temperature. In other words, the temperature of the solar cells in the water-cooled prototypes can reach 38°C, in 'P1 Air' it can reach 70°C and for 'P2 Air' it was 53°C. The reference PV-cell under the same conditions obtained a steady state temperature of 316K (43°C).

TABLE 28, STAGNATION TEMPERATURES OF THE OUTPUT FLOWS AND THE SOLAR CELLS IN STEADY STATE (STC)

Temperatures [°C]	P1 Air	P1 Water	P2 Air	P2 Water	PV only
Output [T_{amb} = 15°C]	67	51	50	51	-
Plate [T_{amb} = 15°C]	70	38	53	38	43
Output [T_{amb} = 20°C]	74	59	56	59	-
Plate [T_{amb} = 20°C]	74	42	56	42	48
Output [T_{amb} = 25°C]	79	66	65	66	-
Plate [T_{amb} = 25°C]	77	47	63	47	50

Table 28 provides an overview of the stagnations temperatures under different ambient temperatures (15, 20 and 25°C) and with 1000 Wh/m² of solar irradiance. Also in Figure 57 are the output and plate (solar cell) temperatures illustrated as a function of the mass flow rate and under standard test conditions, however in this case with an ambient temperature of 20°C.

FIGURE 57, OUTPUT AND PLATE TEMPERATURES, AT 1000 WH/M² AND AMBIENT TEMPERATURE 20°C

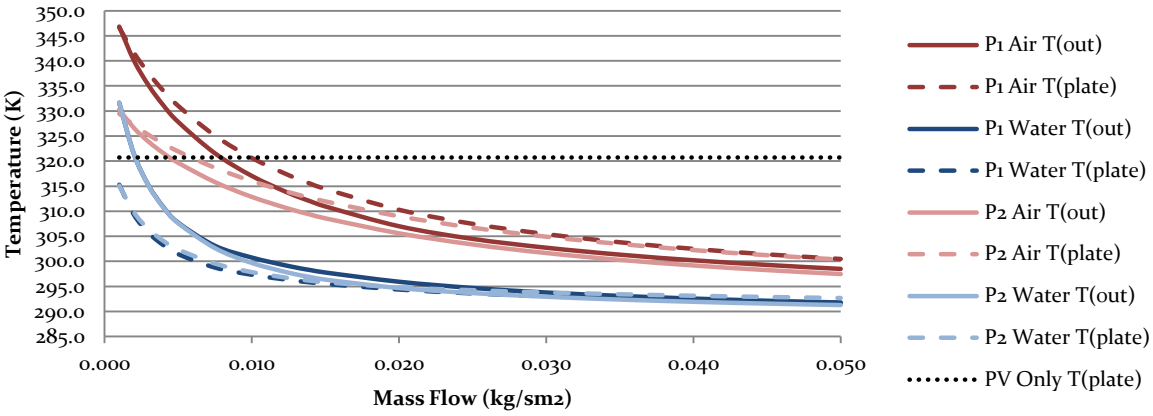

From Table 28 and Figure 57, it can be found that the solar cell temperature in the water collectors could reach temperatures slightly below 50°C. In the air collectors, the solar cell temperature could reach 56-70°C under optimal conditions. The thermal annealing results show that thermal annealing occurred already at 60°C and can be expected to occur at 50°C as well, however the speed of the efficiency improvements will be very limited. For water-cooled PV-T collectors the thermal annealing effect is therefore not very likely to take place. In air-cooled PV-T collectors on the other hand, the temperatures should be sufficient to enable thermal annealing. In this case (60-65°C) the speed of the thermal annealing process is expected to occur with approximately 0.03% of relative efficiency improvement per hour. For a typical a-Si solar module from Hyet Solar with an efficiency of 10.0 percent, this would result in a new efficiency of 10.036 percent after 12 hours of annealing in optimal conditions.

It appears that the annealing effect is relatively small for the temperatures obtained from the calculations. However, the annealing effect occurs much more rapidly at slightly higher temperatures. Also the results from King, Kratochvil and Boyson (2000), proved that thermal annealing during the summer could cause a 5% increase of the normalized performance in Albuquerque, USA (King, Kratochvil, & Boyson, 2000). In the Netherlands however, there are only little days available for effective annealing and the effect is therefore expected to be small. Still, it would be interesting to include this effect in future models. For the case of the Netherlands the outcomes would not change very much, but for more sunny climates this effect could be significant.

In the current model used to predict the performance of the four models and the reference PV-cell, thermal annealing was not included. In future models it would be interesting to also take into account the effect of thermal annealing in amorphous Silicon modules as well, especially for simulations in hot climate conditions. For now, the relative efficiency improvements of approximately 0.031%/hour at 60°C, 0.031%/hour at 90°C and 0.339%/hour at 120°C could be extrapolated to more temperatures. This data can be used in future models to predict an efficiency improvement depending on the temperature of the solar cell in a particular hour. Subsequently, this efficiency improvement is in turn new information that affects the upcoming hour. It should also be taken into account that the Staebler Wronski effect (degradation) will diminish the annealing effect again. During daily operation, there is a constant tradeoff between degradation and efficiency improvement from the increased temperatures.

5.2 Optimal PV-T model

To determine the preferred PV-T model, several criteria are taken into account; qualitative considerations, the key performance indicators (under standard test conditions and annually), the potential for thermal annealing and its compatibility with other equipment. The latter criterion is now based on literature, but should be extended with additional modeling and testing to see how well the PV-T systems could be integrated in larger systems or applications (heat pump, absorption chillers etc). For example, most thermal systems are driven by hot water flows and less by hot air streams which will thus require an additional heat exchanger. See Table 29 for an overview of these above mentioned criteria for the four models.

TABLE 29, OVERVIEW OF THE FOUR MODELS AND THE CRITERIA

	Qualitative	**Performance at 0.015 $\frac{kg}{sm^2}$**			**Thermal annealing**	**Applications**
		Var.	**STC**	**Annual**		
P1 Air	1.Light weight 2.Easy manufacturing 3.Less damage, if leakage 4.No phase change (if freezing)	Eff_{el} [%] $Eff_{el,p}$ [%] Eff_{th} [%] T_{out} [°C]	8.32 8.12 29.61 34.7	8.54 7.88 23.77 20.5	1.Yes, temperatures are sufficient	1.Mainly drying 2.Additional Heat exchanger for water driven equipment
P1 Water	1.Superior properties 2.Economic to pump	Eff_{el} [%] $Eff_{el,p}$ [%] Eff_{th} [%] T_{out} [°C]	9.19 9.17 42.77 22.0	8.67 8.61 35.06 18.01	1.No, temperatures too low	1.Preheat 2.Direct appl. with water driven equipment
P2 Air	1.Light weight 2.Easy manufacturing 3.Less damage if leakage 4.No phase change (if freezing)	Eff_{el} [%] $Eff_{el,p}$ [%] Eff_{th} [%] T_{out} [°C]	9.58 9.22 26.17 32.4	8.61 7.46 14.52 19.34	1.Yes, temperatures are sufficient	1.Mainly drying 2.Additional Heat exchanger for water driven equipment
P2 Water	1.Superior properties 2.Economic to pump	Eff_{el} [%] $Eff_{el,p}$ [%] Eff_{th} [%] T_{out} [°C]	9.86 9.85 43.64 22.1	8.67 8.64 29.70 17.75	1.No, temperatures too low	1.Preheat 2.Direct appl. with water driven equipment

From a practical point of view (see the criterion 'qualitative'), the air-cooled PV-T models are preferred for their light weight, easy to construct and low risk design. This is especially beneficial for the implementation of the PV-T system at large flat roofs of commercial offices. However, from an efficiency perspective, the water-cooled PV-T models show relatively 50-100% higher thermal efficiencies compared to the air-cooled models. Because water provides better cooling and less optical losses (in case of Prototype 1), the water-cooled models also have higher electrical performances. Furthermore, air requires much more pumping power, resulting in even lower electrical efficiencies. As a consequence, the final electrical efficiencies of the water-cooled systems are relatively 5-15% higher for water-cooled PV-T systems compared to the air-cooled models. However, the output temperatures of the air-cooled systems are about 2 to 12 degrees Celsius higher than for the air-cooled systems. This would also enable thermal annealing during the summer, which is not likely to occur in water-cooled systems. Unfortunately, the effect of thermal annealing in actively cooled PV-T systems will be very limited, and should therefore be weighted lightly in the final decision. Considering the design of the models, prototype 1 always enables better thermal efficiencies than prototype2 2, while only compromising little on the electrical efficiencies. For water this implies a relative annual efficiency improvement of approximately 18%, and for air prototype 1 shows an efficiency that is about 60% more efficient than prototype 2. The applications criterion, mainly based on literature, is also more beneficial for water-cooled PV-T systems. Air-cooled systems would require very large heat exchangers and thus also a lot of pumping power. However, when used for drying for example, air-cooled collectors would be preferred.

Considering the reasons above, the best choice would be model 'P1 Water', where the heat is extracted with water from both the front and the backside of the solar cell. First of all, the water-cooled models have superior thermal and electrical efficiencies and require less pumping power. From the water-cooled models, prototype 1 shows a better thermal efficiency compared to prototype 2 and the electrical efficiencies in real climate conditions are very similar. Finally, water is also favorable because it is most likely better compatible with other thermal applications.

Furthermore, the thermal efficiency of 'P1 Water' could be improved by adjusting several parameters. The channel depth is now 8 mm, but the model is expected to perform better when would be made lower. The effect of the width of the channel is not exactly clear, in 'P1 Water' this should be slightly increased, while in 'P2 Water' this should be smaller. In addition, according to the simulations, the angels of the tube should be diminished (almost towards a triangular shape). Those three parameters affect the effective heat transfer area, which is preferably as high as possible. In the literature this was also achieved by adding extra fins inside the tubes or ceramic granulates. The length of the system did not seem to affect the thermal efficiency much. The last parameter that could improve the system is the foil thickness. In the current model the foil thickness was set at 1 mm, but when increased to 2 mm, the thermal efficiency was improved. When all parameters are adjusted in the correct way, the thermal efficiency of 'P1 Water' under standard test conditions could be increased by relative 6 to 9% (from ~43 to ~46%).

SECTION 6: DISCUSSION

The aim of this study was to evaluate four PV-T models on their performance under standard test conditions and under real Dutch climate conditions. In addition, the effect of thermal annealing was investigated by means of an experiment. Throughout this research, the best methods were chosen that were available within the time and resources available. However, also several limitations appeared during this research that should be mentioned.

The model presented in section 3 is based on the model for air-cooled collectors from Hegazy (2000). Via numerical simulations, a steady state situation is calculated for specific input data such as solar irradiance, ambient temperature and wind speed. However, in the case of real climate conditions, the hourly values only represent averages for the whole hour, while in reality each hour comprises large variations. Nevertheless, the hourly data was free available at KNMI and still provides a good estimate of the annual performances. One important and unexpected result was found when the temperature increase was investigated as a function of the tube length, see Figure 42. To study this effect, the model was cut up in smaller tubes where the output of the previous tube was the input for the next tube. It appeared that the output temperatures were slightly different from those found via the original approach. This should be looked into for future simulations.

In the thermal annealing experiment a total of three modules were degraded and heated up. The experiment could be improved by using more modules and by increasing to amount of measurements. More modules would enable to study a wider range of temperatures and more measurements would make the results more accurate. However, the available modules were limited and due the measurement procedure (module needs to cool down for at least one hour before each measurement) only three measurements were possible within one day. In particular within the first 24 hours more measurements are favorable because the largest efficiency improvements occur within this timeframe.

To validate the theoretical results, real prototypes should be constructed and tested under the same standard test conditions and outdoor. Based on this information, an estimate can be made of the difference between the modeling and actual measurements. However, it is always difficult to construct a solid and waterproof prototype. Also it should be taken into account that during the construction also some difficulties will arise that could influence the air or water flows. For example, it is difficult to ensure equal fluid flows through each tube.

A final and essential point of discussion is the integration with other applications. In the current model, only the input and output is considered in the modules. Storage should be included, but will in turn affect the performances; inlet temperatures are dependent on the storage temperature and the storage itself and the transportation will induce additional losses as well. In addition, complete systems should be formulated, where the PV-T provides heat and electricity as input which can be used to drive different combinations of thermal applications. Section 2.1.9 already briefly mentioned the combination of the PV-T modules with a heat pump, an absorption chiller or with aquifer thermal energy storage.

SECTION 7: CONCLUSION

This study was commissioned by the Nanosol project, a consortium of five partners which aims to develop a PV-T module that should be market ready by the end of 2014. A hybrid PV-T module (photovoltaic-thermal module) converts solar radiation into electricity and heat simultaneously and directly at the location where it is desired. In doing so, the solar cell is cooled actively resulting in improved electrical performance, significantly increased yield per unit surface and the PV-T module allows for a more uniform appearance on the roofs.

For the further development of this PV-T module, several factors required clarification. To begin with, it was unclear whether it was favorable to cool the solar cell with air or with water. The preferred design was also undecided; the solar cell could be cooled from both sides of the solar cell or from the backside only. In addition, there was interest in the electrical and thermal annual yields of the PV-T modules. Another issue was how the amorphous Silicon modules would be affected by longer periods of elevated temperatures, also known as thermal annealing. The latter occurs during stagnation of the system when the demand for heat is fully satisfied and heat is not extracted from the solar cell anymore.

In order to investigate these factors, extensive simulations were performed based on the model from Hegazy (2000) for air-cooled collectors. This model was improved and extended to also simulate water-cooled collectors. Two prototypes were designed that could be cooled with either air or water, resulting in a total of four models; P1 Air, P1 Water, P2 Air and P2 Water. Prototype 1 (P1) is cooled from both sides of the solar cell and prototype 2 (P2) is only cooled from the backside. First these models were simulated under standard test conditions (STC) (1000 Wh/m^2 solar irradiance, 15°C ambient temperature and 0.0 m/s wind) and thereafter also under real Dutch climate conditions (RCC). The real climate conditions were retrieved from KNMI and consist of measured hourly data for solar irradiance, ambient temperature and wind speed of the weather station in Deelen, 2012. Besides the simulations, also an experiment was conducted at Hyet Solar to study the temperature dependent effect of thermal annealing. Three modules were degraded in a light soaker for about 300 hours until their efficiencies were stabilized and subsequently the three modules were placed in different ovens for 300 hours at 60°C, 90°C and 120°C. During the two processes the efficiency was regularly measured to keep track of the degradation and annealing process.

Through the simulations it was found that the annual electrical efficiencies of the four models at a mass flow rate of 0.015 $\frac{kg}{sm^2}$, including the required energy for pumping, was 7.88, 8.61, 7.46 and 8.64 percent for 'P1 Air', 'P1 Water', 'P2 Air' and 'P2 Water' respectively. The annual thermal efficiencies appeared to be 23.77, 35.06, 14.52 and 29.70 percent for the four models. The reference PV cell under the same conditions provided an annual electrical efficiency of 8.58 percent. Under standard test conditions and during stagnation, the maximum temperature of the solar cells in the air-cooled models varied between 63°C and 77°C. In the water-cooled PV-T systems a maximum solar cell temperature of 47°C could be achieved. After degradation of the test modules, the annealing experiment showed a relative increase in efficiency of 0.031%, 0.130% and 0.339% per hour during the first 24 hours of thermal annealing at 60°C, 90°C and 120°C respectively.

With respect to the performances, qualitative considerations, possible combinations with other applications and the effect of thermal annealing, the most favorable design proved to be 'P1 Water'. The water-cooled collectors showed superior performances (relative 50-100% better thermal efficiencies and 5-15% better electrical performances), requires much less pumping power and has more possibilities to be integrated with other applications. Additionally, prototype 1 showed higher thermal efficiency compared to prototype 2, while compromising only slightly on its electrical efficiency. However, air provides higher output temperatures and therefore enables thermal annealing of the amorphous Silicon

solar cell, which is less likely to occur in the water-cooled collectors. Unfortunately, the possibilities from thermal annealing at low temperatures appeared to be limited. The thermal efficiencies of the models could be improved further by increasing the effective heat transfer surface of the tubes compared to the fluid volume.

The numerical simulations could be further improved by using more accurate data (e.g. 15 minutes instead of hourly measurements). Also, when the model was cut into smaller tubes behind each other, where the output of the previous tube was input for the next tube to investigate the temperature increase over the distance in the tube, provided different output temperatures than was estimated using the original model. This effect was unexpected and should be look into in further simulations. In addition, heat storage and other thermal appliances should be connected to the simulations to examine the value of the extracted heat. The thermal annealing experiment could be optimized by including more temperatures and by including more measurement points, especially within the first 24 hours of the heating process.

For future research, several suggestions could be made. The results of the annealing process provide handles to include this effect to improve further simulations. Also, the theoretical outcomes should be validated with a real test setup, under similar standard test conditions and outdoor conditions. This would also provide valuable information about difficulties in the manufacturing process. In case real PV-T modules are produced, the production costs should be competitive with the other, few available PV-T modules in the market; between 0.45€/Wp and 0.90€/Wp (combined heat and electricity). In addition, simulations and tests should be performed on PV-T systems integrated with other thermal applications such as storage, heat pumps, absorption chillers and aquifer thermal energy storage. The latter is essential to utilize the obtained heat from the PV-T system to produce electricity, heat and cold simultaneously and enable energy neutral buildings in the near future.

SECTION 8: RECOMMENDATIONS

The Nanosol consortium aims to develop a market ready PV-T system by the end of 2014. Via this study several recommendations can be made with respect to the design of the module and for next steps that are required for the development.

1. According to this study, the most favorable model is 'P1 Water'. Water proofed to have superior properties over air and is therefore much more effective in cooling the solar cell resulting in higher electric and thermal yields. Furthermore, the required power to pump water through the system is much lower than for air. Prototype 1 cools the solar cell from both the front and the backside, which showed to enable increased thermal efficiency without compromising much on the electrical efficiency. Furthermore, the water-cooled collectors are easier to combine with other thermal applications.

2. Model 'P1 Water' can be further improved by increasing the effective heat transfer surface. This can be done by using smaller tubes (decrease depth and width) and adjusting the shape (more triangular or spherical). Also the thickness of the foil should be sufficient to enable better insulating properties. In the simulations this was set at 1 mm, while 2 mm thick foil showed an increase in thermal efficiency of one percent.

3. Real test under standard test conditions and outdoor conditions should be performed to validate the theoretical results. This will also reveal difficulties in the manufacturing process.

4. Theoretical simulations and experimental tests should be conducted to examine the value and the most optimal utilization of the extracted heat. Storage, heat pumps, absorption chillers and aquifer thermal energy storage are interesting options to combine with PV-T.

5. The final PV-T module should cost between 0.45€/Wp and 0.90€/Wp to be competitive with commercially available PV-T system. In these indicative prices, the electrical and thermal yield per square meter are combined and divided over the module price per square meter.

SECTION 9: REFERENCES

Alfegi, M., Sopian, K., Othman, M., & Yatim, B. (2008). Experimental investigation of single pass, double duct photovoltaic thermal (PV/T) air collector with CPC and fins. *American Journal of Applied Sciences*(5), 866-871.

Arndt, R., & Puto, R. (2003). *Basic Understanding of IEC Standard Testing for Photovoltaic Panels.* From http://tuvamerica.com/services/photovoltaics.cfm: http://tuvamerica.com/services/photovoltaics/ArticleBasicUnderstandingPV.pdf

Assoa, Y., Menezo, C., Yezou, R., Fraisse, G., & Lefebvre, T. (2005). Study of a new concept of photovoltaic-thermal hybric collector. *Passive and Low Energy Cooling for the Built Environment*, (pp. 1-6). Santorini, Greece.

Bakker, M., Zondag, H., Elswijk, M., Strootman, K., & Jong, M. (2005). Performance and costs of a roof-sized PV/thermal array combined with a ground coupled heat pump. *Solar Energy, 78*, 331-339.

CBS. (2013, February 23). *Hernieuwbare energie; eindverbruik en vermeden verbruik fossiele energie*. Retrieved from Tabellen per thema: http://statline.cbs.nl/StatWeb/publication/?DM=SLNL&PA=7516

Charalambous, P., Maidment, G., Kalogirou, S., & Yiakoumetti, K. (2007). Photovoltaic thermal (PV/T) collectors: a review. *Applied Thermal Engineering, 27*, 275-286.

Chow, T. (2010). A review on photovoltaic/thermal hybrid solar technology. *Applied Energy, 87*, 365-379.

Dersch, H., Stuke, J., & Beichler, J. (1981). Light-induced dangling bonds in hydrogenated amorphous silicon. *Applied Physics Letters, 38*(456), 456-458.

Dupeyrat, P., Helmers, H., Fortuin, S., & Kramer, K. (2011). *Recent advances in the development and testing of hybrid PV-Thermal collectors.* Freiburg, Germany: Fraunhofer Institute.

ECN. (2005). PVT Roadmap: a European guide for the development and market introduction of PVT technology. In H. Zondag, W. Helden van, M. Bakker, P. Affolter, W. Eisenmann, H. Fechner, . . . Y. Tripanagnostopoulos (Ed.), *European Photovoltaic Solar Energy Conference. 6-10*, pp. 1-4. Barcelona, Spain: PVSEC.

Fang, G., Hu, H., & Liu, X. (2010). Experimental investigation on the photovoltaic-thermal solar heat pump air-conditioning system on water-heating mode. *Experimental Thermal and Fluid Science*, 736-743.

He, W., Chow, T., Ji, J., Lu, J., Pei, G., & Chan, L. (2006). Hybrid photovoltaic and thermal solar-collector designed for natural circulation of water. *Applied Energy*, 199-210.

Hegazy, A. (2000). Comparative study of the performances of four photovoltaic/thermal solar air collectors. *Energy Conversion & Management, 41*, 861-881.

Ibrahim, A., Othman, M., Ruslan, M., Alghoul, M., Yahya, M., & Zaharim, A. (2009). Performance of photovoltaic thermal collector (PVT) with different absorbers. *Transactions on Environment and Development*, 321-330.

IEA. (2013, February 23). *Electricty/Heat in the Netherlands in 2009*. Retrieved from Statistics: http://www.iea.org/stats/electricitydata.asp?COUNTRY_CODE=NL

IPCC. (2007). *Climate Change 2007: Synthesis Report.* Intergovernmental Panel on Climate Change. Geneva, Switzerland: IPCC.

Ishii, T., Otani, K., Takashima, T., & Ikeda, K. (2013). Change in I-V characteristics of thin-film photovoltaic (PV) modules induced by light soaking and thermal annealing effects. *Progress in Photovoltaics: Research and Applications*, 1-9.

King, D., Kratochvil, J., & Boyson, W. (2000). Stabilization and performance characteristics of commercial amorphous-silicon pv modules. *Photovoltaic Specialists Conference* (pp. 1446-1449). Anchorage, AK: IEEE.

KNMI. (2013). Hourly data of all weather stations in the Netherlands. The Netherlands. From http://www.knmi.nl/klimatologie/uurgegevens/selectie.cgi

Kosteki, T., Kherani, N., Stradins, P., Gaspari, F., Shmayda, W., Sidhu, L., & Zukotynski, S. (2003). Tritiated amorphous silicon betavoltaic devices. *Proc.-Circuits Devices Syst., 150*(4), 274-281.

Kumar, R., & Rosen, M. (2011). A critical review of photovoltaic-thermal solar collectors for air heating. *Applied Energy, 88*, 3603-3614.

Merten, J., & Andreu, J. (1998). Clear separation of seasonal effects on the performance of amorphous silicon solar modules by outdoor I/V-measurements. *Solar Energy Materals & Solar Cells, 52*, 11-25.

Othman, M., Sopian, K., Yatim, B., & Daud, W. (2006). Development of advanced solar assisted drying systems. *Renewable Energy*(31), 703-709.

Pathak, M., Girotra, K., Harrison, S., & Pearce, J. (2012). The effect of hybrid photovoltaic thermal device operating conditions on intrinsic layer thickness optimization of hydrogenated amorphous silicon solar cells. *Solar Energy, 86*(9), 2673-2677.

Peercy, P. (1981). Hydrogen in Amorphous Silicon. *Nuclear Instruments and Methods, 182*, 337-349.

Sandnes, B., & Rekstad, J. (2002). A photovoltaic/thermal (PV/T) collector with a polymer absorber plate. Experimental study and analytical model. *Solar Energy*(72), 63-73.

Santbergen, R., & Zolingen, R. (2006). An optical model for the absorption factor of textured crystalline silicon PV-cells. *21st EPSEC.* Dresden, Germany.

Schott-Solar. (2013a). *www.schottsolar.com.* From Products and applications/download/Schott ASI: http://www.schott.com/newzealand/english/download/schott_asi_data_sheet_95-103_en.pdf

Schott-Solar. (2013b). *www.schott.com.* From photovoltaic/english/schott-perform-poly.html: http://www.schott.com/newzealand/english/download/schott_poly_data_sheet_220-235_en_0810.pdf

Senternovum. (2008). Energie verbruik in utiliteitsgebouwen, verdeeld naar functie [MJ/m2]. AgentschapNL. From http://senternovem.databank.nl/

Staebler, D., & Wronski, C. (1977). Reversible conductivity changes in dischargeproduced amorphous Si. *Applied Physics Letters, 31*(292), 1-4.

Twidell, J., & Weir, A. (2006). *Renewable Energy Resources* (Second edition ed.). London and New York: Taylor & Francis.

Virtuani, A., & Fanni, L. (2012). Seasonal power fluctuations of amorphous silicon thin-film solar modules: distinguishing between different contributions. *Progress in Photovoltaics: Research and Applications*, 1-10.

VREG. (2012). Userprofiles for Gas and Electricity. Belgium. From http://www.vreg.be/verbruiksprofielen-0

Zondag, H. A. (2008). Flat-plate PV-Thermal collectors and systems: A review. *Renewable & Sustainable Energy Reviews*, 891-959.

Zondag, H., de Vries, D., van Helden, W., van Zolingen, R., & van Steenhoven, A. (2003). The yield of different combined PV-thermal collector designs. *Solar Energy, 74*, 253-269.

APPENDIX A: AIR AND WATER PROPERTIES

A1. AIR PROPERTIES AS A FUNCTION OF TEMPERATURE

In all cases, the blue line represents actual data from tables from course books, the red line shows the data used for the model. The red line is based on the actual data but contains values for all temperatures. (Twidell & Weir, 2006)

Density [kg/m3]

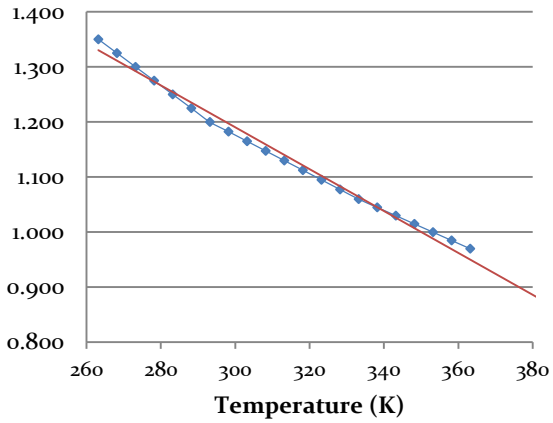

Kin. Viscosity [m2/s]

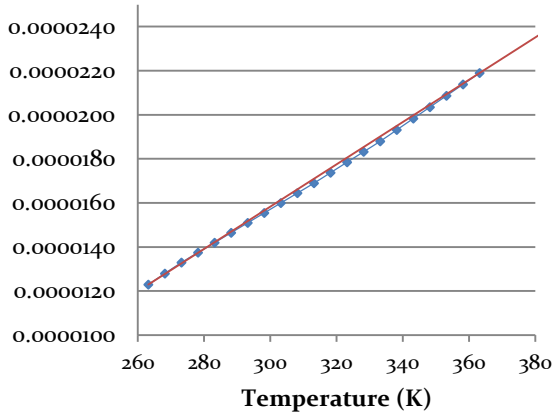

Specific Heat Capacity [J/kgK]

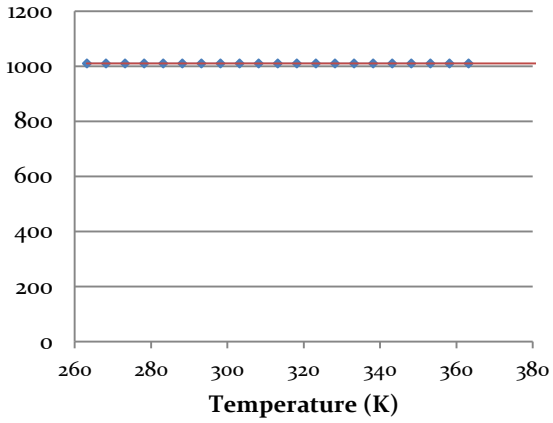

Thermal Diffusivity [m2/s]

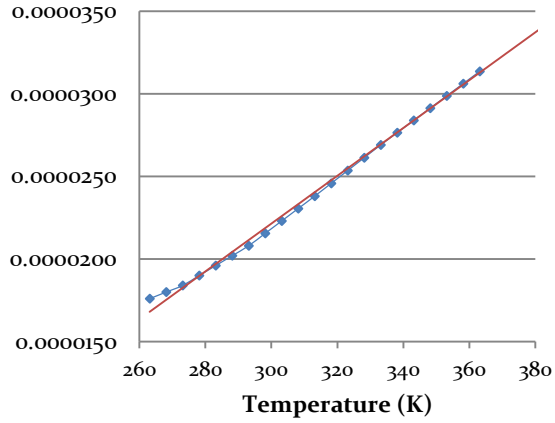

Thermal Conductivity [W/m]

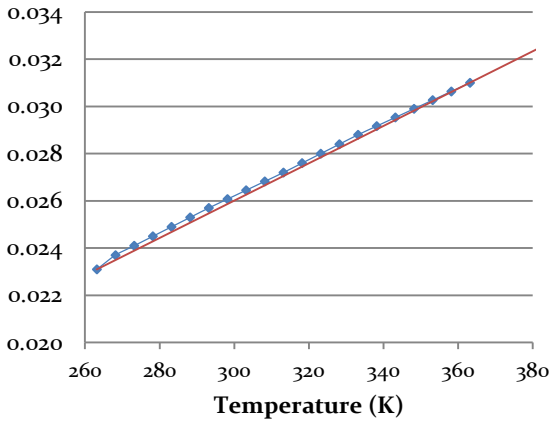

A2. WATER PROPERTIES AS A FUNCTION OF TEMPERATURE

In all cases, the blue line represents actual data from tables from course books, the red line shows the data used for the model. The red line is based on the actual data but contains values for all temperatures. (Twidell & Weir, 2006)

Density [kg/m3]

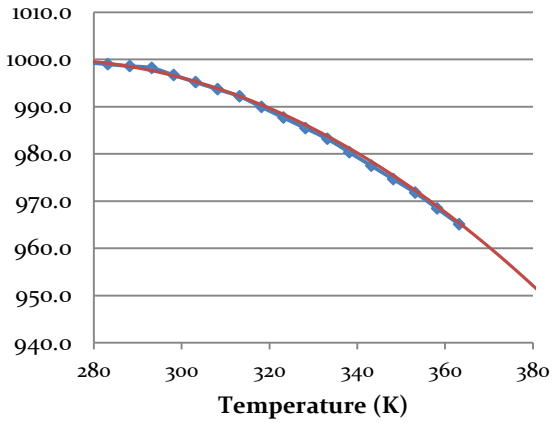

Kinetic Viscocity [m2/s]

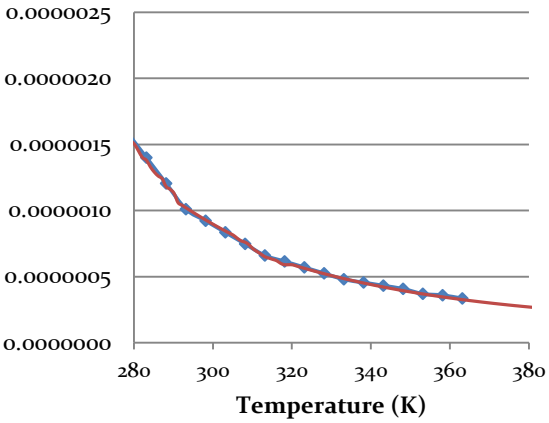

Specific Heat Capacity [J/kgK]

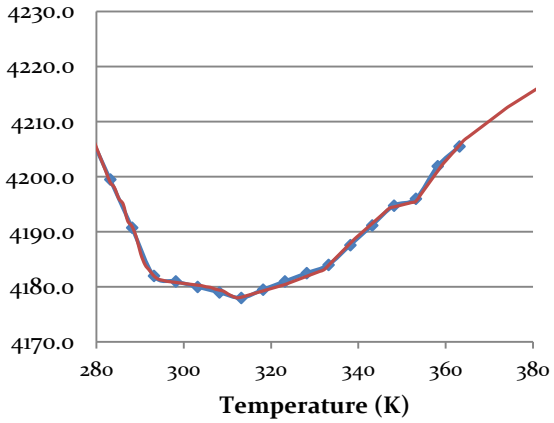

Thermal diffusivity [m2/s]

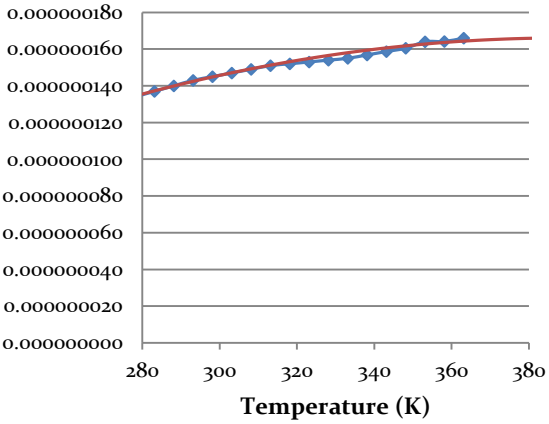

Thermal conductivity [W/m]

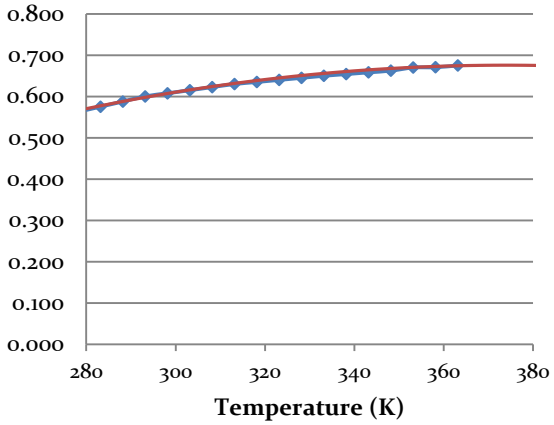

APPENDIX B: THERMAL ANNEALING EXPERIMENT - LAB JOURNAL

PROCESS

1. Place Modules in Light Soaker to degrade until efficiency is stabilized
2. Place Modules in Oven at 60, 90 and 120 degrees Celcius for maximum two weeks
3. Measure efficiency before light soaker, during light soaker, before oven, during oven, after oven

MODULES

1. Three year old, but never used modules will be used for the experiment
2. They have been stored on top of each other in boxes
3. The modules are 30x30 cm in size (28 cells of 1x30cm)

OPERATION PULSAR

1. Turn on the three large condensators, wait until 640 V
2. Turn on the Flasher itself
3. Turn on the computer and start Pulsar (see desktop)
4. Place module correctly on the vacuum plate, below the metal contacts
5. Lower the metal contacts, and turn on the vacuum plate
   (make sure reference detector is uncovered)
6. Fill in the Pulsar data correctly (Use for state, the first time 'remeasure' and thereafter LS or something else)
7. Press 'Start', now a bright flash will appear and the data will be shown on the screen
8. The data is now saved in the correct excel file belonging to the specific role of the module (see desktop → Role Modules)
9. See all the pictures for more clarification

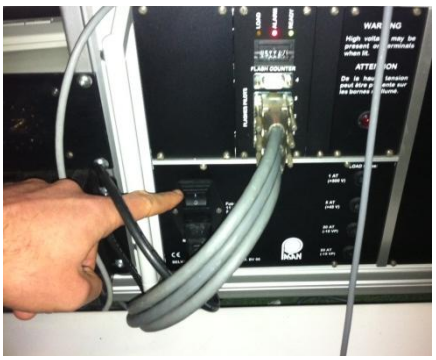

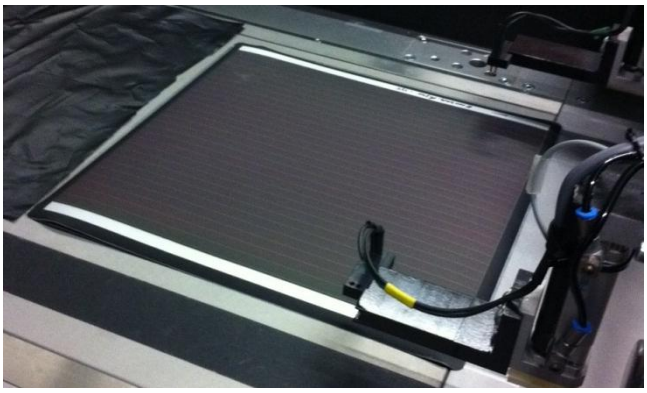

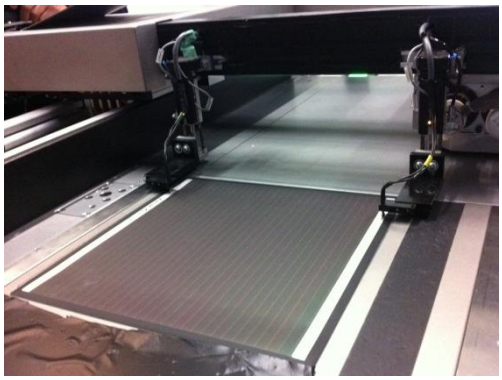

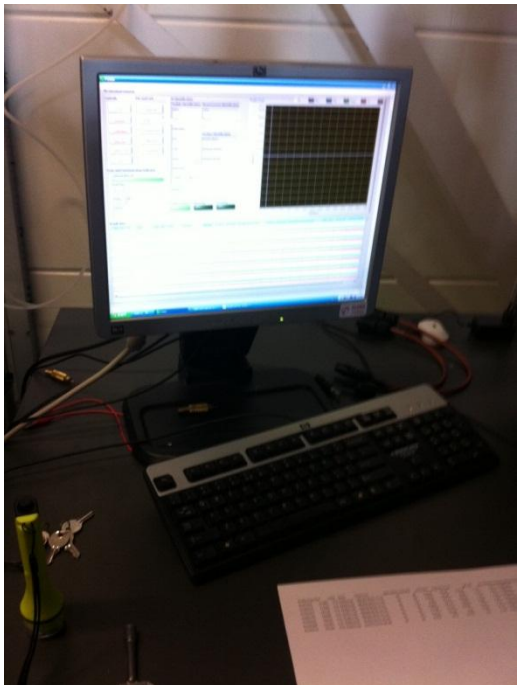

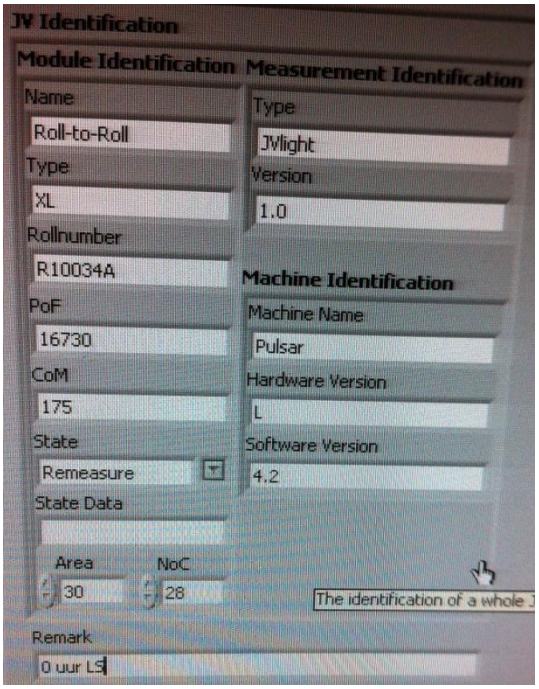

OPERATION LIGHT SOAKER

1. Turn on the lamps
2. Place module in the lower case, in the middle of the chamber
3. Close door
4. Measure the module efficiency every two days under the flasher (let it first cool for 1 hour)
5. After 240-300 hours, the module is probably sufficiently stabilized, check from point 4
6. Note all times in labjournal
7. See pictures for clarification

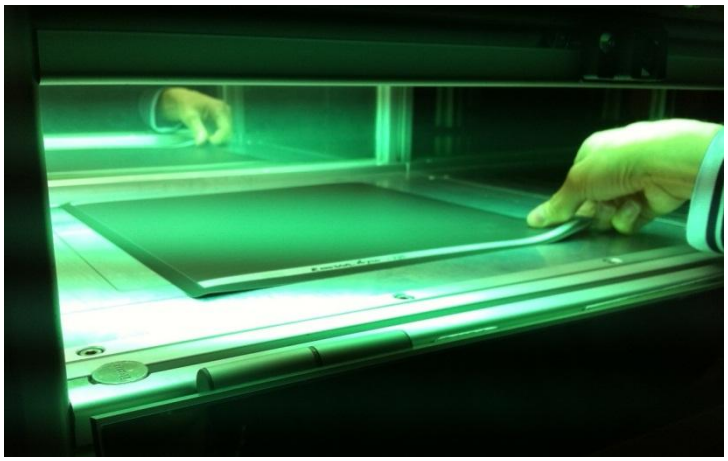

OPERATION OVEN

1. Turn on the Oven and set it to the correct temperature
2. Place module in the oven (placed between two aluminium plates to avoid bubbles)
3. Close door
4. Regularly measure the efficiency with the Flasher (again let it cool to room temperature)
5. Place module back into the oven after measurements
6. Note all times in labjournal
7. See pictures for clarification

TABLE 1, RECEIVED MODULES (SIZE: 30CM X 28 CELLS OF 1 CM)

Mod.	RollNum.	PoF	CoM	State	Date/Time	V_{OC} (V)	J_{SC} (mA)	FF	Eff. (%)
A	R10034A	16730	175	R2REncap	08/06/2010 17:51	0.810	14.14	0.616	7.06
B	R10034A	17430	175	R2REncap	08/06/2010 17:35	0.826	14.07	0.620	7.21
C	R10034A	17480	175	R2REncap	08/06/2010 17:32	0.824	14.05	0.618	7.15

JOURNAL

Date	Time	Activity	Instrument	Mod.	Remarks
14 may	11.55	Measure efficiency (η = ±7.25)	Flasher	A	All efficiencies have increased compared to
	12.00	Measure efficiency	Flasher	B	previous measurement three years ago.
	12.05	Measure efficiency	Flasher	C	Modules were stored in dark closet.
	12.10	Place module in Light Soaker	Light Soaker	A	Temperature 39°C
16 may	09.00	Take module out of LS	Light Soaker	A	Cooling down (44 hours LS)
	09.56	Measure efficiency (η = ±6.29)	Flasher	A	
	10.00	Place module in Light Soaker	Light Soaker	A	
					Extra: Agreed with Klaus to do some Reflection measurements (to find α)
21 may	08.35	Take module out of LS	Light Soaker	A	Cooling down (166 hours LS)
	09.56	Measure efficiency (η = ±6.24)	Flasher	A	
	10.00	Place module in Light Soaker	Light Soaker	A	
24 may	08.30	Take module A out of LS	Light Soaker	A	Cooling down (300 hours LS)
	09.52	Measure efficiency (η = ±6.21)	Flasher	A	NREL: ((Pmax-Pmin)/Paver)< 2% →Stable
	10.16	Module A in oven at 60 degr.	Oven 60	A	
	10.26	Measure efficiency (η = ±7.35)	Flasher	B	0 hours LS
	10.29	Measure efficiency (η =±7.23) /7.20%	Flasher	C	0 hours LS
	10.43	Place module in LS	Light Soaker	B	
	10.45	Place module in LS	Light Soaker	C	
	11.21	Take module out of the oven	Oven 60	A	1 hour of oven
	11.45	Take module out of LS	Light Soaker	B	1 hour LS
	11.45	Take module out of LS	Light Soaker	C	1 hour LS
	12.24	Measure efficiency (η = ±6.21)	Flasher	A	1 hour Oven 60
	12.35	Module back in Oven 60	Oven 60	A	
	12.42	Measure efficiency (η = ±7.01)	Flasher	B	1 hour LS (2x measured)
	12.44	Measure efficiency (η = ±6.92)	Flasher	C	1 hour LS (2x measured)
	12.47	Module back in LS	Light Soaker	B	
	12.47	Module back in LS	Light Soaker	C	
	13.47	Module out of LS	Light Soaker	B	
	13.47	Module out of LS	Light Soaker	C	
	14.35	Module out of Oven 60	Oven 60	A	
	14.45	Measure efficiency (η = ±6.90	Flasher	B	2 hours LS
	14.47	Measure efficiency (η = ±6.81)	Flasher	C	2 hours LS
	14.49	Module in LS	Light Soaker	B	
	14.49	Module in LS	Light Soaker	C	
	15.40	Measure efficiency (η = ±6.21)	Flasher	A	3 hours Oven 60
	15.45	Module back in Oven 60	Oven 60	A	
	15.49	Module out of LS	Light Soaker	B	
	15.49	Module out of LS	Light Soaker	C	
	16.48	Measure efficiency (η = ±6.84	Flasher	B	3 hours LS
	16.50	Measure efficiency (η = ±6.74)	Flasher	C	3 hours LS
	16.52	Module back in LS	Light Soaker	B	
	16.52	Module back in LS	Light Soaker	C	
28 may	08.30	Module out Oven	Oven 60	A	(19 hours and 45 min Oven 60)
	08.30	Module out LS	Light Soaker	B	(16h and 30m LS)
	08.30	Module out LS	Light Soaker	C	(16h and 30m LS)
	09.46	Measure efficiency (η = ±6.26!	Flasher	A	(19.5h in Oven 60)
	09.50	Module back in Oven 60	Oven 60	A	
	09.53	Measure efficiency (η = ±6.67)	Flasher	B	(16.5h in LS) (2x measured)
	09.55	Measure efficiency (η=±6.54 /6.55	Flasher	C	(16.5h in LS) (2x measured)
	09.57	Module back in LS	Light Soaker	B	
	09.57	Module back in LS	Light Soaker	C	
	16.00	Module out of Oven60	Oven 60	A	(26h in oven60)
	16.03	Module out of LS	Light Soaker	B	(23h in LS)
	16.03	Module out of LS	Light Soaker	C	(23h in LS)
	16.56	Measure efficiency (η = ±6.25	Flasher	A	(26h in Oven 60) (2x measured)
	16.58	Measure efficiency (η = ±6.65)	Flasher	B	(23h in LS) (2x measured)

	17.00	Measure efficiency (η = ±6.53)	Flasher	C	(23h in LS) (2x measured)
	17.04	Module back in LS	Light Soaker	B	
	17.04	Module back in LS	Light Soaker	C	
	17.07	Module back in Oven 60	Oven 60	A	
30 may	08.40	Module out of Oven 60	Oven 60	A	(66h in Oven60)
	08.44	Module out of LS	Light Soaker	B	(67h in LS)
	08.44	Module out of LS	Light soaker	C	(67h in LS)
	09.39	Measure efficiency (η = ±6.30	Flasher	A	(66h in Oven 60) (2x measured)
	09.41	Measure efficiency (η = ±6.59	Flasher	B	(67h in LS) (2x measured)
	09.44	Measure efficiency (η = ±6.48	Flasher	C	(67h in LS) (2x measured)
	09.48	Module back in Oven 60	Oven 60	A	
	09.50	Module back in LS	Light Soaker	B	
	09.50	Module back in LS	Light Soaker	C	
03 jun	08.30	Module out of Oven 60	Oven 60	A	(162h in Oven60)
	08.35	Module out of LS	Light Soaker	B	(163h in LS)
	08.35	Module out of LS	Light soaker	C	(163h in LS)
	10.14	Measure efficiency (η = ±6.35	Flasher	A	(162h in Oven 60) (2x measured)
	10.18	Measure efficiency (η = ±6.55	Flasher	B	(163h in LS) (2x measured)
	10.20	Measure efficiency (η = ±6.45	Flasher	C	(163h in LS) (2x measured)
	10.30	Module back in Oven 60	Oven 60	A	
	10.30	Module back in LS	Light Soaker	B	
	10.35	Module back in LS	Light Soaker	C	
06 jun	14.05	Module out of Oven 60	Oven 60	A	(238h in Oven60)
	14.10	Module out of LS	Light Soaker	B	(239h in LS)
	14.10	Module out of LS	Light soaker	C	(239h in LS)
	15.13	Measure efficiency (η = ±6.37	Flasher	A	(238h in Oven 60) (2x measured)
	15.15	Measure efficiency (η = ±6.53	Flasher	B	(239h in LS) (2x measured)
	15.17	Measure efficiency (η = ±6.43	Flasher	C	(239h in LS) (2x measured)
	15.20	Module back in Oven 60	Oven 60	A	
	15.25	Module back in LS	Light Soaker	B	
	15.25	Module back in LS	Light Soaker	C	
10 jun	08.30	Module out of Oven 60	Oven 60	A	(327h in Oven60)
	08.35	Module out of LS	Light Soaker	B	(326h in LS)
	08.35	Module out of LS	Light soaker	C	(326h in LS)
	09.42	Measure efficiency (η = ±6.39	Flasher	A	(327h in Oven 60) (2x measured)
	09.45	Measure efficiency (η = ±6.49	Flasher	B	(326h in LS) (2x measured)
	09.48	Measure efficiency (η = ±6.41	Flasher	C	(326h in LS) (2x measured)
	09.50	-	-	A	MODULE FINISHED
	09.52	Module back in LS	Light Soaker	B	
	09.52	Module back in LS	Light Soaker	C	
12 jun	09.00	Module out of LS	Light Soaker	B	(374h in LS)
	09.00	Module out of LS	Light soaker	C	(374h in LS)
	09.55	Measure efficiency (η = ±6.47	Flasher	B	(374h in LS) (2x measured)
	09.57	Measure efficiency (η = ±6.39	Flasher	C	(374h in LS) (2x measured)
	10.03	Module in Oven	Oven 90	B	
	10.04	Module in Oven	Oven 120	C	
	11.00	Module out Oven	Oven 90	B	(1h in Oven 90) (plates still hot..)
	11.00	Module out Oven	Oven 120	C	(1h in Oven 120) (plates still hot..)
	11.58	Measure efficiency (η = ±6.48	Flasher	B	(1h in Oven 90) (2x measured)
	12.00	Measure efficiency (η = ±6.55	Flasher	C	(1h in Oven 120) (2x measured)
	12.05	Module in Oven	Oven 90	B	
	12.07	Module in Oven	Oven 120	C	
	13.03	Module out Oven	Oven 90	B	(2h in Oven 90) (plates removed after 30m
	13.03	Module out Oven	Oven 120	C	(2h in Oven 120) (plates removed after 30
	14.09	Measure efficiency (η = ±6.49	Flasher	B	(2h in Oven 90) (2x measured)
	14.11	Measure efficiency (η = ±6.62	Flasher	C	(2h in Oven 120) (2x measured)
	14.17	Module in Oven	Oven 90	B	
	14.18	Module in Oven	Oven 120	C	
	15.17	Module out Oven	Oven 90	B	(3h in Oven 90) (plates removed after 30m
	15.17	Module out Oven	Oven 120	C	(3h in Oven 120) (plates removed after 30
	16.20	Measure efficiency (η = ±6.49	Flasher	B	(3h in Oven 90) (2x measured)
	16.22	Measure efficiency (η = ±6.65	Flasher	C	(3h in Oven 120) (2x measured)
	16.30	Module in Oven	Oven 90	B	

	16.30	Module in Oven	Oven 120	C	
13 jun	08.45	Module out Oven	Oven 90	B	(16h in Oven 90) (plates removed after 30
	08.45	Module out Oven	Oven 120	C	(16h in Oven 120) (plates removed after 30
	10.04	Measure efficiency (η = ±6.64	Flasher	B	(16h in Oven 90) (2x measured)
	10.06	Measure efficiency (η = ±6.80	Flasher	C	(16h in Oven 120) (2x measured)
	10.10	Module in Oven	Oven 90	B	
	10.10	Module in Oven	Oven 120	C	
	16.08	Module out Oven	Oven 90	B	(22h in Oven 90) (plates removed after 30
	16.08	Module out Oven	Oven 120	C	(22h in Oven 120) (plate removed after 30
	16.56	Measure efficiency (η = ±6.63	Flasher	B	(22h in Oven 90) (2x measured)
	16.58	Measure efficiency (η = ±6.77	Flasher	C	(22h in Oven 120) (2x measured)
	17.05	Module in Oven	Oven 90	B	
	17.05	Module in Oven	Oven 120	C	
14 jun	17.10	Module out Oven	Oven 90	B	(47h in Oven 90) (plates removed after 20
	17.10	Module out Oven	Oven 120	C	(47h in Oven 120) (plate removed after 20
	17.30	Measure efficiency (η = ±6.68	Flasher	B	(47h in Oven 90) (2x measured)
	17.32	Measure efficiency (η = ±6.77	Flasher	C	(47h in Oven 120) (2x measured)
	17.40	Module in Oven	Oven 90	B	
	17.40	Module in Oven	Oven 120	C	
17 jun	10.50	Module out Oven	Oven 90	B	(47h in Oven 90)
	10.50	Module out Oven	Oven 120	C	(47h in Oven 120)
	12.14	Measure efficiency (η = ±6.77	Flasher	B	(47h in Oven 90) (2x measured)
	12.17	Measure efficiency (η = ±6.74	Flasher	C	(47h in Oven 120) (2x measured)
	12.20	Module in Oven	Oven 90	B	
	12.20	Module in Oven	Oven 120	C	
19 jun	12.53	Module out Oven	Oven 90	B	(161h in Oven 90)
	12.53	Module out Oven	Oven 120	C	(161h in Oven 120)
	14.15	Measure efficiency (η = ±6.73	Flasher	B	(161h in Oven 90) (2x measured)
	14.17	Measure efficiency (η = ±6.64	Flasher	C	(161h in Oven 120) (2x measured)
	14.23	Module in Oven	Oven 90	B	
	14.23	Module in Oven	Oven 120	C	
21 jun	09.45	Module out Oven	Oven 90	B	(204h in Oven 90)
	09.45	Module out Oven	Oven 120	C	(204h in Oven 120)
	10.56	Measure efficiency (η = ±6.79	Flasher	B	(204h in Oven 90) (2x measured)
	10.58	Measure efficiency (η = ±6.66	Flasher	C	(204h in Oven 120) (2x measured)
	11.05	Module in Oven	Oven 90	B	
	11.05	Module in Oven	Oven 120	C	
24 jun	09.36	Module out Oven	Oven 90	B	(275h in Oven 90)
	09.36	Module out Oven	Oven 120	C	(275h in Oven 120)
	10.20	Measure efficiency (η = ±6.78	Flasher	B	(275h in Oven 90) (2x measured)
	10.20	Measure efficiency (η = ±6.60	Flasher	C	(275h in Oven 120) (2x measured)
	10.26	Module Finished	Oven 90	B	
	10.26	Module Finished	Oven 120	C	